Novel CDKL5 substrates and functions in neurodevelopment

Lucas L. Baltussen

University College London

and

The Francis Crick Institute

PhD Supervisor: Sila Ultanir

A thesis submitted for the degree of

Doctor of Philosophy

University College London

July 2018

Declaration

I, Lucas Baltussen, confirm that the work presented in this thesis is my own. Where information has been derived from other sources, I confirm that this has been indicated in the thesis.

Abstract

Cyclin-Dependent Kinase-Like 5 (CDKL5) is a serine/threonine protein kinase important for neuronal development. Mutations in the CDKL5 gene are responsible for CDKL5 deficiency disorder, a rare neurodevelopmental disorder displaying a heterogeneous range of clinical phenotypes. CDKL5 is enriched in the brain during early postnatal development, and is known to be involved in the development of dendritic spines and synapses. However, direct downstream effectors of CDKL5 and its molecular mechanisms of action remain unknown.

We have generated analogue-specific CDKL5 by mutating the gatekeeper residue in the ATP-binding pocket, and introduced a second-site mutation to rescue kinase activity. Based on the utilization of bulky ATP analogues by analogue-specific CDKL5, we used an unbiased chemical genetic screen to identify CDKL5 substrates and phosphorylation sites in mouse brain. *In vitro* validation of ARHGEF2, EB2 and two sites in MAP1S revealed RPxS as a common CDKL5 phosphorylation motif. We show that EB2 and MAP1S phosphorylation is strongly reduced in brains of Cdkl5 KO mice. In neurons derived from CDKL5 patient iPSCs, we observe similar reductions indicating that regulation of these phosphorylation sites is conserved in humans. By using CDKL5 substrate phosphorylation as a read-out, we have been able to show that CDKL5 activity is regulated during brain development and affected by neuronal activity.

These novel CDKL5 substrates share microtubule binding properties, but only phosphorylation of MAP1S by CDKL5 is directly regulating its microtubule binding affinity. Attempts to identify a molecular function of EB2 phosphorylation did not lead to satisfying results. Both MAP1S and EB2 are known to be involved in microtubule dynamic instability, the process of constant growth and collapse of microtubule plus-ends. We show that primary cortical cultures of Cdkl5 KO mice have altered microtubule plus-end dynamics visualised by sparser, but longer EB3 comets. Knockdown of MAP1S, but not EB2, partially rescued this phenotype in Cdkl5 KO neurons, indicating a downstream function of MAP1S in the regulation of microtubule dynamics.

Impact Statement

The work we describe in this thesis is all about one single goal: Cure CDKL5 deficiency disorder. This destructive neurodevelopmental disorder is an extremely heavy burden on many families, but only one of over 7000 rare diseases in the world. Rare diseases are therefore often severely understudied and underfunded, and the same is true for CDKL5. Almost 15 years after discovering CDKL5 as a genetic cause for epileptic encephalopathy, still only 131 publications on Pubmed contain CDKL5 in the title. The vast majority of them describing the severe clinical symptoms of CDKL5 deficiency disorder without going into basic science. This lack of knowledge about the function of CDKL5 has been a major hurdle in advancing therapeutic strategies to find a cure.

We believe that our work on the identification of the first physiological substrates of CDKL5 will provide essential information on the function of the kinase and the reasons behind its pathogenicity. Antibodies that have been produced based on our findings have shown remarkable potential to be used as biomarkers in disease models, and potentially could be further developed as tools for gene therapy and protein replacement strategies. The specific consensus sequence for CDKL5 phosphorylation we have identified has already assisted others in their pursuit of CDKL5 targets as well. Our discovery of a novel phenotype in CDKL5 deficient neurons regarding microtubule dynamics has also opened up new directions for CDKL5 research. All of which are believed to shorten the time between now and a cure for CDKL5 deficiency disorder.

Acknowledgements

I would like to start by thanking Sila for the opportunity to work on this project and trust me as her first PhD student to lead it in the right direction. Also many thanks to past and present members of the lab that helped me in all kinds of ways possible: Suzanne has been there from the beginning to support me with too many experiments to all mention here, and provide me with a daily dose of institute gossip. Noreens expertise in mass spectrometry and sexing have been crucial for this work, and together with Suzanne forms the outstanding culture club. Amy, Kali and Flavia have made the lab a stimulating place to work and gave me plenty of important advice and feedback throughout the years. Raphael, Irene and Max have been outstanding master students that took a lot of work out of my hands that I really did not wanted to do. And although Margaux only started recently, she has already proven herself as more than capable of continuing this project after me.

Special thanks to some instrumental scientific contributors to my work that are outside of our lab (some of which who are also excellent drinking buddies): Donald, for all you need to know about microscopes and kilts. Vangelis, the source of proteins and sports chat. Helen and Bram, who are masters in the modern wizardry of proteomics. Sai, Bobbi and all other BRF staff who have looked after my pets all these years. All my collaborators from all over the world who provided me with knowledge and materials to make my experiments work, or not.

Thanks a lot to the many friends that I have made at work in the last 4.5 years: All Natural Killers that provided the highlight of my PhD by winning the last football league at Mill Hill, which we so dearly miss now. Everyone ever involved in Nimdram, who let me express my inner-diva and provide a platform to take your mind of daily life by pretending to be someone else. The breakfast club, probably the most exclusive club at work, and the best place to complain about everything that is wrong with the world. Francis and the Crickets, who let me sing a song or beat a cowbell once every blue moon, even though I am the most unmusical person ever. And of course everyone else who ever had the pleasure of having a drink with me at the bar.

Finally, I am in great debt to the people closest to me that have kept my feet on the ground and stopped me from going insane sometimes. I love you all. Especially Sarah, who has made my life a million times better than I could have ever imagined for the last 2,5 years. My parents and brothers, who I mainly have to apologise to, instead of thanking, for not coming home enough and not keeping in touch enough. Basically I have to apologise for being a shit son and brother, but thanks for understanding. Oh dear…

Thanks to all of you (and many more) I have been able to do what I love during my PhD, and in a way you all contributed to this thesis. That's why I refused to write the rest of this thesis in the singular form of the first person, as you never walk alone.

Table of Contents

Table of Figures

List of Tables

Abbreviations

+TIP = plus-end tracking protein

AAK1 = AP2-associated kinase 1

ACN = acetonitrile

AMPA = α-amino-3-hydroxy-5-methylisoxazole-4-propionic acid

AMPH1 = amphyphysin 1

AP1 = adaptor protein 1

ARHGEF2 = Rho guanine nucleotide exchange factor 2

AS = analogue-sensitive

ATP = adenosine triphosphate

BDNF = brain-derived neurotrophic factor

BSA = bovine serum albumin

CaMKII = Ca2+/calmodulin-dependent protein kinase II

CAMSAP = calmodulin-regulated spectrin-associated protein family member

CBB = coomassie brilliant blue

CDK5 = cyclin-dependent kinase 5

CDKL = cyclin-dependent kinase-like

CH = calponin homology

CHK2 = checkpoint kinase 2

CIP = calf intestinal phosphatase

CLIP170 = cytoplasmic-linker protein 170

CNS = central nervous system

CRISPR = clustered regularly interspaced short palindromic repeats

CSF = cerebrospinal fluid

dATP = deoxyadenosine triphosphate

DIV = days in vitro

DMEM = Dulbecco's modified Eagle medium

DNA = deoxyribonucleic acid

DNMT1 = DNA methyltransferase 1

dNTP = deoxynucleotide

DTT = dithiothreitol

DYRK1A = dual-specificity tyrosine-(Y)-phosphorylation regulated kinase 1A

E = embryonic day

EB = end-binding protein

EEG = electroencephalography

EPSC = excitatory postsynaptic current

ERK2 = extracellular signal-regulated kinase 2

ERP = event-related potential

FBS = fetal bovine serum

GABA = γ-aminobutyric acid

GAN = gigaxonin

GDP = guanine diphosphate

GFP = green fluorescent protein

GSK3 = glycogen synthase kinase 3

GTP = guanosine triphosphate

HA = hemagglutinin

HBSS = Hank's balanced salt solution

HDAC4 = histone deacetylase 4

HEK = human embryonic kidney

HRP = horseradish peroxidase

ICCS = spatial image cross-correlation spectroscopy

IGF1 = insulin-like growth factor 1

IP = immunoprecipitation

IPSC = induced pluripotent stem cell

IQGAP1 = IQ motif-containing GTPase-activating protein 1

ITK = interleukin 2-inducible T-cell kinase

KALIP = kinase assay linked with phosphoproteomics

KCl = potassium chloride

KO = knockout

LB = lysis buffer

LC3 = light chain 3

LC-MS/MS = liquid chromatography-tandem mass spectrometry

LIC = ligase-independent cloning

LRPPRC = leucine-rich pentatricopeptide repeat-containing

LRRK2 = leucine-rich repeat kinase 2

LTD = long-term depression

LTP = long-term potentiation

MAP = microtubule associated protein

MAP = microtubule-associated protein

MeCP2 = methyl-CpG binding protein 2

MEM = minimum esdential medium

mTOR = mechanistic target of rapamycin

NBM = neurobasal medium

NDR = nuclear dbf2-related

NGL1 = netrin G1-ligand

NMDA = N-methyl-D-aspartate

P = postnatal day

PAK1 = P21-activated kinase 1

PBS = phosphate-buffered saline

PCR = polymerase chain reaction

PDl = poly-D-lysine

PFA = paraformaldehyde

PKR = protein kinase R

PNBM = p-nitrobenzyl mesylate

PSD = postsynaptic density

RAPH1 = Ras-associated and pleckstrin-homology domains-containing protein 1

RASSF1 = Ras-association domain family member 1

RT = room temperature

SEM = standard error of the mean

sgRNA = single guide RNA

shRNA = short hairpin RNA

SILAC = stable isotope labelling of amino acids in cell culture

SLENDR = Single-cell labelling of endogenous proteins by CRISPR-Cas9-mediated homology-directed repair

ssODN = single-stranded oligodeoxynucleotide

STK9 = serine/threonine kinase 9

TBST = tris-buffered saline + Tween-20

TCEP = tris(2-carboxyethyl)phosphine

TEAB = triethylamonium bicarbonate

TFA = trifluoroacetic acid

TPD52 = tumor protein d52

TRIM46 = tripartite motif-containing 46

TTX = tetradotoxin

UV = ultraviolet

VDCC = voltage-dependent calcium channel

VP35 = Ebola virus protein 35

Chapter 1. Introduction

Ever since the discovery that reversible phosphorylation of proteins regulates protein function, there has been great interest in protein kinases, the enzymes that mediate this reaction. Protein kinases regulate a plethora of cellular processes by transferring the γ-phosphate of adenosine triphosphate (ATP) onto serine, threonine or tyrosine residues of substrate proteins (Cohen, 2000). Global mass spectrometry analysis over the last decades resulted in cumulative evidence showing that the vast majority of proteins can be phosphorylated at multiple sites (Hornbeck et al., 2015). The protein kinase complement of the human genome, also referred to as the 'kinome', is comprised of more than 500 kinases responsible for these phosphorylation events (Manning et al., 2002). Many of these kinases are expressed in the mouse brain and neurons as shown by *in situ* hybridization (Lein et al., 2007) and proteomic analysis (Sharma et al., 2015), and provide important functions during neuronal development and functioning. Important examples include cyclin-dependent kinase 5 (CDK5), which phosphorylates several substrates to regulate neuronal migration, synaptic plasticity and dendritic spine morphogenesis (Cheung and Ip, 2012), and Ca^{2+}/calmodulin-dependent protein kinase II (CaMKII), one of the most studied kinases in neuronal function, owing to its postsynaptic localization and requirement for several forms of synaptic plasticity in learning and memory (Ghosh and Giese, 2015).

Due to the numerous roles protein kinases play in cellular events, and the accessibility of their ATP binding pocket, they are one of the most important classes of drug targets in the pharmaceutical industry. Recently it was estimated that 50-70% of current cancer drug discovery programmes are focused on protein kinases (Cohen and Alessi, 2013). Kinase-targeted therapies for neurological diseases are also being developed. For example, glycogen synthase kinase 3 (GSK3) and leucine-rich repeat kinase 2 (LRRK2) have received much interest from the pharmacological industry in attempts to treat Alzheimer's and Parkinson's disease respectively (Chico et al., 2009). However, despite significant advances, there are no approved kinase-targeting drugs for the central nervous system available yet (Gunosewoyo et al., 2017). More basic knowledge about the function and substrates of kinases is often regarded as a necessary step towards unlocking their therapeutic potential.

In this thesis, we will focus on our attempts to understand more about cyclin-dependent kinase-like 5 (CDKL5), a kinase directly responsible for the severe neurodevelopmental symptoms of CDKL5 deficiency disorder. We will introduce this topic by initially elaborating on neurodevelopment with a special focus on the neuronal cytoskeleton, followed by a detailed overview of the current knowledge on CDKL5, and finish with a comprehensive introduction to kinase substrate mapping and the novel CDKL5 substrates identified in this thesis.

1.1 Neuronal development

The mammalian brain is considered to be the most complex organ in the body and development of the central nervous system (CNS) is therefore a complicated and tightly regulated process. The brain and the spinal cord are derived from the neural tube, a structure filled with cerebrospinal fluid (CSF) that is formed during embryogenesis (Greene and Copp, 2009). The anterior part of the neural tube gives rise to the primary anatomical regions of the brain through the formation of a series of vesicles, while dorsal-ventral patterning during neural tube development leads to specification of the tremendous variety of neuronal and glial cells (Le Dreau and Marti, 2012). After progenitor cells develop into differentiated neurons in a process called neurogenesis, newly generated neurons migrate away from their original germinal zones to their final positions in cell assemblies. Post-mitotic neurons in the cortex and hippocampus follow radial migration, where neurons generated in proliferative zones move along radially oriented glial fibres, orthogonal to the surface of the brain. These cells eventually become excitatory pyramidal neurons (Kriegstein and Alvarez-Buylla, 2009). Inhibitory neurons on the other hand, migrate tangentially and move parallel to the surface of the brain, often transgressing regional boundaries (Marin and Rubenstein, 2003). Once neurons have migrated, they begin to differentiate and commit to specialized networks via neurite arborisation and synaptogenesis. We will describe the specific development of axons, dendrites and synapses in more detail.

1.1.1 Axon, dendrite and synapse development

In order for neurons to mediate information flow through the nervous system, they need to be highly polarised. Therefore, two structurally and functionally different processes extend from the neuronal cell body. The axon is typically a single long projection that conducts electrical impulses known as action potentials to convey information to other neurons by the release of neurotransmitters. Input-receiving dendrites are composed of several branched processes that integrate multiple signals and propagate the received electrochemical stimulation to the soma. The exact processes of *in vivo* neuronal polarisation highly depend on cell-type, brain region and developmental stage. For instance, cortical pyramidal cells, the main excitatory neurons in the forebrain, extend multiple minor neurites during migration, of which one becomes a trailing process, while another develops into a leading process. These processes finally develop into the axon and apical dendrite respectively (Cheng and Poo, 2012). Neuronal polarisation is precisely regulated by secreted factors in the extracellular matrix, such as brain-derived neurotrophic factor (BDNF) and insulin-like growth factor 1 (IGF1), and acts via many important intracellular pathways, like Rho GTPase signalling (Takano et al., 2015).

Once the axon is specified, a specialised structure at the tip called the growth cone, leads the way to navigate the extending axon over long distances to the right direction for correct synaptic wiring. Growth cone guidance is classically believed to be regulated via chemoaffinity-based mechanisms by four ligand/receptor systems: Slits, netrins, semaphorins and ephrins can either be attracting or repelling guidance cues depending on the type of receptor that is expressed on the growth cone's surface (Huber et al., 2003). Guidance receptor signalling mechanisms then act locally to modulate actin cytoskeleton dynamics to steer the growth cone, cause growth cone collapse or affect the rate of axonal growth (O'Donnell et al., 2009). The subsequent synaptic targeting with precise laminar, cellular and subcellular specificity seems to be dependent on different cell adhesion molecules, such as netrin G ligands and receptors (Williams et al., 2010). It is important to mention that most neurons do not simply connect one-to-one. Instead, axon branching can result in the formation of collaterals at distinct segments of the main axon or a highly branched synaptic termination zone. Therefore multiple axon terminals, or synaptic boutons, can form synapses onto the soma or dendrites of other neurons (Kalil and Dent, 2014).

For a neuron to form correct and functional dendritic arbours it is necessary to achieve the right shape, size and place of the complex branching pattern. As a developmental strategy to create parallel channels of information flow through, many types of neurons grow their dendrites in specific directions to meet the axon terminals of their presynaptic partners (Wong and Ghosh, 2002). This process if often accompanied by compartmentalisation of dendritic arbours. Pyramidal cells for instance, are made of apical and basal dendritic branches that are further divided into distal and proximal domains corresponding to the layered anatomy of the cortex and hippocampus (Spruston, 2008). The size, or occupied area of the dendritic tree, determines the number of synapses a neuron can form, while the arbour's branching pattern controls the density with which a neuron samples this field. Features such as dendrite diameter, distance from the soma, and the number of branch points that must be crossed to reach the soma, also influence the contribution of any given synapse to the firing of the neuron (Lefebvre et al., 2015; London and Hausser, 2005). The self-awareness of dendritic patterning is especially obvious in fly sensory neurons, which achieve precise tiling of dendritic arbours by homotypic repulsion and self-avoidance, meaning that dendrites are unlikely to overlap with other dendrites of its own or a neighbours' (Grueber and Sagasti, 2010). Dendrite morphogenesis is therefore a highly dynamic process with transient branches constantly forming and retracting. Whether a branch survives to become part of the mature dendritic tree depends on multiple factors, including the formation and activity of synapses (Cline and Haas, 2008).

Synapses are considered inhibitory or excitatory based on their likelihood to generate an action potential in the postsynaptic cell. In the CNS, this is generally decided by which neurotransmitter is released presynaptically and its effect on the postsynaptic membrane potential. Interneurons induce inhibitory postsynaptic potentials via the release of γ-

aminobutyric acid (GABA), while pyramidal neurons depolarise the cell membrane with an excitatory postsynaptic potential through glutamate release. The majority of excitatory synapses are formed on mature dendritic spines, small, mushroom-shaped protrusions that contain a postsynaptic density (PSD) (Yuste and Bonhoeffer, 2004). The PSD is a highly specialised, protein-dense structure consisting of all necessary scaffolding and signalling molecules to receive neurotransmitters released from the presynaptic terminal, and transduce them into electrical and biochemical changes in the postsynaptic neuron. For example, it plays an important role in organising glutamate receptors such as α-amino-3-hydroxy-5-methylisoxazole-4-propionic acid (AMPA) and N-methyl-D-aspartate (NMDA) receptors, to localise at the postsynaptic membrane (Sheng and Kim, 2011). Neuronal activity via these glutamatergic receptors is extremely important for synaptic plasticity, the ability of synapses to strengthen and weaken over time and one of the foundations of learning and memory.

The majority of dendritic arborisation and synaptogenesis starts at late embryonic stages and continues after birth in both humans and rodents. Rodent cortical layer 5 pyramidal cells, often used as *in vivo* models for neuronal morphology, show fast growth of dendrites in the basal compartment and the apical tuft between postnatal day (P) 7 and 14. In the following week dendritic growth slows down, but becomes more branched and sees a sharp increase in dendritic spine density. From P21 until young adulthood, the neuron matures by stabilising its dendritic tree and synapses (Ramaswamy and Markram, 2015). Rodent primary hippocampal cultures have long been established as a model system to study neuronal development *in vitro* (Banker and Goslin, 1988). *In vitro* neuronal development starts as round spheres, as they retract their processes upon isolation. Neurons then form several minor neurites of which one grows out rapidly and becomes the axon within 1-3 days. The remaining neurites develop into primary dendrites between days *in vitro* (DIV) 4 and 6, and synaptogenesis slowly begins. At DIV7-11, the dendritic branches grow rapidly and are very dynamic. DIV12-15 marks the final maturation of dendritic outgrowth and branching, and is paired with an increase in spine density and maturation (Baj et al., 2014).

1.1.2   Neuronal cytoskeleton

During development, neurons go through striking changes in morphology, implying strict regulation of cytoskeletal structuring. The two central components of the neuronal cytoskeleton establishing these morphological transitions are microtubule arrays and actin microfilaments. Microtubules are hollow tubes formed by linear protofilaments made of α- and β-tubulin heterodimers, intrinsically polarised by a minus- and plus-end. Neurons have a very dense microtubule network often organised in bundles that nucleate at the centrosome at early developmental stages, but become non-centrosomal during differentiation (Stiess et al., 2010). Because neuronal microtubules are free at both ends, their relative orientation can vary.

Interestingly, axons still display a uniformly plus-end-out microtubule orientation, while dendrites contain microtubules of mixed polarity (Baas and Lin, 2011). The actin cytoskeleton is a more specialized organisation of dynamic filaments in specific subcellular compartments. Actin filaments (F-Actin) are polymers made from globular actin and very dynamic due to the weak interaction between monomers. The most actin-enriched compartments of neurons are growth cones and dendritic spines.

The mechanisms behind the initial formation of neurites in newborn neurons remain incomplete, but have been shown to be dependent on pushing and pulling forces mediated by both microtubules and actin filaments. Although a model has been proposed where space for a protrusion and microtubule bundling is organised by F-actin severing (Flynn et al., 2012). The subsequent specification of the axon is determined by local stabilisation of microtubules, which has been shown nicely by using photoactivatable taxol, a known microtubule-stabilising drug (Witte et al., 2008). More recent work has provided evidence for the more specific roles of calmodulin-regulated spectrin-associated protein family member 2 (CAMSAP2) and tripartite motif-containing 46 (TRIM46) in creating a local pool of minus-end stabilized, non-centrosomal microtubules to promote plus-end out microtubule growth in the axon initial segment, and establish neuronal polarity (van Beuningen et al., 2015; Yau et al., 2014). Interactions between microtubules and actin filaments are important for further steps of neuritogenesis involving growth cone advance and steering. It is believed that highly dynamic F-actin is stabilised in filopodia on the side of the guidance cue and captures microtubules, as an essential step to turn the growth cone and extend it in the right direction (Geraldo and Gordon-Weeks, 2009). In addition to growth by microtubule assembly, evidence is emerging for translocation of whole microtubule bundles through pulling or pushing forces generated by molecular motors (Suter and Miller, 2011). New axonal branches are formed and protracted in a similar way, but can be generated at the lattice of existing microtubules via a protein complex named augmin (Kalil and Dent, 2014). Knowledge about the exact role of the neuronal cytoskeleton in dendritic development is surprisingly limited, but seems to be dependent on microtubule-associated proteins (Conde and Caceres, 2009).

The neuronal cytoskeleton is not only involved in the macro-morphological changes of neurodevelopment, but actin filaments also form the main structure of dendritic spines. It is widely considered that spine formation, maintenance and plasticity of differentiated neurons are regulated by actin dynamics. Long-term potentiation (LTP) of synapses is known to promote F-actin polymerisation in spines, resulting in an increase in actin filament stability and a consequent enlargement of spine heads (Gordon-Weeks and Fournier, 2014). However, dynamic microtubules also curve out of dendrites and invade spines. Although this only happens for an order of minutes in 1-2% of dendritic spines at the time, microtubule spine entry is shown to contribute to their structural changes. Importantly, frequency and dwell time of spine invasion is prolonged by synaptic activity and BDNF stimulation (Hu et al., 2008; Jaworski et al., 2009). NMDA receptor-dependent long-term depression (LTD) on the other hand, supresses

microtubule growth and reduces dynamic microtubule spine entry (Kapitein et al., 2011). Besides F-actin, these findings indicate a long debated role for microtubules in synapse formation and maintenance.

As well as playing a major role in the morphological transitions of neurons, microtubules also guide active transport of signalling molecules, vesicles and organelles throughout the cell. Moreover, it is believed that microtubule spine entry could facilitate delivery of synaptic cargo to the postsynaptic membrane, where it is further distributed by the actin-based transport machinery (Hoogenraad and Bradke, 2009). Three superfamilies of motor proteins are known to transport cargo along the cytoskeleton: Kinesins move towards the plus-end, and dyneins towards the minus-end of microtubules, while myosins traffic specifically along actin filaments (Vale, 2003). A wide variety of motor proteins share highly conserved motor domains within each superfamily, but contain very diverse tail regions in order to specifically associate with different types of cargo. Together with several other regulatory mechanisms such as post-translational modifications and adaptor protein-binding, this allows for correct cargo delivery in neurons (Hirokawa et al., 2010). The difference in orientation of microtubules between axons and dendrites results in further compartmentalisation of transport targeting. Kinesins are also known as direct regulators of microtubule stability and dynamics in morphogenesis (Niwa, 2015). Examples of neuronal activity regulating the balance between motility and cytoskeletal remodelling of kinesins are starting to emerge and suggest more additional mechanisms of compartmentalising the neuronal cytoskeleton (Ghiretti et al., 2016).

1.1.3   Microtubule dynamic instability

The dynamic nature of microtubules plays a key role in their ability to control morphological changes and supply cargo to demanding destinations. The abrupt switching between periods of growth and shrinkage is known as dynamic instability and allows the microtubule cytoskeleton to explore the interior of the cell (Howard and Hyman, 2009). This behaviour is driven by hydrolysis of guanosine triphosphate (GTP) upon binding to the αβ-tubulin dimer in the microtubule lattice, which is the same mechanism behind the generation of microtubule pushing and pulling forces (Inoue and Salmon, 1995). Although microtubules can grow and shrink at both ends, dynamics of these two processes are very different. The minus-end exposing α-tubulin is generally very stable due to its anchoring to nucleation sites, or its capping by members of the CAMSAP family, as is the case for non-centrosomal microtubules (Akhmanova and Hoogenraad, 2015). The plus-end terminated by β-tubulin, is much more dynamic and grows faster, but also undergoes catastrophe more frequently. Stable growth of the microtubule plus-end is therefore believed to be dependent on the presence of a cap of GTP-tubulin, as GDP tends to destabilise the lattice. Microtubule dynamic instability is therefore highly dependent on the regulation of plus-end GTP-caps (Akhmanova and Steinmetz, 2008).

The combined actions of microtubule-associated proteins (MAPs) are generally believed to provide the mechanisms for the spatiotemporal control of microtubule architecture, and can be categorised in three groups: plus-end tracking proteins (+TIPs), structural MAPs and the previously described motor proteins.

+TIPs accumulate at the end of growing microtubules and tightly regulate microtubule dynamic instability and growth directionality. Multiple families of structurally unrelated +TIPs have been identified and new members are still being discovered on a regular basis. At the core of the microtubule plus-end complex are the end-binding proteins (EB proteins), whose N-terminal calponin-homology (CH) domain recognises a nucleotide-dependent structural cap at growing microtubule plus-ends (Maurer et al., 2012). The C-terminal domain of EB proteins mediates dimerization and acts as an important scaffold for other +TIPs, although several other proteins bind microtubule plus-ends independent of EB proteins (Akhmanova and Steinmetz, 2008). EB proteins have been suggested to mainly regulate microtubule dynamics via other +TIPs rather than working autonomously, as their effect on microtubule instability *in vitro* contradicts that in cells (Komarova et al., 2009). EB1 and EB3 have both been shown to have a positive effect on neurite outgrowth of neuronal progenitor cells (Arens et al., 2013). Interestingly, their role in mediating microtubule-actin interactions seems to be important for their function as well. Upregulated EB1 during neurodevelopment has been linked to axon growth via its interaction with spectraplakins (Alves-Silva et al., 2012), while EB3 targeting of the F-actin-binding protein drebrin is necessary for the formation of growth cones and neurite extension (Geraldo et al., 2008). Drebrin has also been shown to mediate the interaction between actin filaments and microtubules in dendritic spines, and is necessary for activity-dependent spine invasion by growing microtubule plus-ends (Merriam et al., 2013). Fluorescently tagged EB proteins are now widely used to track growing microtubules, and provide an efficient tool to study microtubule dynamics in neuronal cells *in vitro* and even *in vivo* (Kleele et al., 2014; Stepanova et al., 2003).

Structural MAPs are non-enzymatic proteins that bind along the lattice of microtubules and enhance the assembly and stability of tubulin polymers. The structural MAPs that are predominantly expressed in neurons, MAP1A/B, MAP2 and Tau are all capable of bundling microtubules into parallel arrays (Lewis and Cowan, 1990), but can be divided into two pairs. MAP1A and MAP1B are proteolytically cleaved into a heavy and light chain, which form dimers, but can also bind microtubules independently. The two proteins have specific regional and temporal expression patterns in neurons. MAP1B is highly expressed in axons during early neurodevelopment, while MAP1A preferentially localises to dendrites in adult neurons (Halpain and Dehmelt, 2006). MAP2 and Tau are expressed both during development and adulthood, but after neuritogenesis they segregate into dendrites and axons respectively (Dehmelt and Halpain, 2005). Microtubule stability provided by these structural MAPs is crucial for axon formation and dendritic differentiation and maintenance (Conde and Caceres, 2009). Multiple structural MAPs have also been identified as actin-interacting proteins besides their highly preferred binding of

microtubules, suggesting possible functions as cross-linkers between the microtubule and actin cytoskeleton (Mohan and John, 2015). In addition, MAP1B and MAP2 have recently been shown to control the availability of EB proteins in the cytosol of neurons, contributing to the regulation of microtubule dynamic instability (Sayas and Avila, 2014).

1.2 Cyclin-dependent kinase-like 5

Disruptions in the tightly regulated development of the central nervous system can cause a variety of neurodevelopmental disorders. These can manifest as developmental delays including impaired motor function, learning difficulties, language or non-verbal communication deficits, or present neuropsychiatric symptoms later in life. Due to the precise orchestration of brain development, a large range of perturbations can cause neurodevelopmental disorders. Malnutrition, social deprivation and physical trauma are important environmental risk factors that can lead to neurological damage early in life. Immune dysfunction, systemic infections and metabolic diseases during pregnancy in either the mother or child, may also negatively affect neuronal development. Most common neurodevelopmental disorders such as autism and schizophrenia are considered multi-factorial and considered to be influenced by both genetics and environment. However, many other neurodevelopmental disorders, such as trisomy 21 in Down syndrome, are genetically determined. In fact, pathogenic mutations in single genes often result in less common neurodevelopmental disorders. For example, Fragile X syndrome is caused by mutations in *FMR1*, and *MECP2* mutations lead to Rett syndrome. CDKL5 deficiency disorder also belongs to the category of rare neurodevelopmental disorders caused by single gene mutations.

1.2.1 CDKL5 deficiency disorder

CDKL5 was identified by transcriptional mapping of the Xp22 region to isolate genes involved in several genetic disorders (Montini et al., 1998). Due to its sequence homology to serine/threonine kinases it was originally termed serine/threonine kinase 9 (STK9). Disruptions in *CDKL5* were initially found in two female patients affected by X-linked infantile spasms and intellectual disability (Kalscheuer et al., 2003). Shortly after, several studies described *CDKL5* mutations in patients mimicking Rett syndrome phenotypes independent of pathogenic mutations in *MECP2*, establishing *CDKL5* as a new locus associated with epilepsy and X-linked intellectual disability (Scala et al., 2005; Tao et al., 2004; Weaving et al., 2004). Increased awareness and more common screening has resulted in more than 200 patients with likely pathogenic *CDKL5* mutations being described to date (Krishnaraj et al., 2017). As it is difficult to collect information from doctors and patient organisations in multiple countries, an official prevalence estimation is not yet available for CDKL5 deficiency disorder.

Because of the similarities between the symptomatic manifestations of *MECP2* and *CDKL5* mutations, the latter was initially considered an atypical variant of Rett syndrome. The main difference is the onset of signs and symptoms: Patients with classical Rett syndrome typically display normal development up to 6-18 months of age, followed by a strong regression (Chahrour and Zoghbi, 2007). This is lacking in patients with *CDKL5* mutations, where

symptoms usually start within the first six months and do not regress further (Grosso et al., 2007). It was not until recently that enough patients with *CDKL5* mutations had been described to understand that other, less pronounced symptoms also differ from classical Rett syndrome. CDKL5 deficiency disorder is therefore currently considered an independent clinical entity characterised by early onset seizures, severely impaired gross motor, language and hand function skills, and subtle physical features (Fehr et al., 2013). The syndromic character of the disorder can also manifest itself through autistic-like tendencies, hypersensitivity to touch, visual impairment, interruptive sleep and other symptoms.

CDKL5 deficiency disorder is caused by dominant, *de novo* mutations in the X-linked *CDKL5* gene. Still, families with multiple affected children have been described. In these cases, maternal germline mosaicism is suggested, as the mothers have tested negative for *CDKL5* mutations and are not affected themselves (Hagebeuk et al., 2015; Mirzaa et al., 2013). CDKL5 deficiency disorder mainly affects girls, with approximately 15% of the patients being male. In Rett syndrome, the difference in prevalence between genders is a result of embryonic lethality in hemizygous boys. This is not believed to be the case for CDKL5 deficiency disorder. Instead, the low number of boys affected by *de novo* CDKL5 mutations could be explained by the difference in the number of cell divisions between sperm cells and oocytes. In contrast to heterozygous girls, hemizygous boys only carry X-linked mutations that originated in the oocyte. Oocytes are known to go through significantly fewer cell divisions than sperm cells, resulting in a 6-fold bias of *de novo* mutations carried in sperm cells. (Arnheim and Calabrese, 2009). This accurately explains the difference in prevalence of CDKL5 deficiency disorder between genders.

A variety of translocations, deletions, insertions, nonsense and missense mutations throughout the *CDKL5* gene can be pathogenic. Many of these mutations will lead to complete loss of the protein due to nonsense-mediated decay. However, the strong enrichment of missense mutations in exons encoding the N-terminal kinase domain suggests that dysfunctional CDKL5 kinase activity is the main contributor to CDKL5 deficiency disorder (Hector et al., 2016). Genotype-phenotype correlation has also shown that patients with C-terminal truncations are more mildly affected than other cases (Fehr et al., 2016). Differences in mosaic patterning of CDKL5 due to random X-chromosome inactivation in heterozygous females is also believed to play an important role in the manifestation of the disorder, as the small number of recurrent mutations that occur, present a wide variety in symptom severity (Bahi-Buisson et al., 2012). In concordance with this, boys with hemizygous *CDKL5* mutations are in general more severely affected than girls (Fehr et al., 2016).

Although there is currently no targeted treatment or gene therapy available for CDKL5 deficiency disorder, the symptoms can be alleviated in many cases with a robust regimen of therapies, according to the Boston Children's Hospital. In challenging attempts to have better control of the frequent seizures, CDKL5 patients are also often on a combination of anticonvulsants together with a ketogenic diet. This general way of trying to maintain epilepsies is usually a heavy burden with minimal results, but there might be a shimmer of hope on the

horizon for families affected by CDKL5 deficiency disorder. Marinus Pharmaceuticals have recently announced successful phase 2 clinical trials with oral ganaxolone, an allosteric modulator of the $GABA_A$ receptor.

1.2.2   CDKL5 expression and localisation

The CDKL family is a member of the CMGC group of serine/threonine protein kinases, which also include cyclin-dependent kinases. Despite the confusing name, CDKL kinases are not known to interact with cyclins, and not believed to be functionally connected to CDKs. Within the family, CDKL5 is the most distinct member in terms of sequence and evolution. CDKL1 and 2 are similar, found in all eukaryotes other than fungi, and probably derive from an early duplication. CDKL3 and 4 are absent in fish and believed to have more recently originated from CDKL2 and 1 respectively. CDKL5 orthologues have only been found in vertebrates (Kilstrup-Nielsen et al., 2012). All CDKL kinases consist of an N-terminal kinase domain followed by a divergent sequence of amino acids absent of any other known domains. However, the ~700 aa C-terminal tail of CDKL5 is significantly longer than that of any other members of the family. Although not much is known about the function of CDKL1-4, there is some evidence for CDKL2/3 to be expressed in the brain (Sassa et al., 2004) and to be involved in intellectual disability and neuronal morphogenesis (Dubos et al., 2008; Liu et al., 2010).

CDKL5 mRNA is encoded by a gene consisting of 22 exons that was originally thought to give rise to two distinct isoforms named after their molecular weight (Williamson et al., 2012). $CDKL5_{115}$ is the full length protein, but is exclusively expressed in the testis and foetal brains. $CDKL5_{107}$ splicing excludes exons 20-22, and is characterised by an altered C-terminal region, as well as completely different 5' and 3' UTRs. This isoform is strongly expressed in the brain and to a lesser extent in many other tissues (Hector et al., 2016). A similar expression pattern was seen for CDKL5 on a protein level (Chen et al., 2010; Lin et al., 2005). Three additional variants of $CDKL5_{107}$ with small changes in exon 11 and 17 were described later, which resulted in all human isoforms to be renamed: hCDKL5_1 ($CDKL5_{107}$), hCDKL5_2-4 ($CDKL5_{107}$ variants) and hCDKL5_5 ($CDKL5_{115}$) (Hector et al., 2016). Only hCDKL5_1 and _2 have exact orthologues that are expressed in the mouse and rat brain (Hector et al., 2017). In all organisms, CDKL5 transcript isoform 2 expression levels appear to be approximately 10% of that of isoform 1, suggesting CDKL5_1 to be the main transcript in the brain.

The temporal expression pattern of CDKL5 transcripts in mouse brain shows a strong postnatal upregulation, which is maintained throughout adult stages. A similar pattern is seen in humans, where CDKL5 transcript levels are higher in adult compared to foetal brain (Hector et al., 2016). In mice, CDKL5 protein expression has been shown to follow a nearly identical temporal pattern, as it is barely detectable at late embryonic stages and reaches peak levels after three weeks of age (Rusconi et al., 2008). Several *in situ* hybridizations indicate that

CDKL5 mRNA is expressed throughout the brain, but is especially enriched in the forebrain, including the neocortex and hippocampus (Hector et al., 2017; Lein et al., 2007; Mari et al., 2005). In agreement, CDKL5 protein expression is highly enriched in the cortex, hippocampus, striatum and olfactory bulb (Wang et al., 2012). On a cellular level, immunohistochemistry seems to reveal that CDKL5 is primarily expressed in a diffuse pattern in neurons (Chen et al., 2010; Rusconi et al., 2008), although a distinct CDKL5 isoform has been found to be expressed in glia cells (Chen et al., 2010). More in-depth characterisation of cell-type specific CDKL5 expression has been described using commercial CDKL5 antibodies with immunocytochemistry. However, after the generation of the first Cdkl5 mouse model in 2012, validation of these antibodies demonstrated that none of them are CDKL5-specific when used for immunofluorescence. These experiments should therefore be disregarded.

The lack of a reliable CDKL5 antibody for immunofluorescence has also made it challenging to determine the subcellular localisation of the protein, although immunogold electron microscopy recently hinted at accumulation of CDKL5 in the postsynaptic density (Okuda et al., 2017). Western blotting of synaptosomal and nuclear preparations have identified CDKL5 in both fractions, indicating that CDKL5 localisation is not restricted to a specific subcellular compartment (Ricciardi et al., 2012; Rusconi et al., 2008; Zhu et al., 2013). Overexpression of CDKL5 in non-neuronal cell lines has shown that shuttling between cytosol and nucleus is both dependent on its kinase activity and C-terminal tail, which contains multiple putative nuclear localisation and export sites (Bertani et al., 2006; Rusconi et al., 2008). More importantly, the subcellular distribution of endogenous CDKL5 in the mouse brain varies between regions and is dependent on age, as the nuclear fraction of CDKL5 is induced at early postnatal stages (Rusconi et al., 2008). Interestingly, CDKL5's subcellular distribution seems to be mediated via its phosphorylation at serine 308 by dual-specificity tyrosine-(Y)-phosphorylation regulated kinase 1A (DYRK1A), a protein kinase hypothesized to contribute to abnormal brain development in Down syndrome (Oi et al., 2017).

Many forms of autism spectrum disorder have been associated with crucial components of activity-dependent signalling networks that regulate synaptic maturation and function (Ebert and Greenberg, 2013). Multiple pieces of evidence start to emerge that CDKL5 is also regulated by activity-dependent mechanisms. Treatments with multiple pharmacological reagents such as cocaine and serotonin led to decreased Cdkl5 expression in the striatum of rats (Carouge et al., 2010). This effect is believed to be downstream of methyl-CpG binding protein 2 (MeCP2) methylation, and establishes a possible link between Rett syndrome and CDKL5 deficiency disorder. However, this contradicts the unchanged CDKL5 mRNA levels found in Rett syndrome patients and Mecp2 KO mice (Mari et al., 2005; Weaving et al., 2004). Neuronal depolarisation by potassium chloride (KCl) on the other hand, resulted in rapid increases in CDKL5 levels in hippocampal cultures and cortical slices, mainly through local protein translation (La Montanara et al., 2015). However, long term NMDA receptor stimulation led to dephosphorylation of CDKL5 and proteasome-dependent degradation. Interestingly, this seemed to be relying on the

extrasynaptic pool of NDMA receptors, as synaptically evoked bursts of action potentials by blocking GABA$_A$ receptors with bicuculline, does not have the same effect on CDKL5 degradation as glutamate treatment (Rusconi et al., 2011).

1.2.3   Molecular functions of CDKL5

The CDKL5 protein consists of an N-terminal kinase domain and an undefined C-terminal tail (Figure 1A). Like many other kinases, CDKL5 contains a TXY motif in its kinase domain, whose phosphorylation is necessary for maximum kinase activity (Pearson et al., 2001). CDKL5 is capable of autophosphorylation on this motif, but it is unknown if this concerns phosphorylation of the threonine or tyrosine residue (Bertani et al., 2006; Lin et al., 2005). Pathogenic missense mutations in the CDKL5 kinase domain have been shown to reduce its catalytic activity, providing more proof that loss of CDKL5 kinase activity specifically causes the neurodevelopmental disorder (Bertani et al., 2006; Sekiguchi et al., 2013). The C-terminal tail is important for regulating CDKL5 activity, localisation and stability (Bertani et al., 2006; Lin et al., 2005). The effect of CDKL5's C-terminus on the stability of the protein is evident by the failure of many labs to purify full-length CDKL5. Truncated CDKL5$^{1-352}$ on the other hand expresses better and is considered more catalytically active (Lin et al., 2005). So far, it has only been possible to purify truncated forms of CDKL5, which has resulted in the availability of the crystal structure of the kinase domain (Canning, 2013).

Several attempts have been made to characterise the molecular functions of CDKL5 through the identification of interactors and substrates of the kinase. The seemingly partial nuclear localisation of CDKL5 and the close similarities between Rett syndrome and CDKL5 deficiency disorder, suggested that CDKL5 and MeCP2 could possibly be associated. Although a potential interaction between the two proteins was indeed confirmed by pull-down assays in two separate studies (Lin et al., 2005; Mari et al., 2005), very weak *in vitro* MeCP2 phosphorylation by CDKL5 has not always been reproducible and is heavily disputed (Lin et al., 2005; Mari et al., 2005; Sekiguchi et al., 2013). CDKL5 has been found to associate with another nuclear protein via a screen for protein kinase-interactors of DNA methyltransferase 1 (DNMT1) (Kameshita et al., 2008). Although DNMT1 has been reported to be phosphorylated by CDKL5 in the presence of deoxyribonucleic acid (DNA) *in vitro*, this phosphorylation is rather weak, might be indirect and has not been validated *in vivo*, as is the case for MeCP2. The exact status of these nuclear molecular pathways therefore remain to be further characterised.

A potential indirect effect of CDKL5 on nuclear transcription could be via histone deacetylase 4 (HDAC4), a protein that shuttles between the nucleus and cytoplasm in a phosphorylation-dependent manner. Phosphorylation of HDAC4 by CDKL5 was identified in an unbiased phosphospecific antibody microarray of SH-SY5Y neuroblastoma cell lysates (Trazzi et al., 2016). This ELISA-based approach is highly specific for small changes in phosphorylation

levels, but only screens for the small number of phosphospecific antibodies available. Decreased HDAC4 phosphorylation and a resulting increase in activity and nuclear localisation were observed in neuronal progenitor cells of CDKL5 KO mice, which were reverted by re-expression of CDKL5 or inhibition of HDAC4 activity through an inhibitor (Trazzi et al., 2016). Although these findings suggest robust changes in histone deacetylation and neuronal gene expression in CDKL5 deficiency disorder, gene expression profiling of multiple patient cell lines show very little overlap and no particular signature (Livide et al., 2015; Nectoux et al., 2011). This makes it difficult to ascribe CDKL5 loss-of-function phenotypes to specific differentially expressed genes.

Dendritic abnormalities are the most consistent anatomical correlates of intellectual disabilities present in many neurodevelopmental disorders (Kaufmann and Moser, 2000). The developmental expression pattern of CDKL5 together with the manifestation of CDKL5 deficiency disorder, indicates a potential role for CDKL5 in neuronal morphogenesis. Early work by Chen et al. showed that neurite outgrowth and arborisation is disrupted when CDKL5 is downregulated by RNA interference in dissociated neuronal cultures, and via *in utero* electroporation of embryonic rat brains (Chen et al., 2010). In contrast to its proposed function in the nucleus, CDKL5 was found to control dendrite development through a cytoplasmic interaction with Rac1, a small GTPase that regulates actin remodelling and neuronal morphogenesis. CDKL5 was specifically shown to mediate neurite formation upstream of Rho-GTPase signalling via the BDNF-dependent activation of Rac1 in the actin-rich growth cone (Chen et al., 2010).

Yeast two-hybrid screening identified another interactor of CDKL5 in the growth cone as shootin1, a key regulator of polarisation and axon formation in the early steps of neuronal differentiation (Nawaz et al., 2016). Here, it was also shown that short hairpin RNA (shRNA)-mediated knockdown of CDKL5 in mouse primary hippocampal neurons indeed disrupts neuronal polarisation. Shootin1 phosphorylation is known to be required for the formation of traction forces at axonal growth cones, and is thus necessary for axon outgrowth (Toriyama et al., 2013). Phosphorylated shootin1 is reduced in the absence of CDKL5, but it is unknown if this is a direct effect or possibly exerted via Rac1-dependent P21-activated kinase 1 (PAK1) activation (Nawaz et al., 2016). Another interaction between CDKL5 and a known regulator of cell migration and polarity, IQ motif-containing GTPase-activating protein 1 (IQGAP1) has been shown. This interaction is required for IQGAP1 to form a functional complex with its regulators, cytoplasmic-linker protein 170 (CLIP170) and Rac1 (Barbiero et al., 2017). Here they show that, in non-neuronal cells, disruption of this complex eventually leads to disassociation of +TIP CLIP170 from microtubules and impaired microtubule dynamics.

The role of CDKL5 in neurite development was challenged in a separate study that employed the same knockdown approaches as Chen et al., but did not find altered dendritic outgrowth, and instead observed morphological defects in spines (Ricciardi et al., 2012). Moreover, they described that loss of CDKL5 reduced both the amplitude and frequency of

mEPSCs as a result of decreases in excitatory synapse number. These findings were supported by another study that provided evidence for the synaptic recruitment of CDKL5 via its direct binding to palmitoylated PSD95 (Zhu et al., 2013). A potential postsynaptic mechanism regulating spine development has been suggested through the interaction of CDKL5 and netrin G1-ligand (NGL1), a protein related to the netrin family of axon guidance molecules (Ricciardi et al., 2012). Mutations in the netrin G1 gene are also found in patients with atypical Rett-syndrome and early-onset seizures (Borg et al., 2005). Phosphorylation of NGL1, be it directly or indirectly by CDKL5, promotes the NGL1-PSD95 interaction that stabilises dendritic spines and is proposed to be disrupted upon CDKL5 loss-of-function (Ricciardi et al., 2012). Interestingly, the presynaptic protein amphyphysin 1 (AMPH1) was identified as a substrate of CDKL5 in an unbiased screen using radioactive ATP in fractionated mouse brain lysates, indicating a potential dual role for CDKL5 in both the pre- and postsynapse (Sekiguchi et al., 2013). Although the authors only show AMPH1 phosphorylation *in vitro*, it is suggested to regulate its affinity for endophilin, a protein involved in synaptic vesicle endocytosis. *In vitro* phosphorylation of AMPH1 by CDKL5 was later found to be critically dependent on the arginine at -3 and proline at -2 of the phosphorylated serine (Katayama et al., 2015).

The identified interactors and potential substrates of CDKL5, are located throughout the cell and involved in a wide range of molecular pathways, making it difficult to pinpoint CDKL5 to a specific function. The conflicting results regarding neuronal development and morphology upon knockdown of CDKL5 by RNA interference, added to the challenge of focussing on specific CDKL5-dependent phenotypes. The known risk of introducing off-target effects by shRNA-mediated knockdown is especially notorious in experiments related to dendritic morphogenesis and spine formation (Alvarez et al., 2006; Baek et al., 2014). The extent to which the previously described molecular and cellular mechanisms are relevant and reproducible in Cdkl5 KO animal models is therefore crucial to investigate further. Animal models that mimic CDKL5 deficiency disorder are not only important for studying the function of the protein. Robust molecular, cellular and behavioural biomarkers are also absolutely necessary to determine the effects of possible treatments in clinical trials. This includes early phase studies of new potential drugs, but also protein replacement or gene therapy.

1.2.4 CDKL5 animal models

In recent years, two separate Cdkl5 knockout (KO) mouse lines have been generated in order to model CDKL5 deficiency disorder. Here we have called them the American (Wang et al., 2012) and European (Amendola et al., 2014) Cdkl5 KO mouse for simplicity. In both these mice, deletion of an early exon resulted in truncation of the protein in the N-terminal kinase domain and complete loss of CDKL5, likely due to nonsense-mediated decay (Amendola et al., 2014; Wang et al., 2012). Both Cdkl5 KO mice show multiple behavioural phenotypes

associated with motor impairment, intellectual disability and autistic features typical for CDKL5 deficiency disorder, supporting the face validity of constitutive Cdkl5 KO in mice. The American model demonstrated impaired motor control on the rotarod and hind limb clasping, problems with learning and memory in a fear conditioning assay, and autistic-like deficits in sociability and home-cage nesting behaviour (Wang et al., 2012). This mouse also displayed altered auditory-evoked event-related potentials (ERPs), suggesting impairments in cognitive processing. Several consistent phenotypes were observed in the European mouse, including hind limb clasping, impaired working memory and contextual learning, and decreased visual-evoked ERPs (Amendola et al., 2014; Fuchs et al., 2014).

Surprisingly, neither of these mouse models develop spontaneous seizures in C57Bl/6 or mixed genetic backgrounds. No CDKL5-dependent differences were observed in kainate-induced seizure frequency either, except for abnormal electroencephalography (EEG) readings in the European model (Amendola et al., 2014). Interestingly, the recent publication of a third Cdkl5 KO mouse in Japan displayed hyperexcitability to NMDA specifically, which provoked more severe seizures than in WT mice (Okuda et al., 2017). These findings suggest that, despite the absence of spontaneous seizures in Cdkl5 KO mice, there is increased seizure susceptibility. Other unbiased, quantitative biomarkers of high translational value in Cdkl5 KO mice could be visually evoked potentials in adult mice to monitor brain function, and the increase of sleep apneas as a respiratory biomarker (Lo Martire et al., 2017; Mazziotti et al., 2017).

Conditional knockout of Cdkl5 helped identify the cell types in which loss of CDKL5 drives pathological phenotypes. Deletion of floxed Cdkl5 in GABAergic neurons of the forebrain by Dlx5/6-driven Cre recombinase, showed to be specifically associated with the hypolocomotion observed in the European mouse (Amendola et al., 2014). Specific loss of CDKL5 in glutamatergic neurons of the cortex, driven by Emx1-Cre in the European and Nex-Cre in the American model, was shown to replicate the defects in hind limb clasping, head tracking and hippocampal-dependent learning and memory (Amendola et al., 2014; Tang et al., 2017). These results indicate a more pronounced function for CDKL5 in excitatory neurons of the forebrain. However, altered inhibitory transmission has specifically been found in the cerebellum of adult Cdkl5 KO mice (Sivilia et al., 2016).

Glutamatergic neurons can be sparsely labelled and morphologically characterised *in vivo* by expressing a fluorescent Thy1 transgene (Feng et al., 2000). Using this method, distal arborisation of only the apical dendrite was shown to be reduced in cortical and hippocampal layer 5 of constitutive Cdkl5 KO mice (Amendola et al., 2014). These findings were followed by the description of age-dependent instability of spine formation, resulting in significant reductions in dendritic spine density, PSD-95-positive synaptic puncta and frequency of spontaneous miniature excitatory postsynaptic currents (EPSCs) (Della Sala et al., 2015). Surprisingly, conditional knockout of CDKL5 in excitatory neurons do not yield robust reductions in dendritic arborisation of hippocampus CA1, but only mild disruptions in branching are observed. Also in

contrast to constitutive Cdkl5 KO, is a small increase in spine density and volume, and enhanced synaptic activity was observed (Tang et al., 2017). Interestingly, the authors observed both increased excitatory and inhibitory synaptic activity. This is in line with increased glutamatergic presynaptic structures, as well as hyperconnected parvalbumin-expressing interneurons described in the constitutive Cdkl5 KO mouse (Pizzo et al., 2016). Therefore, CDKL5 could also potentially regulate inhibitory synaptic function and may cause a shift in the excitation/inhibition balance.

Kinome profiling of both the European and American Cdkl5 KO mouse models identified altered PI3K/Akt signalling downstream of CDKL5, although it is not clear how directly involved CDKL5 is with these pathways (Amendola et al., 2014; Wang et al., 2012). Interestingly, pathogenic mechanistic target of rapamycin (mTOR) signalling has been linked to many other neurodevelopmental disorders, including Rett syndrome (Crino, 2011). A specific function of CDKL5 in neurogenesis and dendritic growth of neurons in the dentate gyrus, was shown to be dependent on Akt/GSK3b signalling (Fuchs et al., 2014). Inhibition of GSK3b rescues hippocampal development and learning problems in Cdkl5 KO mice (Fuchs et al., 2015). Similarly, exogenous administration of IGF1, a potential activator of the Akt/mTOR pathway, recuperated defective ribosomal protein S6 phosphorylation, spine density, and PSD95 expression (Amendola et al., 2014).

CDKL5 clearly has a key role in regulating neuronal development in the brain, but the limited characterisation of animal models makes it difficult to assign a specific function to the protein. CDKL5 seems to be important for proper dendritic arborisation and synapse formation, but contradicting results between animal models imply these could be secondary and not cell autonomous effects in pyramidal neurons. Differences in age, brain region and cell-type could have significant impact on the results. Neuronal primary cultures of KO mice could simplify the way CDKL5 is studied, and reveal potential new directions without having adverse off-target effects introduced by RNA interference. So far only one study has used this opportunity, and showed reduced dendritic length and synapse number in Cdkl5 KO primary hippocampal neurons (Trazzi et al., 2016). Induced pluripotent stem cell (IPSC)-derived neurons from patients with CDKL5 deficiency disorder are starting to become available as well, and will provide essential information about the translational value of molecular and cellular phenotypes (Amenduni et al., 2011). These human disease models have been invaluable for other neurodevelopmental disorders (Chailangkarn et al., 2016). So far only two patient-derived neuronal lines have been briefly described, which also exhibited aberrant dendritic spines (Ricciardi et al., 2012). In summary, although significant advances have been made in the ten years since discovering CDKL5's involvement in neurodevelopment, a lot more knowledge about this kinase is necessary. Especially focus on the identification of the molecular and cellular mechanisms through which CDKL5 exerts its function is essential in order to uncover potential druggable targets and cure CDKL5 deficiency disorder.
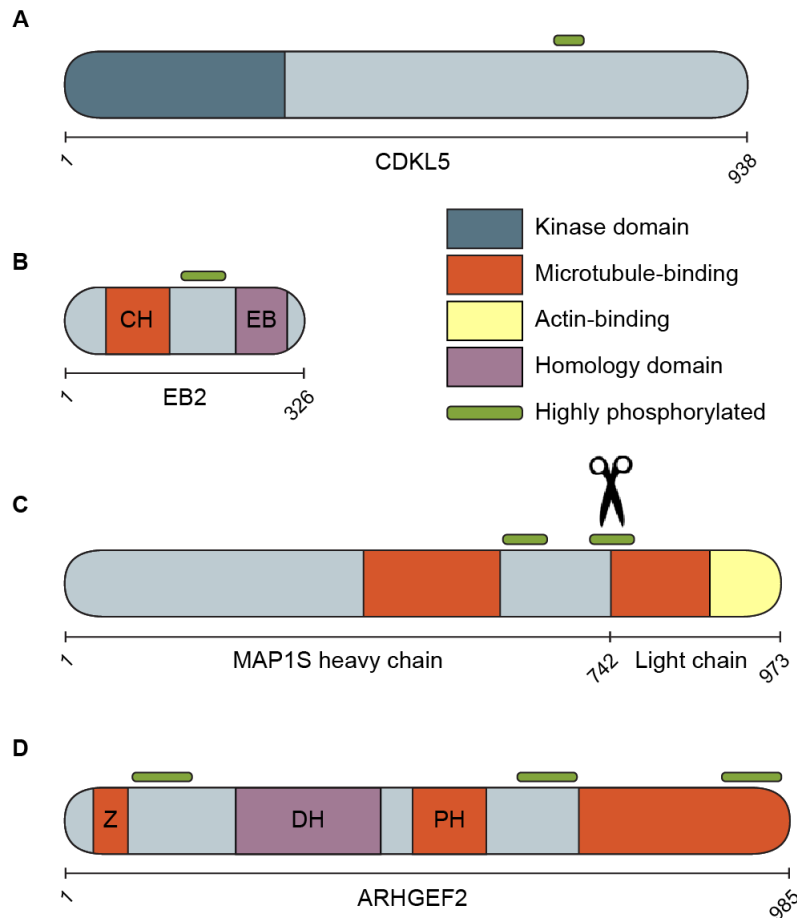
Figure 1: CDKL5, EB2, MAP1S and ARHGEF2 protein schematics.

Schematics of the four proteins that form the basis of this thesis. (A) CDKL5 contains an N-terminal kinase domain and is devoid of other structured regions. The C-terminal tail is believed to be important for regulating CDKL5 localisation and activity. (B) The calponin-homology (CH) domain of EB2 binds microtubules, while the EB homology domain interacts with other +TIPs. (C) MAP1S is proteolytically cleaved into a heavy and light chain, which can bind microtubules independently. The C-terminal end of the light chain is also capable of binding F-actin. (D) ARHGEF2 demonstrates Rho GEF activity via its Dbl-homology (DH) domain. Its activity is inhibited when wrapped around microtubules via its multiple microtubule-binding domains. Z = zinc finger region, PH = pleckstrin-homology domain. All schematics drawn are based on the mouse protein. Regions containing multiple phosphorylation sites that are identified more than five times on PhosphoSitePlus are depicted in green.

1.3   Kinase substrate mapping

To determine the function and downstream pathways of any kinase, the identification of direct phosphorylation targets is regarded as crucial information. For example, the revelation that LRRK2 directly phosphorylates and regulates multiple Rab GTPases *in vivo*, massively boosted the hypothesis that altered vesicular transport is the underlying reason for the high number of signalling pathways suggested to be under the control of this kinase (Berwick and Harvey, 2011; Steger et al., 2016). Direct substrate phosphorylation also acts as an important molecular biomarker for kinase activity, and is a vital read-out for upstream effectors. For instance, multiple small-molecule regulators that behaved as kinase inhibitors *in vitro*, acted as kinase agonists *in vivo*. This was only possible to observe via the phosphorylation of known targets (Dar and Shokat, 2011). However, the unbiased identification of robust, physiological substrates of kinases is a daunting task that requires powerful screening techniques and strong *in vivo* validation (Cohen and Knebel, 2006; Johnson and Hunter, 2005).

1.3.1   High-throughput screening techniques

The most commonly used biochemical method to determine substrate phosphorylation is the *in vitro* kinase assay, where purified proteins are incubated in the presence of ATP to establish an enzymatic reaction. This labour intensive method is still considered the golden standard to validate kinase-substrate interactions when combined with mutagenesis of candidate proteins, but does have the limitation that physiological conditions are not exactly replicated and reduced specificity is often observed. *In vivo* validation is therefore always necessary. Potential substrate candidates of a kinase are often based on genetic screening or protein-protein interactions. However, the transient interaction between kinases and substrates is not believed to efficiently trigger reporter gene transcription in yeast-two-hybrid screens, and is hard to capture with affinity purification (Xue and Tao, 2013). These methods could therefore theoretically identify physiologically relevant proteins directly, but are likely to introduce unwanted bias and false positives.

By applying the idea of *in vitro* kinase assays to surface-based methods such as protein microarrays, unbiased high throughput screening of *in vitro* substrates of a kinase of interest became much more straightforward (Mok et al., 2009; Ptacek et al., 2005). However, incorrect folding and steric hindrance could result in inefficient kinase-substrate interactions. For a long time only yeast proteome microarrays existed, although the human proteome is now available as well (Jeong et al., 2012). With a similar strategy, peptide arrays can be used to identify preferred phosphorylation motifs of a kinase, called the consensus sequence (Hutti et al., 2004; Miller and Turk, 2016). Kinase-substrate binding conforms to a lock and key model, where the semi-linear peptide sequence that surrounds the phosphorylation site fits into the kinase active

site. This consensus sequence can therefore act as a useful handle towards the identification of novel direct substrates.

The recent advances in throughput and sensitivity of mass spectrometry have massively changed the field of characterising protein post-translational modifications, and has become the dominant method of identifying phosphorylation events. A big advantage compared to microarray-based screening is the immediate localisation of the phosphorylated residue. Global phosphoproteomic changes can be mapped by knocking out or pharmacologically inhibiting kinases of interest in order to determine downstream effects (Lai et al., 2015; Steger et al., 2016). Stable isotope labelling of amino acids in cell culture (SILAC) is often the preferred method in order to quantitatively analyse altered phosphorylation between peptides that incorporated 'heavy' or 'light' isotopes (Mann, 2006). A drawback of this approach is not knowing which substrates are directly phosphorylated by the kinase of interest opposed to other kinases further downstream. To avoid this, phosphoproteomic analysis can be combined with *in vitro* kinase assays in a method named KALIP, kinase assay linked with phosphoproteomics (Xue et al., 2016). Here, the pool of phospho-enriched peptides or proteins used for global phosphoproteomics, is also treated with phosphatases and exposed to an *in vitro* kinase assay. This double method is proposed to be both kinase and cell-type specific, and provides an improvement on false positive rates. Another recent study even claims that the sensitivity of mass spectrometry has come so far that it is possible to detect phosphoproteomic changes in the small amount of transient-binding substrates after affinity purification (Amano et al., 2015).

The specific identification of direct substrates of a kinase remains an issue in all the previously described methods. This is mainly due to the shared enzymology between the very conserved family of protein kinases. A chemical genetic method utilising modified ATP-binding pockets and bio-orthogonal ATP analogues, has been shown to overcome this problem (Hertz et al., 2010). Analogue-sensitive (AS)-kinase can be generated by making a single point mutation in the ATP binding pocket at the 'gatekeeper' residue, which enables the AS kinase to utilize bulky ATP analogues (Gregan et al., 2007; Shah et al., 1997). A subset of kinases loses catalytic activity upon the gatekeeper mutation, but this can be restored by second site suppressor mutations previously shown to rescue these so-called intolerant kinases (Zhang et al., 2005). By also modifying bulky ATP analogues to include a thiophosphate to be transferred during protein phosphorylation (ATPγS), AS-kinases can specifically thiophosphorylate their substrates. The thiophosphate-group can subsequently be used as a specific tag to measure AS-kinase activity or identify direct substrates. To achieve the latter, active AS-kinase is incubated with protein lysates from tissues or cell lines of interest, and is allowed to thiophosphorylate substrates using its preferred bulky ATPγS analogue. After trypsin digestion, by covalent capture of thiophosphorylated peptides, only direct substrates of the AS-kinase are purified (Hertz et al., 2010). Specific putative phosphorylation sites can then be identified by tandem mass spectrometry using kinase-dead negative controls to determine false-positive background. This method is widely applicable and has been used to identify novel substrates of

multiple kinases involved in synaptic development and neurological diseases (Baltussen et al., 2017). Similar to other substrate identification methods, putative hits need to be verified by *in vitro* kinase assays and *in vivo* validation experiments using phosphospecific antibodies. Major advantages of this method are the usage of tissue homogenates in which protein interactions are maintained, the use of bulky ATP analogues aiding few false positives, and finally the immediate identification of phosphorylation sites allowing the generation of phosphospecific antibodies to facilitate validation.

We decided to use chemical genetic kinase-substrate mapping to identify substrates of CDKL5. CDKL5 has no other known functional domains, thus direct physiological substrates are currently key to understanding its function. As discussed before, potential CDKL5 substrates have been proposed, but either the direct phosphorylation by CDKL5 has not been established (NGL1), or they have not been validated *in vivo* (MeCP2, DNMT1, AMPH1). The recent discovery of HDAC4 phosphorylation in an unbiased antibody array was validated *in vivo*, and seems to be more promising as a credible CDKL5 substrate (Trazzi et al., 2016). However, the very limited reduction of HDAC4 phosphorylation in Cdkl5 KO mice indicates a minor role for CDKL5 in phosphorylating this site. Nevertheless, direct CDKL5 phosphorylation targets under physiological conditions and the roles they play in neuronal development and CDKL5 deficiency, remain open questions which we hope to address in this thesis.

1.3.2   Novel CDKL5 substrates

In this thesis you will find that we identified three novel direct CDKL5 substrates: EB2, MAP1S and ARHGEF2. These proteins share microtubule-binding properties and are known to act on the cytoskeleton. The implications this could have on neuronal development has already been introduced by describing some of the close relatives of these proteins. The results chapters in this thesis will describe how exactly we discovered these novel substrates of CDKL5, and what function these interactions might have in neuronal development. Without spoiling too much of the results, we would like to finish this introduction by providing a bit more background on the specific CDKL5 substrates identified in this thesis.

Microtubule end-binding protein 2 (EB2) is the least characterised member of the EB protein family that forms the core of the microtubule plus-end tracking complex. Although EB2 is structurally very similar to EB1 and EB3, it contains specific substitutions in the calponin-homology domain, which result in less explicit interactions with the growing microtubule plus-end (Figure 1B). It is therefore less competent at suppressing microtubule catastrophes than the other EB proteins (Komarova et al., 2009). In addition, the affinity of other +TIPs for direct binding to EB1 and EB3 is much higher than for EB2, suggesting critical differences between the EB proteins in the C-terminal domain as well (Komarova et al., 2005). EB2 also does not significantly participate in the formation of heterotypic +TIP complexes (De Groot et al., 2010).

Together, these properties make EB2 generally not suitable as a fluorescent plus-end marker, because it is much more evenly distributed on the microtubule lattice. Interestingly, this seems to be dependent on competition with EB1 (Komarova et al., 2009). Because of these reasons, neuronal functions of EB proteins are almost exclusively ascribed to EB1 and EB3, suggesting a different and still elusive role for EB2 in neurons. However, *MAPRE2*, the gene encoding EB2, might be the genetic cause for a rare congenital disease, involving intellectual disability and dysmorphic features (Isrie et al., 2015), is defined as a susceptibility risk factor for ADHD (Vilor-Tejedor et al., 2016), and is dysregulated in both trisomy 18 and 21 (Volk et al., 2017). These genetic links indicate a more prominent function of EB2 in neurodevelopment than currently known.

End-binding proteins are ubiquitously expressed, and in non-neuronal cell types, a potentially specific role for EB2 in regulating cell adhesion is starting to emerge. Overexpression of EB2 results in impaired adhesion in cell culture, while loss of the protein leads to increased cell adherence (Stenner et al., 2013). This is in concordance with stabilised focal adhesions found in skin epidermal cells after knockdown of EB2 *in vitro* and *in vivo* (Liu et al., 2015). Microtubules are known to serve as tracks to deliver proteins necessary for focal adhesion turnover (Krylyshkina et al., 2003), and EB2 seems to play an important role in this, as it has been found to recruit multiple proteins essential for focal adhesion dynamics to microtubules (Goldspink et al., 2013; Liu et al., 2015; Yue et al., 2014). Interestingly, high phosphorylation of the linker region between the calponin- and EB-homology domains has been shown to play an important role in EB2's affinity for microtubules and its effect on cell adherence (Iimori et al., 2016; Stenner et al., 2013).

Microtubule-associated protein 1s (MAP1S) is a more recently identified member of the MAP1 family of structural MAPs (Wong et al., 2004). In contrast to MAP1A and MAP1B, MAP1S is ubiquitously expressed and has a much shorter heavy chain (Figure 1C). Like the other MAP1 proteins, MAP1S heavy and light chains form dimers, but can independently bind, bundle and stabilise microtubules (Ding et al., 2006; Orban-Nemeth et al., 2005). MAP1 light chains are also capable of binding actin filaments, but it is unknown if this can happen while they are bound to microtubules as well. While the functions of MAP1A and MAP1B are well characterised in neurons, our knowledge of MAP1S in the brain is limited. Our main understanding comes from one paper on giant axonal neuropathy, an autosomal recessive disorder caused by mutations in gigaxonin (GAN). Here, the authors describe a toxic accumulation of MAP1S in GAN KO mice that results in defective axonal transport and neurite degeneration (Ding et al., 2006). Interestingly, MAP1S has also been shown to bind NMDA receptor subunit NR3A, although no function has been attributed to this interaction (Eriksson et al., 2007).

The bulk of literature on MAP1S in non-neuronal cells is about its proposed role in autophagy. Through its interactions with autophagosome-associated light chain 3 (LC3) and mitochondrion-associated proteins leucine-rich pentatricopeptide repeat-containing (LRPPRC)

and Ras-association domain family member 1 (RASSF1), MAP1S is important in both basal autophagy for clearance of abnormal mitochondria as nutritive stress-induced autophagy for nutrient recycling (Xie et al., 2011). These pathways are believed to be the cause for abnormalities in the cell cycle and eventual mitochondria-mediated mitotic cell death upon MAP1S depletion (Dallol et al., 2007; Liu et al., 2009). MAP1S-mediated autophagy has therefore been implicated in multiple forms of fibrosis and carcinomas (Song et al., 2015; Xu et al., 2016; Yue et al., 2017). Interestingly, MAP1S downregulation also results in altered microtubule dynamic instability during cell division, demonstrating a converging function with EB2 (Tegha-Dunghu et al., 2014). Finally, MAP1S has also been shown to interact with known CDKL5 substrate HDAC4, which seems to destabilise MAP1S, causing suppressed autophagy flux (Yue et al., 2015).

Rho GTPases are molecular switches that control a wide variety of signal transduction pathways in all types of cells. Rho guanine nucleotide exchange factor 2 (ARHGEF2) is a Rho GEF which activates Rho GTPase signalling by enhancing the rate of guanine diphosphate (GDP) release of inactive GDP-bound Rho GTPases. ARHGEF2 is unique among the Rho GEFs, as its activity is regulated by its binding of microtubules, and it therefore couples microtubule dynamics to Rho GTPase activation. ARHGEF2 contains three domains that sequester the protein in an inhibited state wrapped around the microtubule lattice (Figure 1D). Multiple kinases have been shown to regulate ARHGEF2 microtubule-binding affinity and thus Rho GEF activity, by phosphorylating the linker between the zinc finger and Dbl-homology domain (Sandi et al., 2017; Takano et al., 2017; Yoshimura and Miki, 2011). This linker region interacts with dynein light chain Tctex-1, a known inhibitor of ARHGEF2 (Meiri et al., 2012). ARHGEF2 is ubiquitously expressed and is associated with many different cellular functions and human diseases (Birkenfeld et al., 2008).

One of the well-known functions of Rho GTPase signalling is its role in organising the actin cytoskeleton (Sit and Manser, 2011). ARHGEF2 seems to play a crucial part in this pathway by linking microtubule dynamics to the actin cytoskeleton via its Rho GEF activity. It provides control of multiple cellular processes involved in cell morphology and polarity, including focal adhesion formation (Huang et al., 2014; Sandi et al., 2017). In neurons this expresses itself through the negative regulation of active ARHGEF2 on neurite sprouting and axon formation (Conde et al., 2010; Takano et al., 2017), and inhibition of neurogenesis upon ARHGEF2 knockdown (Gauthier-Fisher et al., 2009). In mature neurons, ARHGEF2 subcellular distribution is dependent on neuronal activity, and translocates from dendritic shafts to spines upon stimulation (Muly et al., 2008). Via its interaction with actin-binding proteins neurabin and spinophilin, ARHGEF2 is recruited to dendritic spines, where its Rho GEF activity negatively regulates spine density, length and size in an activity-dependent manner (Kang et al., 2009; Ryan et al., 2005).

Chapter 2. Materials & Methods

2.1 Biochemistry and molecular biology

2.1.1 Recombinant DNA constructs

Multiple recombinant DNA constructs were made by subcloning DNA of interest into plasmids through restriction endonuclease digestion. Primer pairs were designed to generate insert DNA flanked by two suitable restriction sites. Polymerase chain reaction (PCR) reactions were set up containing 0.2 µM of each primer, 100 ng template DNA, 0.2 mM deoxynucleotide (dNTP) mix, 1x Kapa Hifi buffer and 2.5 U Kapa Hifi Taq polymerase. The following PCR program was used: 1. 95 °C for 3 minutes, 2. 98 °C for 20 seconds, 3. 58 °C for 15 seconds, 4. 72 °C for 1 minute, 5. 72 °C for 5 minutes, 6. hold at 4 °C. Steps 2-4 were repeated 35 times. PCR product is ran on an agarose gel, cut out and purified by QIAquick gel extraction kit (Qiagen). Sticky end overhang of purified PCR product was created by digestion with suitable restriction enzymes (New England Biolabs) in the appropriate buffer for 2 hours at 37 °C. Endonuclease activity was quenched by heat inactivation at 65 °C for 20 minutes. The same protocol was followed to open the insert-receiving plasmid, which was additionally dephosphorylated by calf intestinal phosphatase (CIP) for 30 minutes at 37 °C to prevent re-ligation. Vector and insert DNA in a 1:3 molar ratio were ligated by T4 ligase at room temperature (RT) for 2 hours, and transformed into DH5α library efficient cells (Thermo Scientific). Colonies were inoculated overnight in lysogeny broth with antibiotics and purified with QIAprep spin miniprep kit (Qiagen). Correct insertions were verified by repeating the enzyme restriction steps.

By following this protocol, full-length $CDKL5_{115}$ and truncated $CDKL5^{1-352}$ were cloned into pRK5-HA using restriction sites SalI/NotI to contain an N-terminal hemagglutinin (HA)-epitope tag. The same restriction sites were also used to clone EB2, MAP1S, ARHGEF2 and TPD52 into pRK5-HA. $CDKL5^{1-352}$ was also ligated into pFastBac HTB using restriction sites SalI/NotI and transformed into DH10Bac cells to isolate recombinant bacmid DNA for insect cell purification. FLAG-tagged full-length $CDKL5_{107}$ in pcDNA3 was a kind gift from Charlotte Kilstrup-Nielsen at the University of Insubria.

Through restriction endonuclease digestion, MAP1S and ARHGEF2 were also ligated into pEGFP-C1 for an N-terminal green fluorescent protein (GFP)-tag, while GFP-tagged EB2 was a kind gift from Niels Galjart at the Erasmus University. mCherry-Mito-7 was a gift from Michael Davidson (Addgene plasmid # 55102) and EB3-tdTomato was a gift from Erik Dent (Addgene plasmid # 50708).

Ligase-independent cloning (LIC) was used to N-terminally tag EB2, MAP1S and ARHGEF2 with Strep-tag II, a synthetic peptide, by cloning them into pTriEx-6 (Novagen). With this method two PCR primers were designed to flank the insert with specific sequences that create long sticky overlaps after polymerase exonuclease activity: 5' CAGGGACCCGGT – insert 3' (forward), 5' GGCACCAGAGCGTTA – insert 3' (reverse). PCR product was generated as described before, but subsequently incubated with T4 DNA polymerase and only deoxyadenosine triphosphate (dATP) at RT for 30 minutes. After heat inactivation, the insert spontaneously ligated with LIC-ready pTriEx-6 (provided by Vangelis Christodoulou) in 5 minutes at RT. This reaction was quenched by 5 mM ethylene-diamine-tetraacetic acid (EDTA), and ready to transform in competent cells to be treated like other recombinant DNA constructs.

shRNAs against CDKL5, MAP1S and EB2 in pLentilox3.7 were designed by Sila Ultanir and made by Suzanne Claxton.

20-base sequences that precede a 5-NGG protospacer-adjacent motif were selected to induce DNA double strand breaks close to the HA-tag insertion sites. To minimize off-targeting effects, the clustered regularly interspaced short palindromic repeats (CRISPR) design tool was used (http://crispr.mit.edu/), resulting in the following sgRNA target sequences: 5' TCTGTGGCTCACATCAAAAG 3' (N-terminal CDKL5), 5' GGCCTTCCCCGCCTGCAAGG 3' (C-terminal MAP1S), 5' GTTTGGGTCGGCCCGGGCAT 3' (N-terminal EB2), 5' GCTCACGCTGGATTATGTCT 3' (N-terminal ARHGEF2). For each target, a pair of oligos was annealed by 5 minutes of incubation at 95 °C and gradually cooled down. Annealed oligos were subsequently ligated via BbsI restriction sites into the human codon-optimized S. pyogenes Cas9 (SpCas9) and single guide RNA (sgRNA) expression plasmid pX330, a gift from Feng Zhang (Addgene plasmid # 42230). Single-stranded oligodeoxynucleotides (ssODNs) for homology-directed repair were purchased from IDT, and contained the 27-base HA-tag sequence flanked by sequences of 86 bases that were homologous to the target region (full seguences in appendix). pX330 containing CaMKIIa sgRNA, and pCAG-hyPBase and pPB-CAG-mEGFP of the piggyback transposon system were kind gifts from Ryohei Yasuda at the MPFI.

All recombinant DNA constructs were verified by Sanger sequencing (Source Bioscience).

2.1.2 Site-directed mutagenesis

Point mutations were introduced into recombinant DNA constructs using QuikChange site-directed mutagenesis (Agilent). Pairs of complementary primers were designed with the mutagenic site flanked by 20 nucleotides. Two separate PCR reactions with each primer were set up containing 0.2 µM primer, 100 ng template DNA, 0.2 mM dNTP mix, 1x Pfu buffer and 2.5 U Pfu Ultra HF. The following PCR program was used: 1. 94 °C for 30 seconds, 2. 95 °C for

30 seconds, 3. 55 °C for 1 minute, 4. 68 °C for 1.5 minutes/kb, 5. hold at 4 °C. Steps 2-4 were repeated 4 times after which the two samples were combined and the same program is repeated 20 times for steps 2-4. Samples were incubated with DpnI for 2 hours at 37 °C to cut methylated template DNA, and transformed into XL10-Gold ultracompetent cells (Agilent). On average 4 colonies were inoculated overnight in lysogeny broth with antibiotics and purified with QIAprep spin miniprep kit (Qiagen). All mutations were verified by Sanger sequencing (Source Bioscience).

2.1.3 Antibodies

Commercially available primary antibodies				
Antigen	Species	Clonality	Source	Catalog #
ARHGEF2	Mouse	Monoclonal	Abcam	ab90783
CDKL5	Rabbit	Polyclonal	Abcam	ab22453
CDKL5	Rabbit	Polyclonal	Sigma	HPA002847
Ctip2	Rat	Monoclonal	Abcam	ab18465
dsRed	Rabbit	Polyclonal	Clontech	632496
EB2	Rat	Monoclonal	Abcam	ab45767
FLAG	Rat	Monoclonal	Thermo Scientific	MA1-142
GFP	Chicken	Polyclonal	Aves	GFP-1020
HA	Rabbit	Monoclonal	Cell Signaling	3724
HA	Rat	Monoclonal	Roche	11 867 423 001
LC3	Rabbit	Polyclonal	Abcam	ab48394
MAP1S LC	Rabbit	Polyclonal	Sigma	HPA050934
MAP2	Mouse	Monoclonal	Sigma	M9942
total OXPHOS	Mouse	Monoclonal	Abcam	ab110413
p62	Rabbit	Polyclonal	Cell Signaling	5114S
Strep-tag II	Mouse	Monoclonal	IBA	2-1507-001
Thiophosphate ester	Rabbit	Monoclonal	Abcam	ab92570
α-Tubulin	Rabbit	Polyclonal	Abcam	ab18251
α-Tubulin	Mouse	Monoclonal	Sigma	T9026

Table 1: Primary antibodies used for western blotting and immunofluorescent staining.
Dilutions of primary antibodies is assay-specific. All secondary antibodies used in this thesis were obtained from Jackson ImmunoResearch, and conjugated to horseradish peroxidase (HRP) for Western blotting, and Alexa Fluor or cyanine for immunocytochemistry. Immunofluorescent secondary antibodies were used at 1:500, and HRP-conjugated secondary antibodies at 1:20,000, unless stated otherwise.

2.1.4 Phosphospecific antibodies

Rabbit polyclonal phosphospecific antibodies were raised against the following phosphorylated (*) peptides by Covalab: TTRERPTS*AIY (mouse ARHGEF2 pS122), PGSTPSRPSS*AKRA (mouse EB2 pS222), RKAPARPSS*ASAT (mouse MAP1S pS786), AGDRNRPLS*ARSE (mouse MAP1S pS812). The peptide sequence for EB2 pS222 also matches 100% with rat and human sequences. Final bleeds of immunized New Zealand White rabbits are purified with affinity purification by Covalab: The immune serum is loaded onto a column with the control peptide coupled to agarose beads, thus retaining unmodified peptide-specific antibodies. The flow-through is then loaded onto a column with the modified peptide coupled to agarose beads, thus retaining the modified peptide-specific antibodies. After elution the eluate is assayed by ELISA against both peptides to control its immunoreactivity and its specificity against the modification.

2.1.5 Adherent cell lines

Human embryonic kidney 293T (HEK293T) and COS7 cells were grown in Dulbecco's modified Eagle medium (DMEM) supplemented with fetal bovine serum (FBS) and penicillin/streptomycin at 37 °C with 5% CO_2 for ~25 passages. $1/10^{th}$ of the cells was passaged every 3-4 days into new T75 flasks by dissociation with 0.25% trypsin-EDTA for 2 minutes at 37 °C. Depending on the assay, cells were split into 10 cm dishes (protein purification), 6-well plates (other lysates) or onto uncoated glass coverslips (immunofluorescence). 24-48 hours after passage, cells were transfected with Xtremegene 9 (Sigma) in a 1:3 ratio of µg DNA to µl transfection reagent for 24-48 hours at 37 °C. 6, 2 and 1 µg of total DNA was used per 10 cm dish, 6-well or coverslip respectively. Cells that were not used in further experiments such as protein purification, co-IP or IF, were lysed directly in 1x sample buffer supplemented with 0.1 mM dithiothreitol (DTT).

2.1.6 Protein purification from HEK293T cells

HA-CDKL5$_{1-352}$ and StrepII-tagged EB2, MAP1S and ARHGEF2 were purified by overexpressing these proteins in an assay-dependent number of 10 cm dishes of HEK293T cells. HEK293T cells were lysed in lysis buffer (LB) containing 50 mM Tris-HCl pH 8.0, 150 mM NaCl, 1% NP-40 or 0.1% TX100, 5% glycerol, 1x protease inhibitor cocktail (Roche) and 1:100 phosphatase inhibitor III (Roche) on ice for 30 minutes with occasional pipetting up and down. Lysate was subsequently centrifuged at 20,000 g for 15 minutes at 4 °C and supernatant was taken.

For HA-affinity purification of CDKL5$_{1-352}$, supernatant was cleared with IgG sepharose 6 Fast Flow beads (GE Healthcare) rotating for 30 minutes at 4 °C and subsequently incubated with 50 ul 50% anti-HA affinity beads (Roche) rotating for 2 hours at 4 °C. Beads were washed four times with washing buffer (LB without glycerol or detergent) of which one high-salt wash containing 1 M NaCl rotating at 4 °C for 10 minutes. Three subsequent washes with kinase buffer containing 20 mM Tris-HCl pH 7.5, 10 mM MgCl$_2$, 1x protease inhibitor cocktail (Roche) and 0.5 μM okadaic acid, prepared CDKL5 bound on HA-beads for *in vitro* kinase assays.

For StrepII-affinity purification of CDKL5 substrates, no IgG clearing was done. Lysates were ran on columns over 100 μl 50% Strep-tactin resin (IBA) and washed three times with washing buffer. Proteins were eluted of the resin by washing buffer supplemented with 50 mM desthiobiotin. Protein concentrations were measured by comparison to bovine serum albumin (BSA) standards with coomassie brilliant blue, flash frozen in liquid N$_2$ and stored at -80 °C.

2.1.7 Insect cell protein purification

Large-scale purification of CDKL5$_{1-352}$ was done by infection of insect cells. His-tagged CDKL5-containing bacmid DNA was transfected in SF9 insect cells using Cellfectin Reagent (Invitrogen) and incubated for 72 hours at 28 °C to produce P1 viral stock. P1 was amplified by infecting SF9 cells in suspension in order to generate high-titer P3 viral stock. Small-scale expression with 0.1-2 ml P3 infection per 25 ml of cells incubated for 48 hours at 28 °C, was tested to determine optimal infection for large-scale expression (600-1800 ml cells). Cell pellets were resuspended in 25 mM NaHCO$_3$ and lysed with 2x lysis buffer containing 100 mM Tris-HCl pH 7.5, 1 M NaCl, 20-30 mM imidazole pH 8.0, 5% glycerol, 10 mM MgSO$_4$, 0.2-0.3 % Triton X-100, 2 mM TCEP, 1x protease inhibitor cocktail (Roche) and 1:1000 nuclease. Lysate was centrifuged at 20,000 rpm for 30 minutes at 4 °C. Supernatant was then ran over 2 ml 50% Hispur cobalt resin (Thermo Scientific) and washed three times with wash buffer containing 50 mM Tris-HCl pH 7.5, 500 mM NaCl, 5% glycerol, 1 mM TCEP, 0.01% Triton X-100 and 10-15 mM imidazole. Bound His-tag proteins were eluted in 1 ml wash buffer containing 500 mM imidazole, ran over the column multiple times. Protein concentrations were measured by comparison to BSA standards with coomassie brilliant blue, flash frozen and stored at -80 °C. Further concentration using Vivaspin 6 10,000 MWCO (GE Healthcare), or purification by gel filtration with an S75 16/60 column or anode ion exchange by Vangelis Christodoulou, resulted in loss of the protein.

StrepII-MAP1S LC WT and S786/812A were purified on large scale from insect cells by Vangelis Christodoulou for the microtubule co-sedimentation assay. AMPH1 was purified from E. coli by Richard Li for *in vitro* kinase assays.

2.1.8 *In vitro* kinase assays

Purified proteins were incubated with kinase buffer containing 20 mM Tris-HCl pH 7.5, 10 mM $MgCl_2$, 1x protease inhibitor cocktail (Roche), 1 µM okadaic acid, 1 mM DTT, 100 µM ATP and 0.5 mM ATPγS (Biolog, containing a 6-benzyl, 6-furfuryl, 6-phenylethyl or no bulky group) at 30 °C for 30 minutes, unless stated otherwise. The reaction was quenched by adding 20 mM EDTA and followed by and alkylation reaction with 5 mM p-nitrobenzyl mesylate (Abcam) for 1 hour at RT. The resulting thiophosphate ester was detected by an antibody on Western blots.

2.1.9 Western blotting

Protein samples were denatured by 1x sample buffer supplemented with 0.1 M DTT and incubation at 95 °C for 5-10 minutes. Samples were ran at 140 V on a NuPAGE 4-12% Bis-Tris polyacrylamide gel (Thermo Scientific) unless stated otherwise, together with a Precision Plus Protein standard (Bio-Rad). Gel electrophoresis was stopped when the front reached the bottom or satisfactory protein separation was observed. Proteins were transferred onto an Immobilon PVDF membrane (Millipore) at 300-350 mA for 2 hrs on ice. Membranes were blocked with 5% milk in TBST for 30 minutes and probed with the following primary antibodies in blocking buffer o/n at 4 °C: ARHGEF2 (1:2000, Covalabs), CDKL5 (1:1000, Abcam), CDKL5 (1:1000, Sigma), EB2 (1:1000, Abcam), EB2 pS222 (1:2000, Covalabs), FLAG (1:2000, Thermo Scientific), HA (1:2000, Cell Signalling), HA (1:2000, Roche), LC3b (1:1500, Abcam), MAP1S LC (1:1000, Sigma), MAP1S pS786 (1:2000, Covalabs), MAP1S pS812 (overexpressed 1:2000, endogenous 1:500, Covalabs), total OXPHOS (1:1000, Abcam), p62 (1:5000, Cell Signallin), StrepII (1:1000, IBA), Thiophospate ester (1:30,000, Abcam) and αTubulin (1:50,000, Sigma). Membranes were subsequently washed three times with tris-buffered saline + Tween-20 (TBST) and probed with 1:20,000 HRP-conjugated secondary antibodies for 2 hrs at RT, washed three times again and developed using enhanced chemiluminescence (Pierce). Band intensities on Western blots were quantified using Fiji Gel Analyzer.

2.1.10 Microtubule co-sedimentation assay

5 µg purified MAP1S LC was thiophosphorylated by 0.5 µg AS-CDKL5$_{1-352}$ with 0.5 mM benzyl-ATPγS in kinase buffer for 60 minutes at 37 °C. MAP1S LC S786/812A and kinase dead CDKL5$_{1-352}$ were used as negative controls. Co-sedimentation of taxol-stabilised microtubules with thiophosphorylated MAP1S LC was based on a method described before (Campbell and Slep, 2011). Taxol-stabilised microtubules were prepared by incubating 20 µM purified tubulin protein (Cytoskeleton) with 1 mM GTP and DTT in BRB80 buffer, while gradually increasing the

taxol concentration to 20 uM at 37 °C. 10 uM taxol-stabilised microtubules was incubated with 3 µM phosphorylated or non-phosphorylated MAP1S LC for 20 minutes at 25 °C. 10% of the protein samples was saved as 'input', while the rest was loaded on top of a 40% glycerol cushion in an ultracentrifuge tube, and centrifuged at 100,000 xg for 30 minutes at 25 °C. The supernatant was saved as the 'unbound' fraction, and the pellet as the 'bound' fraction after washing three times with BRB80. 10 µl of each fraction was analysed by Western blotting.

2.1.11 Co-immunoprecipitation

StrepII-EB2 and HA-TPD52 were co-transfected in a 1:1 ratio in HEK293T cells as described in 2.1.4. Single transfections and EB2 S218/221/222A were used as negative controls. Protein complexes were immunoprecipitated for HA- and StrepII-affinity with slightly milder conditions than described in 2.1.5. This means that only 0.1% NP40 used and two mild washing steps were done. 5% of the lysate before IP was saved as input.

2.2 Neurobiology

2.2.1 Mouse lines

Cdkl5 KO and floxed Cdkl5 conditional KO mice were kindly provided by Cornelius Gross, and are described elsewhere (Amendola et al., 2014). These lines were expanded to maintain a healthy population of heterozygous females. Cdkl5 +/- females were used for breeding with wild type C57BL/6J males to produce Cdkl5 -/Y and +/Y littermates. Males expressing Thy1-YFP or Thy1-GFP transgenes were used to produce experimental litters where a subset of pyramidal cells is labelled for neuronal reconstruction. Daily care of the animals was handled by staff of the biological research facility.

2.2.2 Genotyping

Tail or toe biopsies were lysed with lysis buffer containing 25 mM NaOH and 200 uM EDTA for 30 minutes at 95 °C, and neutralised with 1 M Tris-HCl pH 7.5. Three PCR primers were used to genotype Cdkl5: 5' ACGATAGAAATAGAGGATCAACCC 3' (forward), 5' CCCAAGTATACCCCTTTCCA 3' (reverse) and 5' CTGTGACTAGGGGCTAGAGA 3' (CasR). PCR reactions were set up containing 0.2 μM of each primer, 2 μl lysate, 0.2 mM dNTP mix, 1x Kapa Hifi buffer and 2.5 U Kapa Hifi Taq polymerase. The following PCR program was used: 1. 94 °C for 4 minutes, 2. 94 °C for 45 seconds, 3. 58 °C for 30 seconds, 4. 72 °C for 45 seconds, 5. 72 °C for 7 minutes, 6. hold at 4 °C. Steps 2-4 are repeated 32 times. PCR product is ran on an agarose gel and resulted in 230 bp for Cdkl5 WT and 344 bp for Cdkl5 KO. Most genotyping was done by Suzanne Claxton.

2.2.3 *In utero* electroporation

Mice were given 50 μg oral meloxicam (Metacam) as an analgesic the day before surgery. At E13.5, pregnant mice were deeply anaesthetised with isoflurane and injected subcutaneous with 2 mg/kg meloxicam (Metacam) and 0.1 mg/kg buprenorphine (Vetergesic) for analgesia. Mice were shaved and the uterine horns were exposed using aseptic techniques. Every embryo was injected using a Femtojet Pico Injector (Eppendorf) in the lateral ventricle with 1-2 μl of solution containing 1 μg/μl pX330-derivatives, 0.7 μg/μl pCAG-hyPBase, 0.5 μg/μl pPB-CAG-mEGFP, 20 μM ssODN and 1x fast green dye. Electric pulses of 36 V for 50 ms were delivered with 5.0 mm forceps-shaped electrodes connected to an electroporator with the plus-end on the side of the injection. After uterine horns were reinserted, the abdominal cavity was

sewed up with a continuous stitch and the skin with a subcuticular stitch. Mice were kept in a recovery chamber until signs of good health, and were given 50 µg oral meloxicam (Metacam) the day after surgery. Successful injections were verified after birth using ultraviolet (UV) goggles.

2.2.4 Brain harvesting

Fresh brains were harvested from mice after cervical dislocation and decapitation, and flash frozen in liquid N_2. When necessary, the cortex and hippocampus were dissected out first. For Western blotting, mouse brain regions were lysed directly in 1x sample buffer supplemented with 0.1 M DTT. For substrate labelling, mouse brains were lysed in lysis buffer containing 20 mM Tris-HCl pH7.5, 100 mM NaCl, 10 mM $MgCl_2$, 0.5 mM DTT, 1x Protease Inhibitor Cocktail (Roche), 1 uM okadaic acid and 0.25% IGEPAL NP40. Lysates were sonicated briefly three times and incubated for 30 minutes on ice. Lysates were subsequently centrifuged at 20,000 g for 15 minutes at 4 °C and supernatant was flash frozen after measuring the total protein concentration using BCA protein assay (Pierce).

For immunocytochemistry, mice were put under surgical anaesthesia with 80-100 mg/kg ketamine (Vetalar) + 10 mg/kg xylazine (Rompun) injected intraperitoneal. While deeply anaesthetised, mice were fixed by cardiac perfusion with ~0.5 ml/mg bodyweight phosphate-buffered saline (PBS) to clear the blood, followed by ~1 ml/mg bodyweight 4% paraformaldehyde (PFA) until the mouse was stiff. The brain was removed and soaked in 4% PFA for 24 hours. After rinsing with PBS, fixed brains were cut into 50-100 µm thick coronal sections using a Leica VT1000S vibrating blade microtome, and floating sections were stored in PBS with 0.01% sodium azide.

2.2.5 Primary neuronal cultures

Rat and mouse primary cortical or hippocampal cultures are prepared in identical ways. Pregnant rats are ordered from Jackson. Mice are time-mated and plug checked to know the age of embryos when pregnant. E16.5 mouse or E18 rat embryos were removed from the uterus, and the cortex and hippocampus are dissected out. For pregnant Cdkl5 +/- females all embryos were sexed by Noreen Eder, after which every male embryo is cultured separately and genotyped later. In other cases, cortices and hippocampi of all embryos were combined. Cortices and hippocampi were washed three times with Hank's balanced salt solution (HBSS), incubated with 0.25 % trypsin for 20 minutes at 37 °C, and washed four times with HBSS. Cells were dissociated by titrating 20 times and counted using a haemocytometer. Coverslips, 6-well plates or glass-bottom dishes were coated o/n with 0.1 M borate buffer containing 60 ug/ml poly-D-lysine (PDL) and 2.5 ug/ml laminin at RT. 300,000 cells were plated on each coverslip,

and 1,000,000 cells in each 6-well or glass-bottom dish with plating media containing 10% FBS, 0.5% dextrose, sodium pyruvate, 2 mM glutamine and penicillin/streptomycin in minimum essential medium (MEM). After 3-4 hours plating media was replaced for maintenance media containing B27, 0.5 mM glutamine, 12.5 uM glutamate, penicillin/streptomycin and ciprofloxacin in neurobasal medium (NBM, dye-free for glass-bottom dishes). Primary neuronal cultures were grown at 37 °C and 5% CO_2. Every 3-4 days, 25% of maintenance media was refreshed. The majority of primary neuronal cultures was prepared by Suzanne Claxton.

2-5 days before immunocytochemistry or live imaging, Neurons were transfected with Lipofectamine 2000 (Thermo Scientific) in a neuronal stage-dependent ratio (DIV1-6: 1:1, DIV7-11: 1:2, DIV12+: 1:3) of µg DNA to µl transfection reagent for 15 minutes at 37 °C. 1 and 2 µg of total DNA was used per coverslip or glass-bottom dish respectively. Before transfection, half of the maintenance media was taken off and supplemented with the same amount of fresh maintenance media. This was used to replace the media after transfection. EB3-tdTomato was transfected 24-36 hours before live imaging to avoid high protein expression and accumulation at the microtubule lattice.

2.2.6 Neuronal treatments

Neuronal activity was altered by directly adding reagents to the maintenance media of rat primary cortical neurons at DIV7 or DIV14. 3 M KCl to a final concentration of 50 mM, 5 M NaCl to a final concentration of 50 mM, 20 mM NMDA to a final concentration of 50 µM, 200 mM glycine to a final concentration of 200 µM, and 1 mM tetradotoxin (TTX) to a final concentration of 0.5 µM. Neurons were incubated at 37 °C for assay-dependent lengths of time up to 60 minutes, when they were lysed directly in 1x sample buffer supplemented with 0.1 mM DTT. 0 minute-controls were lysed without adding reagents. 30 minutes of pre-incubation with 100 µM AP5 was done before KCl treatment when blocking NMDA receptors.

2.3 Proteomics

2.3.1 SILAC

Primary neuronal cultures were made as described in 2.2.4, but instead 8 million cells were plated in coated 10 cm dishes. Arginine- and lysine-depleted NBM was used in the maintenance media, and instead supplemented with L8R10 (heavy) or L4R6 (light), and additional 200 mg/l proline to prevent conversion. After DIV4, fresh maintenance media also included 1 uM AraC to prevent glial growth. At DIV12, neurons were lysed in the same conditions as described for fresh brains in 2.2.3. SILAC label incorporation and arginine to proline conversion were assessed by Helen Flynn.

2.3.2 Substrate labelling and covalent capture

Direct CDKL5 or nuclear dbf2-related 1 (NDR1) substrates were isolated by capturing thiophosphorylated peptides based on method described before (Hertz et al., 2010). P12 mouse brain lysate (2.5 mg total protein) or SILAC rat cortical culture lysate (1 mg total protein) was labelled by 3-5 ug AS or KD kinase using a kinase labelling mix including 1 µM PKA inhibitor, 0.2 µM PKC inhibitor, 3 mM GTP, 100 µM ATP, 0.5 mM DTT, 0.5 µM okadaic acid and 0.5 mM benzyl- or furfuryl-ATPγS for 1 hour at 30 °C on a nutator. Samples were denatured with 60% urea and 10 mM tris(2-carboxyethyl)phosphine (TCEP) for 1 hour at 55 °C. After dilution with 2x volume 50 mM ammonium bicarbonate while keeping TCEP at 10 mM, samples were digested by 30 µg Sequencing Grade Modified Trypsin (Promega) at pH 8.0 rotating o/n at 37 °C. Trypsinization is quenched by 0.5-1.0% trifluoroacetic acid (TFA). Clean up of the digested peptides is done with Sep-Pak Classic C18 Cartridges (Waters) and completely dried on a Speedvac. Dried samples are resuspended in 50% acetonitrile and 50 mM HEPES, set to pH 7.0 and incubated with Sulfolink Coupling Resin (Thermo Scientific) and 25 µg BSA rotating o/n at RT. Resin was subsequently washed with MQ, 5M NaCl, 50% ACN and 5% formic acid respectively, then incubated with 10 mM DTT for 20 minutes, when eventually thiophosphorylated peptides are eluted with Oxone after 30 minutes of incubation. A final pre-MS desalting and clean up step was done with Zip Tips – P10, 0.6 µL C18 resin (Millipore) and purified peptides were flash frozen in liquid N_2 to be analysed with mass spectrometry.

Optional dimethyl labelling was performed after trypsin digest, but the rest of the protocol was the same as described above, except that Tris-HCl in the lysis buffer and ammonium bicarbonate were replaced by 100 mM triethylamonium bicarbonate (TEAB). 4 mg protein digest reacted with 128 µl 20% formaldehyde and 154 µl cyanoborohydride

(hydrogenated 'light' or deuterated 'heavy') for 1 hour at 25 °C at 750 rpm. Samples were quenched by adding 128 µl 25% ammonia for 10 minutes and acidified with 120 µl TFA until no more gas was produced. 'Heavy' and 'light' mixes were combined and continued for Sep-Pak clean up and following steps as described previously.

2.3.3 Global phosphoproteomics

Lysates of Cdkl5 +/Y and -/Y SILAC labelled primary cortical cultures were mixed according to Table 2. Each mix contained 0.5 mg of light and 0.5 mg of heavy lysate determined by BCA protein assay (Pierce). Mixed protein lysates were digested by trypsin and cleaned up with Sep-Pak cartridges as described in 2.3.2. Additional titanium dioxide enrichment of phosphorylated peptides was achieved. 5 mg of Titansphere titanium dioxide beads (GL Sciences) was added to each sample in loading buffer containing 80% acetonitrile (ACN), 5% TFA and 1M glycolic acid, and agitated on a thermomixer at 1400 rpm for 10 minutes at RT. After centrifugation, supernatant was removed. These steps were repeated to wash with wash buffer 1 containing 80% ACN and 1% TFA, and wash buffer 2 containing 10% ACN and 0.2% TFA. Phosphopeptides were eluted via these same steps with 1% ammonium hydroxide, and 5% ammonium hydroxide. Final clean-up was done with Zip Tips as described in 2.3.2, and samples were flash frozen to be analysed with mass spectrometry.

	x	Heavy (K8R10)								
		WT 2.1	WT 2.2	WT 2.3	WT 2.5	WT 3.2	WT 3.5	KO 2.4	KO 3.3	KO 3.4
Light (K4R6)	WT 2.1	C1								
	WT 2.2		C2							
	WT 2.3			C3						
	WT 2.5				C4			E4		
	WT 3.2								E5	
	WT 3.5									E6
	KO 2.4				E1					
	KO 3.3					E2				
	KO 3.4						E3			

Table 2: SILAC mixing table for global phosphoproteomics of Cdkl5 KO mice.
SILAC labelled primary cortical cultures of three Cdkl5 WT and three Cdkl5 hemizygous KO males were mixed to create six experimental samples (green). Four mixes from cultures of the same animal were used as control samples (orange). Samples from two different cultures have been used for this experiment.

2.3.4 Phospho-EB2 peptide-binding assay

Peptide pull-down using SILAC labelled lysates was described before (Ultanir et al., 2014). Peptides were synthesized for phosphorylated (ASKPGSpTPpSRPSpSAKRA) and non-phosphorylated (ASKPGSpTPSRPSSAKRA) EB2. Peptides were conjugated to Sulfolink Resin iodoacetyl agarose beads (Thermo Scientific) in coupling buffer containing 50 mM Tris pH 8.5 and 5 mM EDTA for 30 minutes at RT. 30 µl resin conjugated to 22 nmol of peptide will be used to for pull-down in 1.6 mg SILAC labelled protein lysate. Coupling efficiency was not possible to be determined as these peptides do not contain amino acids with aromatic rings necessary for 280 nm spectroscopy. Non-specific binding sits on the resin were blocked with 50 mM cysteine for 15 minutes at RT. 30 µl resin conjugated to 22 nmol of peptide was used for pull-down of peptide-binding proteins in 1.5 mg of total SILAC labelled protein lysate of DIV12 rat primary neurons by incubation for 1.5 hours at RT. Beads were washed four times with washing buffer (lysis buffer without protease inhibitors or detergent). Samples are mixed according to Table 3, subsequently solubilized in 30 µl sample buffer and ran on a 10% NuPage Bis-Tris gel for short gel lane extraction and in-gel trypsin digestion done by Helen Flynn.

		Heavy (K8R10)	
	x	Phosphorylated EB2	Non-phosphorylated EB2
Light (K4R6)	Phosphorylated EB2		Mix 1
	Non-phosphorylated EB2	Mix 2	

Table 3: SILAC mixing table for phospho-EB2 peptide-binding assay.
Two mixes were made containing reverse labelled proteins bound to phosphorylated and non-phosphorylated EB2 peptide.

2.3.5 Mass spectrometry

The majority of liquid chromatography-tandem mass spectrometry (LC-MS/MS) data acquisition and processing was done by Helen Flynn. For phosphoproteomic analysis of 2.3.2 and 2.3.3, each sample was resuspended in 35 µl 1% TFA, sonicated for 15 minutes and injected 3 times (10 µl per injection). Digests extracted from each gel band of 2.3.4 were transferred to autosampler vials and 10 µl of each was injected for LC-MS/MS analysis. Peptide mixtures were separated on a 50 cm, 75um I.D. Pepmap column over a 3-hour gradient and eluted directly into the mass spectrometer (Orbitrap Velos). Xcalibur software was used to

control the data acquisition. The instrument ran in data dependent acquisition mode with the top 10 most abundant peptides selected for MS/MS by CID, MSA or HCD fragmentation techniques (one fragmentation technique per replicate).

Data processing was performed using the MaxQuant bioinformatics suite and protein database searching was done by the Andromeda search engine using a Uniprot database of *mus musculus* or *rattus norvegicus* proteins amended with common contaminants. A protein, peptide and phosphosite estimated false discovery rate of 1% was used to generate tables with protein and phosphopeptide identifications and quantifications, which featured matching between runs for peptide identification. Phosphosite tables were subsequently uploaded into the Perseus analysis program for further statistical analysis and data visualisation. The following parameters were reported: Peptide posterior error probabilities for identification using a target-decoy approach. For sites found on multi phosphorylated peptides, the least modified peptide ratio was reported. Phosphosite localisation probabilities for site identification.

2.4 Imaging and analysis

2.4.1 Immunocytochemistry

Coverslips with cultured primary neurons were fixed with cold 4% PFA, 4% sucrose for 10-15 minutes. For microtubule localisation, coverslips containing primary neurons were first fixed with methanol supplemented with 1 mM EGTA for 5 minutes at -20 °C, followed by 5 minutes of standard PFA fixation based on Jaworski et al. Coverslips with COS7 cells were fixed with methanol for 5 minutes at -20 °C. Both were subsequently washed three times with cold PBS. Coverslips and floating brain sections were simultaneously blocked and permeabilised with 0.3% TritonX-100 in 10% normal goat serum for 60 minutes at RT. In the same buffer, the following primary antibodies were incubated o/n at 4 °C: ARHGEF2 (1:50, Abcam), Ctip2 (1:2000, Abcam), FLAG (1:100, Thermo Scientific), GFP (1:2000, Aves), HA (1:1000, Cell Signalling), MAP1S LC (1:500, Sigma), αTubulin (1:1000, Sigma) and αTubulin (1:100, Abcam). After three 5-minute washes with PBS, 1:500 secondary antibodies in PBS were incubated for 2 hours at RT. Coverslips and sections were washed three times again, of which one contained 1:2000 DAPI stain (Thermo Scientific). Coverslips and floating brain sections were mounted with Fluoromount-G (Southern Biotech) on glass slides or under #1.5 cover glass (VWR) respectively.

2.4.2 Neuronal morphology

Complete basal dendritic arbours of Thy1-GFP labelled neurons were imaged without immunostaining in 100 um thick coronal brain sections. Somatosensory layer 5 pyramidal cells were localised with help of the mouse brain atlas. Only bright neurons in the middle of the cross-section were imaged to prevent dendrites being cut. Z-stacks were acquired with a Leica SP5 inverted confocal microscope and a Leica HyD photodetector (20x / 0.5 NA oil, 1.5x optical zoom, 1.5 um z-step size, 2 airy pinhole). Images were processed with Leica Application Suite and Fiji. Basal dendritic arbours were reconstructed using Neurolucida 360 (MBF Bioscience) and analysed with Neurolucida Explorer (MBF Biosocience). Three-dimensional total dendrite length was calculated using Fiji plugin NLmorphologyviewer.

Basal secondary dendrites of Thy1-YFP labelled neurons were imaged without immunostaining in 50 um thick coronal brain sections. Somatosensory layer 5 and hippocampal CA3 and CA1 pyramidal cells were localised with help of the mouse brain atlas. Z-stacks were acquired with a Leica SP5 inverted confocal microscope and a Leica HyD photodetector (100x / 1.46 NA oil, 2x optical zoom, 0.25 um z-step size, 1 airy pinhole). This was set up to sample

close to the ideal Nyquist rate of 78 nm calculated by c . λ / NA / 2.3, while keeping the image as large as possible. Images were processed with Leica Application Suite and Fiji. Spine density and head diameter were manually measured using a custom Fiji plugin.

Axonal and dendritic arbours of GFP-expressing primary neurons were imaged after staining at DIV4 and DIV11 respectively. Pyramidal neurons were identified by typical morphological hallmarks like the presence of an axon and a branched dendritic arbour. Hippocampal CA3 neurons were specifically selected by negative Ctip2 staining. Images were acquired with an Olympus IX83 widefield microscope and a Hamamatsu ORCA-Flash4.0 camera in one focal plane (axons: 10x / 0.4 NA air, dendrites: 20x / 0.75 NA air). Images were processed in Olympus cellSens Dimension and Fiji. Axons and dendrites were reconstructed using Neurolucida 360 (MBF Bioscience) and analysed with Neurolucida Explorer (MBF Bioscience). Z-stacks of secondary dendrites were acquired at DIV18 with a Leica SP5 inverted confocal microscope and a Leica HyD photodetector (63x / 1.4 NA oil, 4x optical zoom, 1 um z-step size, 1 airy pinhole). Images were processed with Leica Application Suite and Fiji. Spine density was manually measured using a custom Fiji plugin.

2.4.3   Dendrite dynamics

Live imaging of the dendritic arbour of GFP-expressing primary neurons at DIV12 was done at 37 °C and 5% CO_2 in glass-bottom dishes containing dye-free media. Pyramidal neurons were identified by typical morphological hallmarks like the presence of an axon and a branched dendritic arbour. Z-stacks were acquired with an Olympus IX83 widefield microscope and a Hamamatsu ORCA-Flash4.0 camera (20x / 0.75 NA air, 1 um z-step size). Images of the same neurons were acquired 24 hours later in an identical manner. Neurons that died in this timespan were disregarded. Images were processed with Olympus cellSens Dimension and Fiji using the Stack Focuser plugin. Formed and retracted dendrites were measured manually using composites in Fiji. Growth or retraction smaller than 5 um was not taken into account.

2.4.4   Live imaging

Live imaging of EB3-tdTomato or mCherry-Mito-7 expressing primary neurons at DIV11-14 was done at 37 °C and 5% CO_2 in glass-bottom dishes containing dye-free media. Flat stretches of dendrite were selected based on their thickness and protein expression levels. Especially correct EB3 expression levels are crucial for visualisation of growing microtubule plus-ends, as it tends to accumulate at the lattice when protein levels get too high. 3-minute videos were acquired at 1 frame/second with an Olympus IX81 spinning disk confocal microscope and a Hamamatsu C9100-13 CCD camera in one focal plane (150x / 1.45 NA oil). Videos were processed using Volocity and Fiji. Background correction was applied for EB3

videos by subtracting the average intensity. Kymographs were generated using the KymographClear 2.0 Fiji plugin and manually analysed.

2.4.5   Microtubule colocalisation

Methanol-fixed COS7 cells overexpressing CDKL5 and substrates were imaged after staining. High CDKL5-expressing cells were selected for healthy nuclei and a distinct microtubule cytoskeleton. Multichannel images were acquired with an Olympus IX83 widefield microscope and a Hamamatsu ORCA-Flash4.0 camera in one focal plane (60x / 1.42 NA oil). Images were processed with Olympus cellSens Dimension and Fiji. Colocalisation of MAP1S and microtubules was quantified manually, but also by Pearson coefficient and spatial image cross-correlation spectroscopy (ICCS) measured with HK means segmentation and Colocalization Studio in Icy.

2.4.6   Graphs and statistics

All graphical data was visualised with GraphPad Prism 7, which also performed all statistical analyses. Statistical significance was visualised as follows: not significant $p > 0.05$, * $p < 0.05$, ** $p < 0.01$, *** $p < 0.001$, **** $p < 0.0001$.

Chapter 3. CDKL5 substrate identification

It is still largely unknown which proteins CDKL5 directly phosphorylates under physiological conditions. In order to understand more about the exact function of CDKL5 and the role it plays in neurodevelopment, it is absolutely crucial to get a better grasp on this basic function of the kinase. This might open up more pathways for developing essential tools and therapeutic strategies in the battle against CDKL5 deficiency disorder. We therefore decided to tackle this problem by establishing chemical genetic kinase-substrate mapping in the lab, and apply it to CDKL5. This method has been very successful for other kinases in the developing brain (Ultanir et al., 2012; Ultanir et al., 2014), is well documented (Hertz et al., 2010), and was therefore believed to give us good results.

This first of two results chapters in this thesis is dedicated to our successful identification of novel physiological CDKL5 substrates. We will show how we generated analogue-sensitive CDKL5 by introducing mutations in the ATP-binding pocket of the kinase, which made it capable of specifically thiophosphorylating its substrates. We then describe how we identified putative CDKL5 targets using covalent capture of thiophosphorylated peptides and mass spectrometry, followed by the steps we took to validate these novel targets with *in vitro* kinase assays. Finally, we demonstrate how we confirmed the loss of CDKL5 substrate phosphorylation with phosphospecific antibodies *in vivo*, and the possibilities these antibodies bring as biomarkers for CDKL5 activity.

Gatekeeper mutation							
CDKL5	Y	L	V	F89A	E	F	M
ERK2	Y	I	V	Q103G	E	F	M	(Eblen et al., 2003)
NDR1	Y	L	I	M166A	E	F	L	(Ultanir et al., 2012)
Second-site rescue mutation							
CDKL5	L	K	L	C152A	D	F	G
NDR1	V	K	L	S229A	D	F	G	(Ultanir et al., 2012)
CHK2	I	K	I	T410A	D	F	G	(Unpublished)

Table 4: Protein alignment of AS-CDKL5 generating mutations.

The CDKL5 gatekeeper and second-site rescue mutation are based on homology with similar mutations in previously described analogue-sensitive kinases. ERK2 = extracellular signal-regulated kinase 2, NDR1 = nuclear Dbf2-related kinase 1, CHK2 = checkpoint kinase 2.
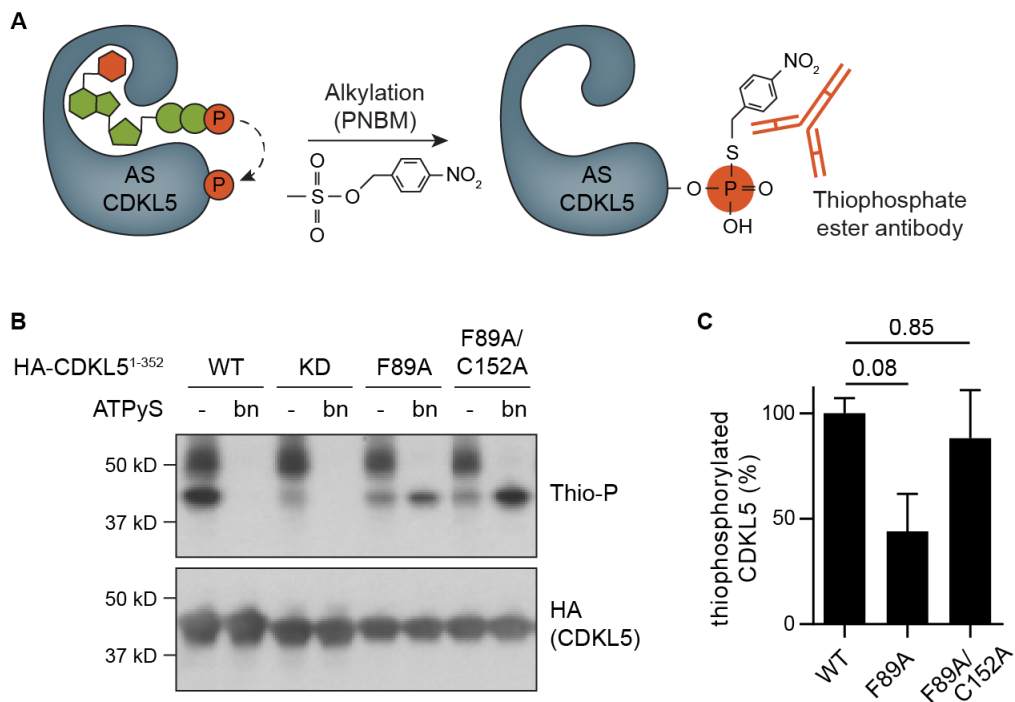
Figure 2: CDKL5$^{1\text{-}352}$ F89A/C152A is analogue-sensitive.

(A) Schematic of the detection of auto-thiophosphorylation. AS-CDKL5 can use bulky ATPyS to thiophosphorylate itself. After alkylation with PNBM, the resulting thiophosphate esters can specifically be detected by an antibody. (B) *In vitro* auto-thiophosphorylation is visualised by Western blotting. Reduced AS activity of CDKL5 F89A is rescued with an additional C152A mutation. - = no bulky side group, bn = benzyl, 1:30,000 Thio-P, 1:2000 HA. (C) Quantification of B. Normalised for HA and with KD background subtracted. Dunnett's multiple comparison: n = 4 repeats, error bars are SEM.

3.1   Generation of analogue-sensitive CDKL5

A compulsory first step that has been done in all previous cases of kinase-substrate mapping via chemical genetics, is the generation of an analogue-sensitive kinase. AS-kinases have the advantage that they can utilise bulky ATP analogues to thiophosphorylate their substrates, enabling the identification of direct targets specifically. In order to identify putative CDKL5 targets with this technique, it was necessary to generate large amounts of analogue-sensitive CDKL5 that could specifically thiophosphorylate its substrates. Therefore, we first had to establish which mutations make CDKL5 analogue-sensitive, then needed to purify the AS kinase in large amounts from insect cells, and finally validate its activity with known substrate AMPH1 using *in vitro* kinase assays.

3.1.1   CDKL5$^{1-352}$ F89A/C152A is analogue-sensitive

In most cases, AS-kinases are simply made by a single point mutation in the so-called 'gatekeeper' residue located in the ATP-binding pocket. Sequence alignment to other kinases and crystal structure analysis predicted that the gatekeeper residue in CDKL5 is the phenylalanine at position 89 (Table 4). The mutation of this bulky amino acid to a smaller, hydrophobic residue was hypothesized to enlarge the ATP-binding pocket and allow CDKL5 to utilize bulky ATPγS analogues. However, multiple 'intolerant' kinases have been reported, which require second-site mutations to rescue loss of kinase activity upon the gatekeeper mutation (Zhang et al., 2005).

Thiophosphorylation of proteins with *in vitro* kinase assays can be observed after alkylation of the transferred thiophosphate by p-nitrobenzyl mesylate (PNBM). The resulting thiophosphate ester is recognised by an antibody on a Western blot and acts as a specific read-out for AS-kinase activity (Figure 2A). Like most kinases, CDKL5 phosphorylates its own kinase domain that can be used as a read-out for catalytic activity. By making use of this auto-phosphorylation it is possible to determine the effect of potential AS-creating mutations without requiring any known substrates. Mutated N-terminal HA-tagged CDKL5 was therefore precipitated from HEK293T cells to measure its analogue sensitivity with *in vitro* kinase assays, while still being bound on the anti-HA beads. Consistent with anecdotal information, early experiments showed difficulties in reliably purifying full-length CDKL5. We therefore quickly switched to a kinase domain-containing truncation (CDKL5$^{1-352}$) known to be more stable and active than the full-length protein.

It soon became obvious that mutating the gatekeeper residue in CDKL5 did not directly lead to analogue-sensitive kinase activity. The experiment was repeated four times and as expected, WT CDKL5$^{1-352}$ shows strong auto-phosphorylation with normal ATPγS, but not with

Gatekeeper mutation	Second-site mutation	Kinase activity	Reasoning	Reference
none	none	++	Wild type CDKL5	
F89A	none	+	Small hydrophobic gatekeeper	(Blethrow et al., 2004)
F89A	L28Y	+	β-sheet homology	(Zhang et al., 2005)
F89A	L64P	-	Sequence homology	
F89A	V73A	+	Second gatekeeper	(Eblen et al., 2003)
F89A	V73I	+	Second gatekeeper	(Eblen et al., 2003)
F89A	L87I	+	Rescues ITK activity	(Joseph and Andreotti, 2011)
F89A	W125Y	+	Sequence homology	
F89A	C152A	++	Rescues NDR1 kinase activity	(Ultanir et al., 2012)
F89A	C152I	-	Variant of C152A/T	
F89A	C152T	+	Rescues NDR1 kinase activity	(Ultanir et al., 2012)
F89A	T169E/Y171D	-	Activation of TEY motif	(Fu et al., 2005)
F89C	none	-	Rescues Src kinase activity	(Garske et al., 2011)
F89G	none	-	Small hydrophobic gatekeeper	(Blethrow et al., 2004)
F89G	L28Y	+	β-sheet homology	(Zhang et al., 2005)
F89G	V73A	-	Second gatekeeper	(Eblen et al., 2003)
F89G	V73I	-	Second gatekeeper	(Eblen et al., 2003)
F89G	A78I	-	Sequence homology	
F89G	A78V	-	Sequence homology	
F89G	L87I	-	Rescues ITK activity	(Joseph and Andreotti, 2011)
F89G	C152A	-	Rescues NDR1 kinase activity	(Ultanir et al., 2012)
F89G	C152G	-	Variant of C152A/T	
F89G	C152I	-	Variant of C152A/T	
F89G	C152S	-	Variant of C152A/T	
F89G	C152T	-	Rescues NDR1 kinase activity	(Ultanir et al., 2012)
F89G	Q69H/E70P	-	Sequence homology	
F89V	none	-	Small hydrophobic gatekeeper	(Blethrow et al., 2004)

Table 5: All gatekeeper and second-site rescue mutations tested in CDKL5.

Most of the mutations introduced to generate AS-CDKL5 resulted in loss of kinase activity. Kinase activity measurements are relative to WT CDKL5 activity with normal ATPyS. - no detected activity, + reduced activity, ++ similar activity to WT. ITK = interleukin 2-inducible T-cell kinase

any bulky ATPyS analogues (Figure 2B). This auto-phosphorylation is absent in the K42A kinase dead control. However, all of the gatekeeper mutations to smaller amino acids resulted in strongly reduced, or completely lost CDKL5 kinase activity with either normal or bulky ATPyS (Table 5). This loss of kinase activity was thought to be caused by two possible explanations: the ATP-binding pocket is altered so that neither normal ATP, nor bulky ATP, can be used for phosphorylation, or the complete structure of kinase domain is destabilized in such a way that all activity is lost. It was therefore necessary to introduce second-site mutations to restore CDKL5's ability to utilise bulky ATPyS.

Most of the successful second-site rescue mutations in other intolerant kinases are located around the ATP-binding pocket or stabilizing β-sheets. So in order to restore CDKL5 kinase activity, we tried various mutations based on the rescue of previously described intolerant kinases, or a lack of CDKL5 sequence homology to otherwise conserved regions of kinase domains (Table 5). However, only in combination with mutation C152A, the analogue-sensitive kinase activity of CDKL5 F89A was consistently similar to WT levels with normal ATPyS (Figure 2B and C, F89A: 44.0 ± 17.8 % of WT, n = 4, p = 0.08, F89A/C152A: 88.3 ± 22.8 % of WT, n = 4, p = 0.85). Three types of bulky ATPyS analogues were tested. CDKL5 F89A/C152A shows no preference for benzyl- or furfuryl-ATPyS, but is not capable of using phenyl-ethyl-ATPyS (data not shown).

CDKL5 C152 is located right before the conserved DFG motif in the kinase domain. Mutating this residue has rescued multiple other intolerant kinases, and is thought to restore the ability of the kinase to utilize bulky ATP by making the ATP-binding pocket more flexible (Table 4). This mutation likely has a similar function in CDKL5, showing that CDKL5[1-352] F89A/C152A is capable of analogue-sensitive auto-thiophosphorylation to a similar extend as WT CDKL5[1-352], and will be referred to as AS-CDKL5 from now on.

3.1.2   Large amounts of AS-CDKL5 are purified from insect cells

AS-CDKL5 was generated to specifically label and capture novel substrates in a chemical genetic screen. For previously described kinases-substrate interactions identified with this method, 10-20 μg of kinase per labelling reaction of ~2 mg total protein lysate has been the most successful (Hertz et al., 2010). However, HA-affinity purification from HEK293T cells, used to identify the AS mutations, only resulted in approximately 0.5 ug of HA-CDKL5[1-352] per 10 cm dish (~10x10^6 cells, Figure 3A). There clearly had to be an improvement in CDKL5 purification yield to get the order of magnitude that is useful for future experiments.

We attempted to increase CDKL5 expression in HEK293T cells by co-transfection with Ebola virus protein 35 (VP35). VP35 has been shown before to massively increase recombinant protein expression by antagonizing protein kinase R (PKR) activation, which otherwise inhibits protein translation (Gantke et al., 2013). However, VP35 co-transfection did not lead to
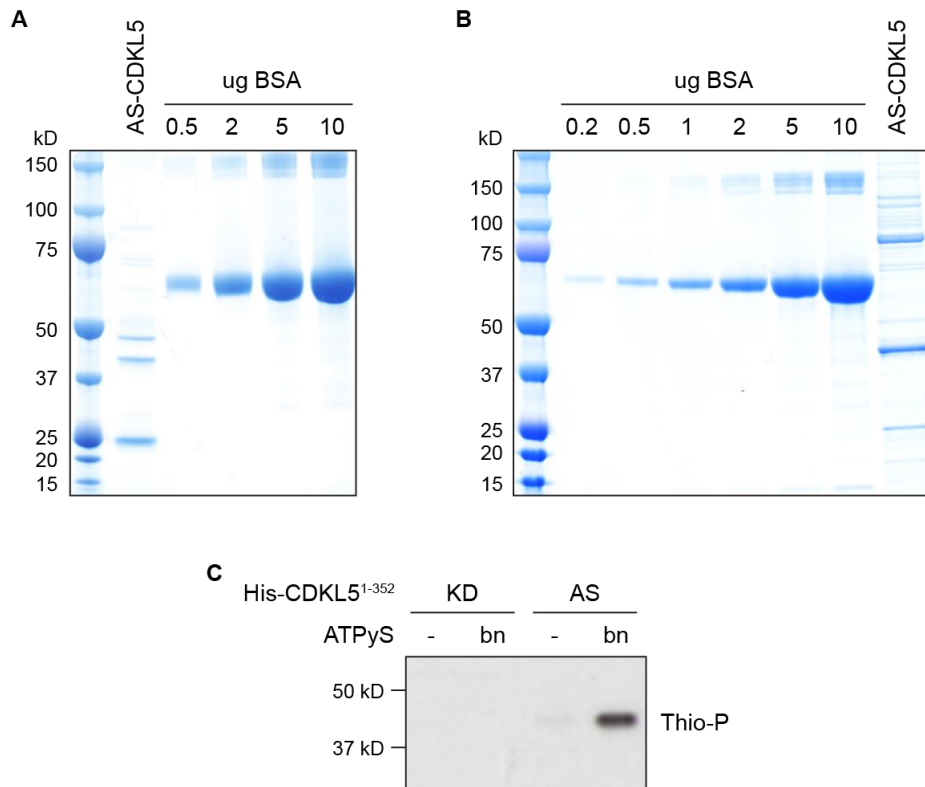
Figure 3: AS-CDKL5 purification from HEK293 and Sf9 insect cells.

(A) HA-affinity purification from HEK293 cells is visualised by coomassie blue staining after gel electrophoresis, and results in ~0.5 ug of AS-CDKL5$^{1-352}$ per 10 cm dish. 25% loaded, BSA is used to quantify yield. Tagged CDKL5$^{1-352}$ is expected to migrate around 40 kD. (B) His-tagged AS-CDKL5$^{1-352}$ purification from Sf9 insect cells with a Hispur cobalt column is visualised by coomassie blue staining after gel electrophoresis, and contains ~0.1 ug/ul protein. 10 ul loaded. (C) *In vitro* auto-thiophosphorylation of 0.5 ug (40 uM) soluble CDKL5$^{1-352}$ is visualised by Western blotting, and only AS-CDKL5 shows to preferentially use benzyl-ATPyS. 1:30,000 Thio-P.

significant changes in CDKL5 expression in our cell culture system (data not shown). Exchanging the N-terminal HA-tag for different epitope tags like FLAG or Strep-tag II did not result in any improvements either, indicating that it is a more intrinsic property of CDKL5[1-352] which is causing problematic expression and/or stability of the protein.

Instead of trying to improve the expression and purification efficiency of CDKL5 in HEK293T cells, we decided to abandon the adherent cell lines, and use a different expression system that is more suitable for large-scale purification. The quickest, easiest and cheapest method would be the expression of proteins in E. coli, but proteins expressed in prokaryotes do not contain any post-translational modifications and might not be folded properly. Kinases expressed via baculovirus infection of insect cells however, are post-translationally modified and therefore tend to retain their activity. Compared to mammalian HEK293T cells, Sf9 insect cells are much easier to grow in large quantities in suspension.

N-terminal His-tagged CDKL5[1-352] was overexpressed by baculovirus infection of Sf9 insect cells, captured by a Hispur cobalt column and eluted with imidazole. Interestingly, additional gel filtration or ion-exchange purification revealed very weak solubility of CDKL5[1-352], as the protein was consistently lost during concentration steps necessary after these techniques. This made it impossible for us to further purify the protein after His-tag affinity capture. We therefore used more stringent washing buffer (500 mM NaCl, 15 mM imidazole) and a small amount of elution buffer to obtain the purest and most concentrated CDKL5[1-352] possible after His-tag affinity without any further purification. With this method we managed to produce relatively clean 0.1 ug/ul analogue-sensitive (Figure 3B) and 0.3 ug/ul kinase dead CDKL5[1-352] (data not shown).

Like AS-CDKL5 purified from HEK293T cells, AS-CDKL5 purified from Sf9 insect cells showed clear auto-thiophoshorylation when incubated with benzyl-ATPyS, but not with normal ATPyS (Figure 3C). This activity was not observed in kinase-dead CDKL5[1-352]. Using eluted His-tagged CDKL5 in the kinase assay also made the results a lot cleaner compared to on-bead assays with HA-tagged CDKL5. This showed that we were able to obtain large amounts of active analogue-sensitive CDKL5[1-352] and inactive kinase-dead control.

3.1.3   AS-CDKL5 thiophosphorylates AMPH1 *in vitro*

Before we attempted to use AS-CDKL5 in a chemical genetic kinase-substrate screen, we tested to see if AS-CDKL5 retained its catalytic activity towards its substrates, besides being capable of auto-phosphorylation. AMPH1 had been the only CDKL5 substrate extensively studied with *in vitro* kinase assays at the time (Sekiguchi et al., 2013), and was therefore considered the most suitable candidate for this experiment.

A notorious feature of *in vitro* kinase assays is the unspecific protein phosphorylation you can observe when you use high protein concentrations and enough time. We tried to avoid
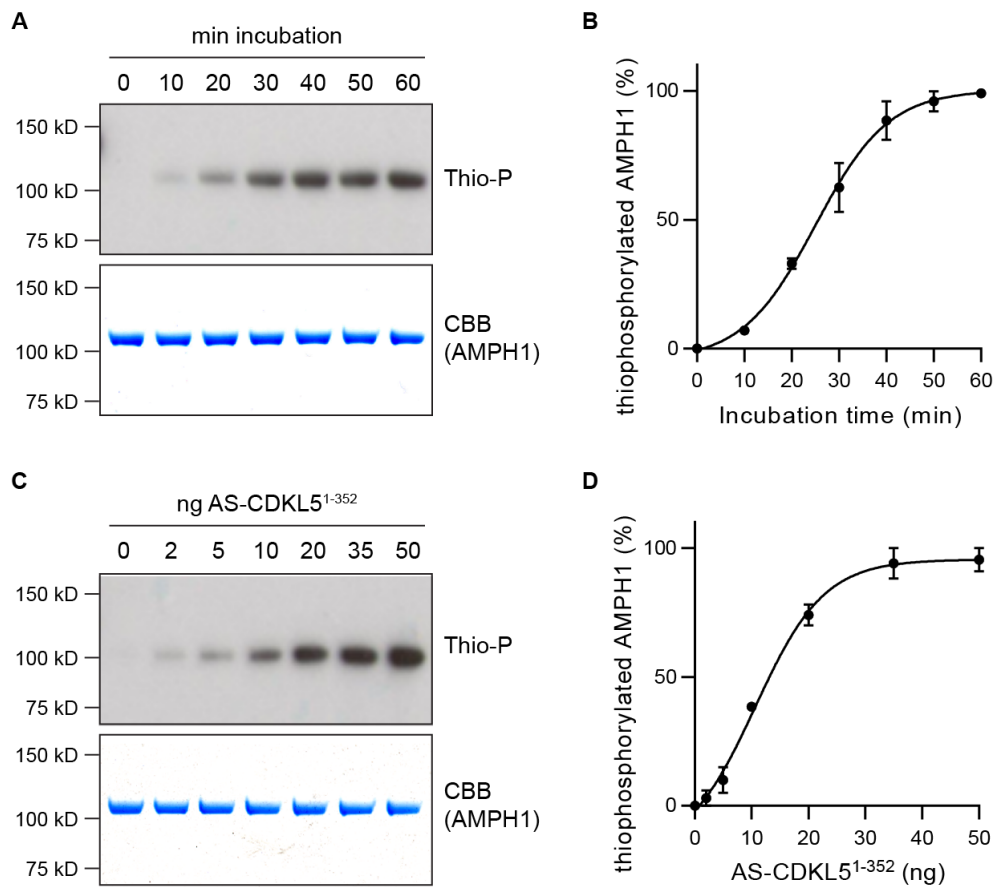
Figure 4: Amphiphysin 1 is thiophosphorylated by AS-CDKL5[1-352].

(A) 300 ng (0.13 uM) AMPH1 is incubated with 50 ng (0.04 uM) AS-CDKL5[1-352] for increasing amounts of time, and visualised by Western blotting (1:30,000 Thio-P) and coomassie blue (CBB) staining. (B) Quantification of A. Maximum phosphorylation is reached after 60 min. Sigmoidal curve fit: n = 2 repeats, R^2 = 0.983, error bars are SEM. (C) 300 ng (0.13 uM) AMPH1 is incubated for 60 min with increasing amounts of AS-CDKL5[1-352] and visualised like A. (D) Quantification of C. Half of the maximum phosphorylation is reached with 15 ng CDKL5. Sigmoidal curve fit: n = 2 repeats, R^2 = 0.988, error bars are SEM.

this by introducing a two-step control experiment to determine the most suitable incubation time and kinase-substrate ratio, while staying in the range of nanomolar protein concentrations. Experiments were performed in duplo.

First the substrate and kinase amount in the assay were fixed, but the incubation time was steadily increased. 300 ng (130 nM) AMPH1 and 50 ng (40 nM) AS-CDKL5 were therefore incubated with benzyl-ATPyS for up to an hour. We saw that AMPH1 thiophosphorylation by 50 ng of AS-CDKL5 reaches a maximum after roughly 60 minutes of incubation. Surprisingly, we did not observe the quick, steep increase in phosphorylation we expected from an efficient enzymatic reaction (Figure 4A and B, 95% = 47.7 minutes, R^2 = 0.983).

We used this information to set the incubation time to the point of maximum substrate phosphorylation, while steadily decreasing the amount of kinase from 50 to 0 ng. We expected to see that this shows that even very small amounts of kinase are capable of phosphorylating its substrate, and that this follows a sigmoidal dose-response curve. 300 ng (0.130 nM) AMPH1 and up to 50 ng (40 nM) of AS-CDKL5 were incubated with benzyl-ATPyS for 60 minutes. As expected, we already observed AMPH1 thiophosphorylation with very small amounts of AS-CDKL5, and this reaction followed a sigmoidal curve (Figure 4C and D, 50% = 13.1 ng CDKL5, R^2 = 0.988). The thiophosphorylation of AMPH1 is absent with kinase-dead CDKL5 negative controls (data not shown). These findings confirm AMPH1 as a direct substrate of CDKL5 *in vitro*, and provide more evidence that the analogue-sensitive CDKL5 kinase domain is active and capable of thiophosphorylating other proteins.

In this subchapter, we showed that by introducing the F89A gatekeeper mutation together with the C152A second-site rescue mutation, CDKL5[1-352] is analogue-sensitive. This means that it can use benzyl-ATPyS to thiophosphorylate itself and, more importantly, known substrate AMPH1 *in vitro*. We managed to purify large amounts of AS-CDKL5 from Sf9 insect cells that can be used for chemical genetic kinase-substrate mapping and further *in vitro* validation of novel CDKL5 substrate candidates.
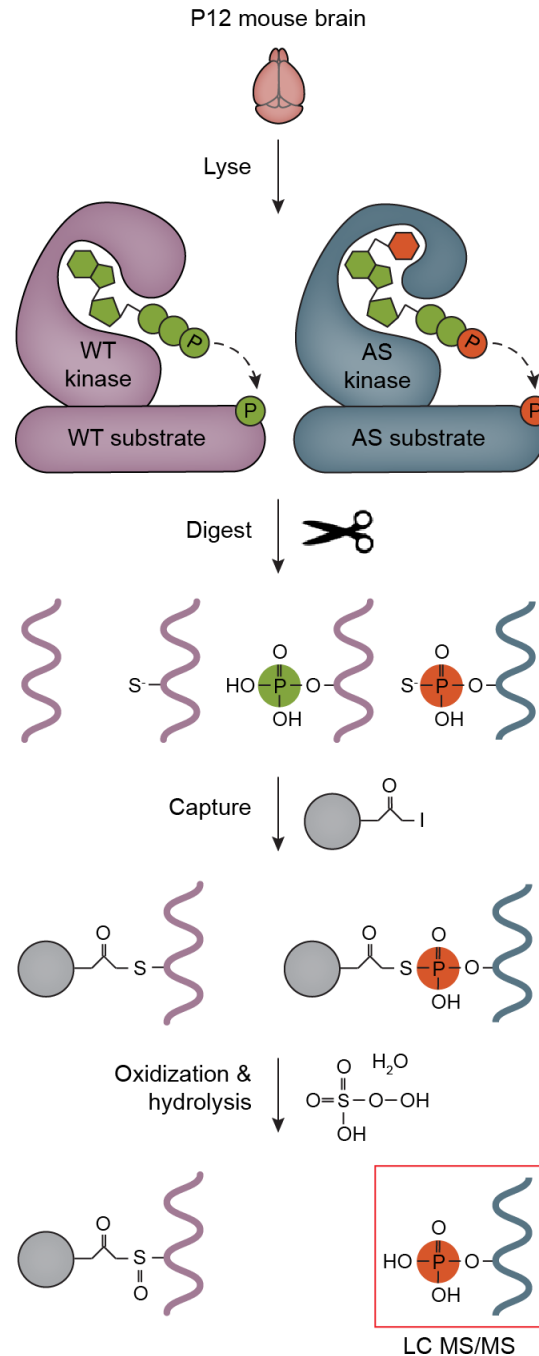
Figure 5: Chemical genetics kinase-substrate mapping.

Schematic of the chemical genetic substrate identification technique. Proteins in P12 mouse brain lysates are phosphorylated by WT kinases, but thiophosphorylated by AS-kinases. After trypsin digestion, thiol-containing peptides are captured by iodine-acetyl agarose beads. Only thiophoshorylated peptides are spontaneously hydrolysed upon oxidisation by Oxone and released from the beads. The purified peptides and phosphorylated sites are identified by mass spectrometry, and provide an unbiased and highly specific screen for direct phosphorylation targets of the AS-kinase of interest.

3.2 Chemical genetic kinase-substrate mapping

With the availability of large amounts of analogue-sensitive CDKL5, we could use chemical genetics to map direct substrates of CDKL5 in mouse brain lysate. We first had to validate and optimise this technique by using the identification of previously described NDR1 kinase substrates as controls. Afterwards we attempted to screen for novel putative sites that were specifically thiophosphorylated by analogue-sensitive CDKL5.

3.2.1 Known NDR1 substrates are validated by chemical genetics

Purified analogue-sensitive kinases are added to complex mouse brain protein lysates together with bulky ATPγS to specifically thiophosphorylate substrates. After trypsin digestion, thiophosphorylated peptides are captured by iodoacetyl agarose beads that bind all thiol-containing peptides. This includes all cysteine-containing peptides. However, oxidative hydrolysis induced by potassium peroxymonosulfate (Oxone) only releases the thiophosphate ester-linked peptides. The phosphopeptides released from the resin are then analysed by tandem mass spectrometry to identify substrate proteins and phosphorylation sites (Figure 5). All mass spectrometry data acquisition discussed in this chapter has been done by Helen Flynn and Bram Snijders in the Proteomics platform.

To verify if this complex method works in our hands, we used NDR1 kinase as a positive control. Five novel NDR1 substrates have previously been described using the same technique (Ultanir et al., 2012). We labelled 2.5 mg P12 mouse brain lysate with 3-5 μg analogue-sensitive or kinase-dead NDR1. Although the use of AS kinases already greatly reduces background compared to conventional techniques, KD negative controls are necessary to distinguish unspecific phosphorylated peptides. Only phosphorylation sites repeatedly identified in the eight AS samples and never in any of the four KD negative controls are considered specific to the kinase of interest and potential substrate candidates.

We detected four of the five previously identified NDR1 substrates in our samples (Table 6). Three of these NDR1 substrates were detected in almost all eight repeats and therefore show even higher sensitivity than in the original publication. Two other important statistics for quality control of mass spectrometry data are the localisation probability and the posterior error probability (PEP). The localisation probability is the confidence that the detected phosphorylation is on the correct residue. PEP is a statistical value for the probability that the observed peptide-spectrum match is incorrect. Both of these values show high confidence in our capability of detecting NDR1 kinase substrates. It is interesting to see that based on the known consensus sequence of NDR1 phosphorylation (HxRxxS) we also identified two novel NDR1 substrate candidates, Ras-associated and pleckstrin-homology domains-containing protein 1 (RAPH1) and Synergin γ (Table 6). Synergin γ is a protein that interacts with the

Protein	Position	Sequence	# of repeats		Loc. Prob.	PEP
			Our screen	Ultanir et al.		
AAK1	Ser635	**HRR**IL**S**D	8/8	7/8	1.000	1.51E-37
PI4Kβ	Ser277	**HQR**SK**S**D	8/8	2/8	0.998	1.64E-29
Rabin 8	Ser240	**HTR**NK**S**T	7/8	3/8	0.996	5.73E-16
Rab11FIP5	Ser307	**HKR**TY**S**D	2/8	1/8	1.000	6.62E-04
Pannexin 2	Ser514	**HTR**HF**S**L	0/8	2/8	n/a	n/a
RAPH1	Ser192	**HRR**TA**S**A	5/8	0/8	0.999	4.62E-06
Synergin γ	Ser1067	**HKR**SL**S**L	4/8	0/8	1.000	6.58E-04

Table 6: Validation of chemical genetic kinase-substrate mapping with NDR1.
Four of the five NDR1 substrates identified by Ultanir et al. are repeatedly detected with high confidence localisation probability and posterior error probability. Two novel NDR1 substrate candidates have also been identified based on the HxRxxS consensus sequence. Red = phosphorylated residue, bold = NDR1 consensus sequence.

Protein	Position	Sequence	# of repeats (> 2)		Loc. Prob. (> 0.750)	PEP (< 10E-05)
			Exp #1	Exp #2		
ARHGEF2	Ser122	RE**RP**T**S**A	3/4	3/4	0.998	9.75E-10
EB2	Ser222	PS**RP**S**S**A	3/4	0/4	0.859	2.77E-13
MAP1S	Ser786	PA**RP**S**S**A	3/4	0/4	0.834	3.48E-06
CDKL5	Tyr168	LSEGN**Y**T	0/4	3/4	0.993	6.45E-58
CDKL5	Tyr171	GNYTE**Y**V	4/4	4/4	1.000	6.52E-160

Table 7: Identification of novel direct CDKL5 substrate candidates.
Three putative CDKL5 substrate phosphorylation sites were detected with chemical genetics. The requirements set to distinguish potential CDKL5 substrates from unspecific background are shown in brackets. Two auto-phosphorylation sites of CDKL5 have also been confirmed. Red = phosphorylated residue, bold = potential CDKL5 consensus sequence.

adaptor protein 1 (AP1) clathrin-adaptor complex, which is known to function in vesicle trafficking like NDR1 itself.

Although these results show that we are capable of identifying analogue-sensitive kinase substrates with high confidence, we tried to optimise this by integrating isotope labelling methods. By labelling AS and KD samples with isotopes of different masses, we would have the advantage of combining pairs so that chemically identical peptides of different stable-isotope composition can be differentiated in a mass spectrometer. This gives you more confidence that signal detected in AS samples is certainly absent in KD controls, instead of simply not being picked up. However, exchanging mouse brain lysate for SILAC labelled mouse primary neurons resulted in only AP2-associated kinase 1 (AAK1) being identified in one of the two AS samples tested (data not shown). This suggests that lysates of primary neuronal cultures are inferior to mouse brain as a complex protein source. Instead of SILAC, stable-isotope dimethyl labelling can be done on mouse brain lysates after trypsin digestion. However, this method seemed to interfere with the covalent capture of thiophosphorylated peptides, as none of the NDR1 substrates were ever identified (data not shown). This means that traditional chemical genetic kinase-substrate mapping provides us with the most convincing results to identify novel phosphorylation sites of analogue-sensitive kinases.

3.2.2 Chemical genetics identifies novel CDKL5 substrate candidates

We were able to consistently identify NDR1 kinase substrates without additional isotope labelling, using only 3 µg kinase in 2.5 mg total protein of P12 mouse brain lysate. We therefore assumed that we could achieve similar results with a comparable CDKL5 substrate screen. Although it is important to keep in mind that AS-NDR1 contains extra mutations to make it constitutively active (Ultanir et al., 2012), and therefore it is difficult to compare the catalytic activity of the two kinases. CDKL5 is highly expressed throughout the brain of P12 mice, so potential substrates are also expected to be present at this age.

In the first attempt to identify novel CDKL5 substrates, an estimated 3 µg of CDKL5 was purified by HA-affinity from HEK293T cells. Substrate labelling of P12 mouse brain lysate was subsequently performed on the beads. Four AS and three KD repeats were analysed with mass spectroscopy, and between them 985 unique phosphorylation sites were detected. 59 of these sites repeated at least twice in the AS samples, but were completely absent in KD negative controls. However, only very few of these phosphorylation sites had PEP values low enough to be considered reliable (< 10E-05). We hypothesized that this was either a result of low kinase activity or a loss of peptides during covalent capture.

Higher amounts of CDKL5 purified from Sf9 insect cells were therefore used for a second experiment. Although due to its low concentration, we only succeeded to slightly
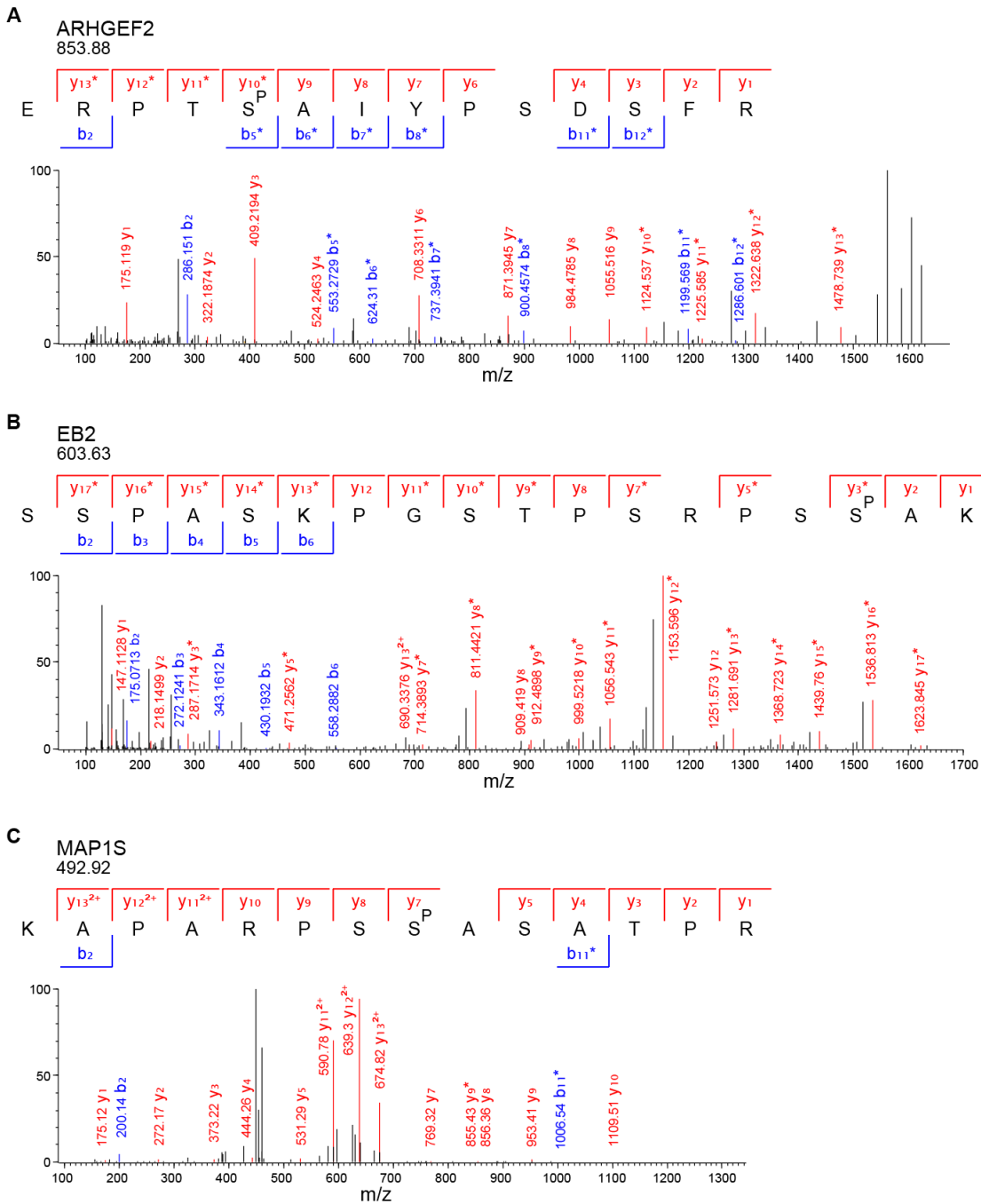
Figure 6: Mass spectra of putative CDKL5 substrate phosphorylation sites.

The individual spectra of the three potential sites directly phosphorylated by CDKL5 show the differences in coverage and explains the higher PEP value for MAP1S. (A) Best spectrum available for ARHGEF2 pS122 (B) Best spectrum available for EB2 pS222. (C) Best spectrum available for MAP1S pS786.

increase the amount of purified kinase to ~4-5 µg. After trypsin digestion, the samples were also acidified more to enhance the binding to C18 Sep Pak clean-up cartridges, and reduce the loss of peptides. In this experiment, four AS and four KD repeats resulted in 1136 unique phosphorylation sites with much lower PEP values over all. However, only 20 sites repeated in the AS samples and were absent in negative controls. The improved detection of peptides therefore seems to have come at the cost of losing AS specific thiophosphorylation. Most likely because the thiophosphate group is very labile towards acid-promoted hydrolysis (Hertz et al., 2010).

Combining the two CDKL5 experiments resulted in 11 unique phosphorylation sites with significant detection values (Loc. Prob. > 0.750, PEP < 10E-05) that repeated at least twice and were absent in KD negative controls. In order to further decrease the number of false positives, we compared these sites to the unspecific background we obtained in the NDR1 negative controls. This way we concluded that there were three putative sites likely to be phosphorylated by CDKL5: ARHGEF2 Ser122, EB2 Ser222 and MAP1S Ser786 (Table 7). The differences in detection values between the three target sites can be explained by the coverage of the peptides in mass spectrometry (Figure 6). This is most likely to be dependent on abundance of the substrate proteins and the ability to detect the specific peptides. These values are therefore not necessarily reflecting the physiological efficiency of the phosphorylation. Interestingly, this data also suggested that CDKL5 auto-phosphorylates tyrosines 168 and 171, which are located in the TEY activation loop. It is unknown if this concerns trans- or cis-phosphorylation.

What was striking is the similarity between the sequences of the three substrate phosphorylation sites, indicating that CDKL5 might have a preference for phosphorylating the RP(S/T)SA motif (Table 7). This is partially in agreement with the phosphorylation of AMPH1, where corresponding arginine and proline residues are critical for substrate recognition by CDKL5 (Katayama et al., 2015). All three phosphorylation sites are conserved in humans and could therefore be important in the pathogenic loss of CDKL5 kinase activity. Interestingly, the three potential CDKL5 substrates are all microtubule-binding proteins, which suggests a possible new direction for CDKL5 function.

In this subchapter, we have shown that we are capable of using chemical genetics to identify novel kinase substrates by validating known sites phosphorylated by NDR1 kinase. Performing the screen under similar conditions with AS-CDKL5 resulted in the convincing detection of three putative CDKL5 substrate phosphorylation sites. The shared phosphorylation motif between these sites indicate a possible consensus sequence for CDKL5. To validate these potential CDKL5 substrates and consensus sequence, direct phosphorylation of these sites has to be shown with *in vitro* kinase assays and mutagenesis.

Figure 7: ARHGEF2 is phosphorylated by CDKL5 only at serine 122 *in vitro*.
(A) 150 ng (50 nM) ARHGEF2 is incubated with 50 ng (40 nM) AS-CDKL5$^{1-352}$ for increasing lengths of time, and visualised by Western blotting (1:30,000 Thio-P) and coomassie blue (CBB) staining. (B) Quantification of A. Maximum phosphorylation is reached after 60 min. Sigmoidal curve fit: n = 2 repeats, R^2 = 0.921, error bars are SEM. (C) 150 ng ARHGEF2 is incubated for 60 min with increasing amounts of AS-CDKL5$^{1-352}$, and visualised as in A. (D) Quantification of C. Half of the maximum phosphorylation is reached with 20 ng CDKL5. Sigmoidal curve fit: n = 2 repeats, R^2 = 0.926, error bars are SEM. (E) 150 ng WT or phosphomutant ARHGEF2 is incubated with 20 ng (15 nM) KD or AS-CDKL5$^{1-352}$, and visualised as in A. (F) Quantification of E. Tukey's multiple comparison: n = 2 repeats, *** $p < 0.001$, error bars are SEM.

3.3   Validation of CDKL5 substrates *in vitro*

In vitro kinase assays similar to the ones performed with AMPH1, can be used to validate the targets found in the chemical genetic screen as direct substrates of CDKL5. In addition, it is possible to verify the correct phosphorylation site of the substrate by mutating the phosphorylated serine to an alanine, and create phosphomutant proteins that should not act as CDKL5 substrates.

3.3.1   CDKL5 phosphorylates ARHGEF2 only at serine 122

Full-length ARHGEF2 WT was cloned into pTriEx-6 and purified by its StrepII-tag from mammalian HEK293T cells. To establish an idea for the kinetics of ARHGEF2 phosphorylation by CDKL5, 150 ng (50 nM) ARHGEF2 WT was incubated with 50 ng (40 nM) AS-CDKL5[1-352] and benzyl-ATPγS for increasing lengths of time. We can see that maximum phosphorylation of ARHGEF2 is achieved after approximately 60 minutes (Figure 7A and B, 95% = 55.8 minutes, $R^2 = 0.921$). Like with AMPH1, we do not see the quick, sharp increase in ARHGEF2 phosphorylation expected from a high efficiency enzymatic reaction.

150 ng (50 nM) ARHGEF2 was then incubated with increasing amounts of AS-CDKL5[1-352] for 60 minutes. As we know that maximum phosphorylation is achieved with 50 ng of CDKL5 under these conditions, it makes it possible to determine the amount of CDKL5 necessary to reach half of the maximum phosphorylation. This would be the kinase:substrate ratio that gives the most contrast without saturating the signal, which is important to define for more sensitive phosphomutant experiments. In the case of 150 ng (50 nM) ARHGEF2, approximately 20 ng (15 nM) CDKL5 was necessary to phosphorylate half of the maximum signal in 60 minutes (Figure 7C and D, 50% = 20.5 ng CDKL5, $R^2 = 0.926$).

ARHGEF2 S122A was purified the same way as WT ARHGEF2. This phosphomutant form of ARHGEF2 was expected not to be phosphorylated by CDKL5, as the identified serine 122 is the only site in the protein containing the suspected RPxS consensus sequence. 150 ng (50 nM) ARHGEF2 WT or S122A was therefore incubated with 20 ng (15 nM) analogue-sensitive or kinase-dead CDKL5[1-352] for 60 minutes. CDKL5-dependent phosphorylation was indeed completely absent in phosphomutant ARHGEF2 (Figure 7E and F, KD: 9.5 ± 3.50%, WT: 100 ± 1.00%, S122A: 13.5 ± 2.50%, n = 2, p = 0.0003, p = 0.57, p = 0.0003), confirming that ARHGEF2 is phosphorylated by small amounts of CDKL5 only at serine 122 *in vitro*. Experiments were only repeated twice due to the obvious differences in ARHGEF2 phosphorylation which were highly significant with n = 2.
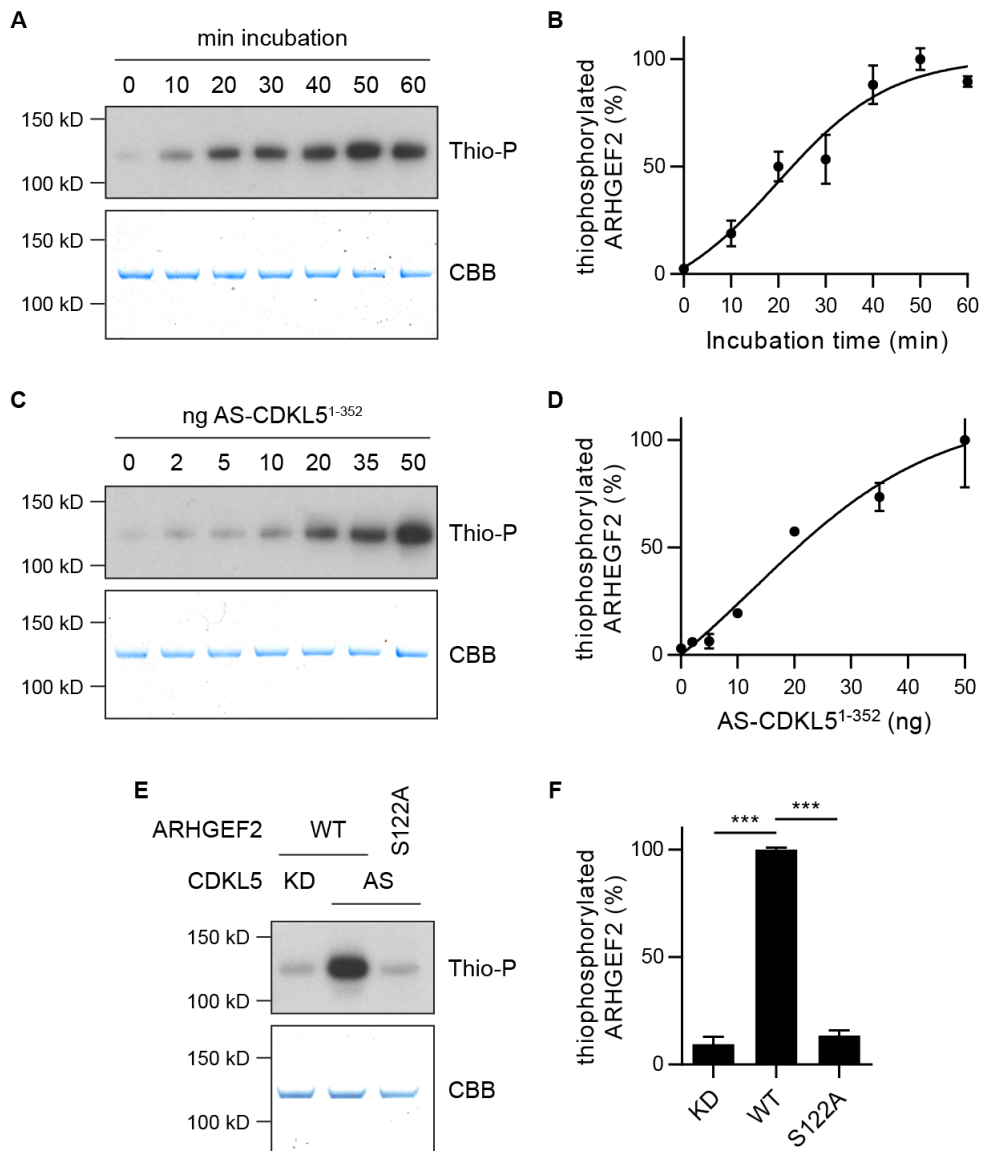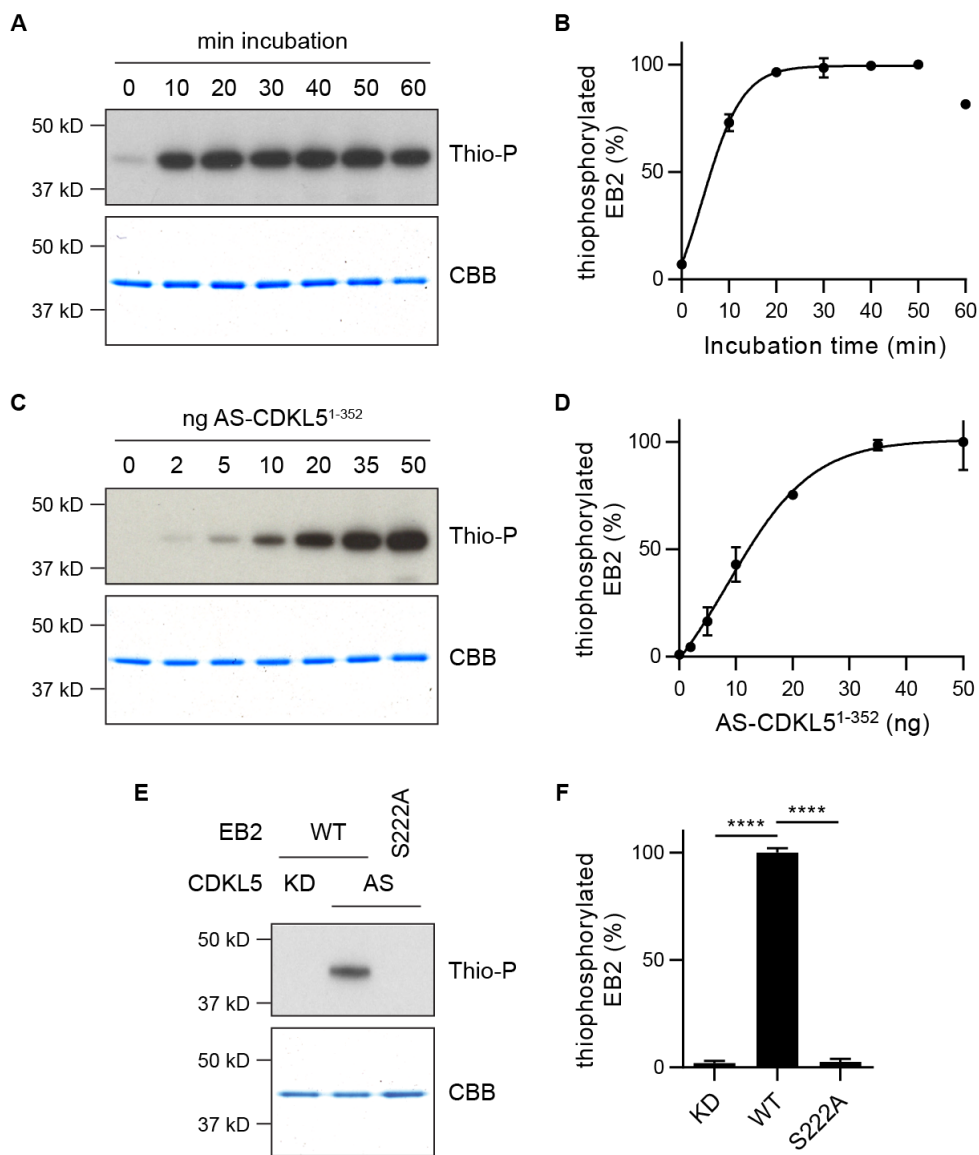
Figure 8: EB2 is phosphorylated by CDKL5 only at serine 222 *in vitro*.

(A) 200 ng (170 nM) EB2 is incubated with 50 ng (40 nM) AS-CDKL5[1-352] for increasing lengths of time, and visualised by Western blotting (1:30,000 Thio-P) and coomassie blue (CBB) staining. (B) Quantification of A. Maximum phosphorylation is reached after 20 min. Sigmoidal curve fit: n = 2 repeats, R^2 = 0.994, error bars are SEM. (C) 200 ng EB2 is incubated for 30 min with increasing amounts of AS-CDKL5[1-352], and visualised as in A. (D) Quantification of C. Half of the maximum phosphorylation is reached with 10 ng CDKL5. Sigmoidal curve fit, n = 2 repeats, R^2 = 0.974, error bars are SEM. (E) 200 ng WT or phosphomutant EB2 is incubated with 10 ng (8 nM) KD or AS-CDKL5[1-352], and visualised as in A. (F) Quantification of E. Tukey's multiple comparison: n = 2 repeats, **** $p < 0.0001$, error bars are SEM.

3.3.2   CDKL5 phosphorylates EB2 only at serine 222

Full-length EB2 WT was cloned into pTriEx-6 and purified by its StrepII-tag from mammalian HEK293T cells. 200 ng (170 nM) EB2 WT was incubated with 50 ng (40 nM) AS-CDKL5$^{1-352}$ and benzyl-ATPγS for increasing lengths of time. Compared to AMPH1 and ARHGEF2, we did observe a sharp increase in EB2 phosphorylation, quickly reaching a maximum in under 30 minutes. This indicates that EB2 phosphorylation by CDKL5 is a more efficient enzymatic reaction (Figure 8A and B, 95% = 18.5 minutes, R^2 = 0.994).

200 ng (170 nM) EB2 was then incubated with increasing amounts of AS-CDKL5$^{1-352}$ for 30 minutes to define the optimal kinase:substrate ratio. We see that in the case of 200 ng (170 nM) EB2, only ~10 ng (8 nM) CDKL5 is necessary to reach half of the maximum EB2 phosphorylation in 30 minutes (Figure 8C and D, 50% = 12.2 ng, R^2 = 0.974).

Like EB2 WT, StrepII-tagged EB2 S222A was purified from HEK293T cells. Serine 222 is the only RPXpS-containing residue in the protein and therefore hypothesized to be the only CDKL5 phosphorylation site in EB2. When 200 ng (170 nM) EB2 S222A was incubated with 10 ng (8 nM) analogue-sensitive CDKL5$^{1-352}$, we indeed see a complete loss of phosphorylation compared to WT EB2 (Figure 8E and F, KD: 2.0 ± 1.00%, WT: 100 ± 2.00%, S222A: 2.5 ± 1.50%, n = 2, p < 0.0001, p = 0.97, p < 0.0001). This confirms that small amounts of CDKL5 phosphorylates EB2 only at serine 222 *in vitro*. Experiments were only repeated twice due to the obvious differences in EB2 phosphorylation which were highly significant with n = 2.

3.3.3   CDKL5 phosphorylates MAP1S at both serine 786 and 812

Although MAP1S gets proteolitically cleaved into a heavy and light chain, full-length MAP1S WT was cloned into pTriEx-6 and purified by its StrepII-tag from mammalian HEK293T cells. 150 ng (50 nM) MAP1S WT was incubated with 50 ng (40 nM) AS-CDKL5$^{1-352}$ and benzyl-ATPγS for increasing lengths of time. Like EB2, MAP1S phosphorylation by CDKL5 is an efficient enzymatic reaction. We observe a similar sharp increase in MAP1S phosphorylation over time that quickly reaches a maximum in under 30 minutes (Figure 9A and B, 95% = 22.2 minutes, R^2 = 0.909).

150 ng (50 nM) MAP1S was then incubated with increasing amounts of AS-CDKL5$^{1-352}$ for 30 minutes. For 150 ng (50 nM) MAP1S, half of the maximum phosphorylation is achieved with only ~5 ng (4 nM) CDKL5 (Figure 9C and D, 50% = 7.0 ng, R^2 = 0.977), confirming MAP1S as a highly efficient CDKL5 substrate *in vitro*.

A second sequence containing the alleged CDKL5 phosphorylation motif was identified in the MAP1S protein. Besides serine 786, which was found to be phosphorylated by CDKL5 in the chemical genetic screen, serine 812 is a potential target of CDKL5 as well. MAP1S serine 812 contains a very similar sequence as the other CDKL5 phosphorylation sites we identified
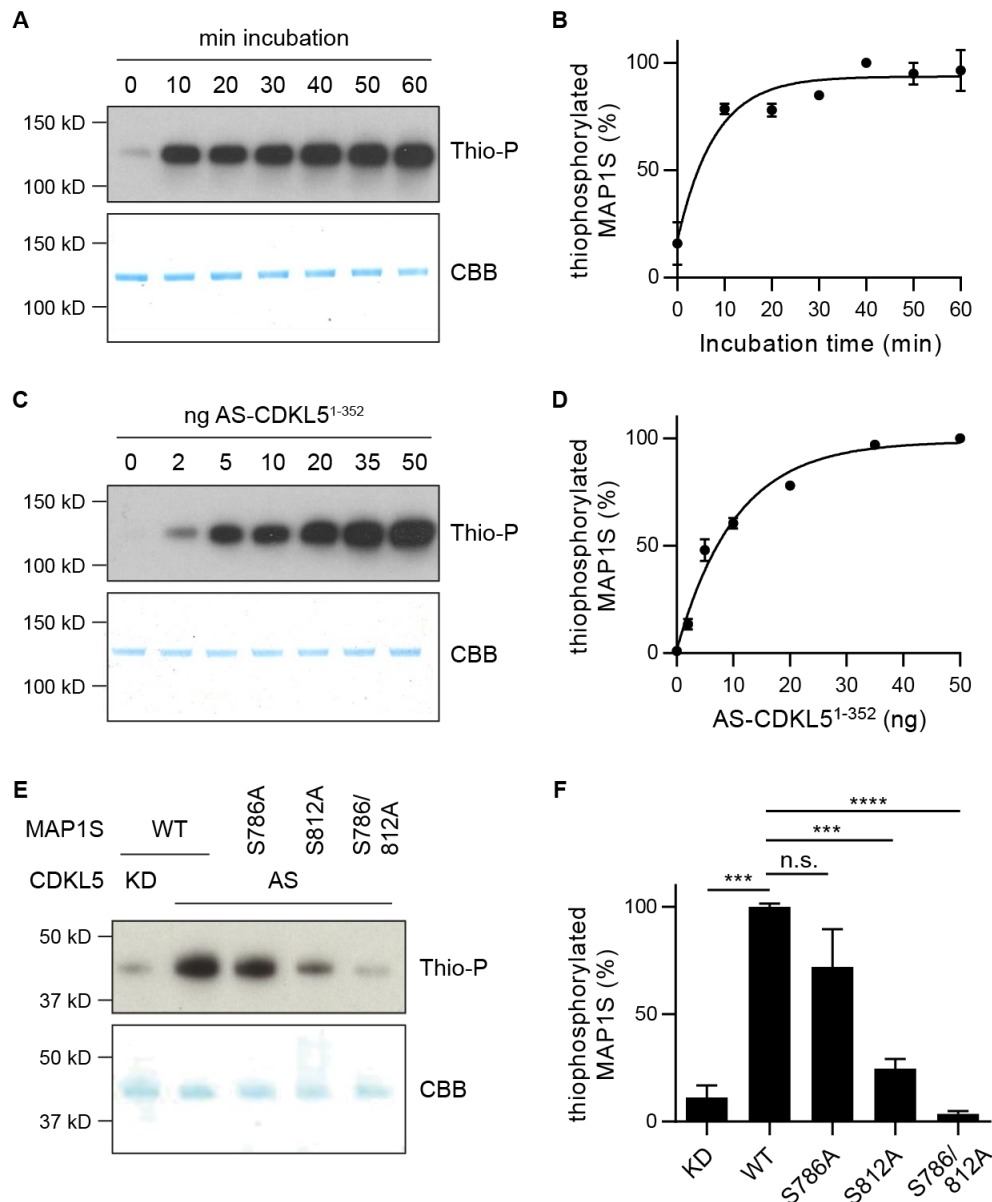
Figure 9: MAP1S is phosphorylated by CDKL5 at serine 786 and 812 *in vitro*.
(A) 150 ng (50 nM) MAP1S is incubated with 50 ng (40 nM) AS-CDKL5$^{1-352}$ for increasing lengths of time, and visualised by Western blotting (1:30,000 Thio-P) and coomassie blue (CBB) staining. (B) Quantification of A. Maximum phosphorylation is reached after 30 min. Sigmoidal curve fit: n = 2 repeats, R^2 = 0.909, error bars are SEM. (C) 100 ng MAP1S is incubated for 30 min with increasing amounts of AS-CDKL5$^{1-352}$, and visualised as in A. (D) Quantification of C. Half of the maximum phosphorylation is reached with 5 ng CDKL5. Sigmoidal curve fit: n = 2 repeats, R^2 = 0.977, error bars are SEM. (E) 100 ng WT or phosphomutant MAP1S is incubated with 5 ng (4 nM) KD or AS-CDKL5$^{1-352}$, and visualised as in A. (F) Quantification of E. Dunnett's multiple comparison: n = 3 repeats, n.s. = not significant, *** $p < 0.001$, **** $p < 0.0001$, error bars are SEM.

(**RPL*S*A**). CDKL5 is therefore expected to be capable of phosphorylating MAP1S on both sites. Single and double phosphomutant forms of MAP1S were therefore purified from HEK293T cells.

150 ng (50 nM) MAP1S WT, S786A, S812A or S786/812A was incubated with 5 ng (4 nM) analogue-sensitive or kinase-dead CDKL5[1-352] for 30 minutes. CDKL5 indeed phosphorylates both serines in MAP1S, as the phosphorylation is only completely absent in the double phosphomutant (Figure 9E). Surprisingly, even though it was not detected in the chemical genetic screen, CDKL5 seems to have a clear preference for phosphorylating MAP1S serine 812 *in vitro*. Only ~25% of MAP1S phosphorylation is accounted for serine 786 (Figure 9F, KD: 11.3 ± 5.49% of WT, $p = 0.0001$, S786A: 72.0 ± 17.6% of WT, $p = 0.13$, S812A: 24.7 ± 4.49% of WT, $p = 0.0003$, S786/812A: 3.67 ± 1.20% of WT, $p = 0.0001$, $n = 3$). These findings confirm that MAP1S is phosphorylated by small amounts of CDKL5 at both serine 786 and serine 812 *in vitro*. It also highlights the importance of the identification of the RPxS motif as a consensus sequence for CDKL5 phosphorylation.

In this subchapter, we have shown that, *in vitro*, CDKL5 is capable of directly phosphorylating all putative substrates we identified with chemical genetics. With the identification of a second MAP1S phosphorylation site containing the same consensus sequence, it has clearly emerged that CDKL5 has a strong preference for RPxS phosphorylation. This *in vitro* data also suggests that CDKL5-dependent phosphorylation of EB2 and MAP1S is more efficient than AMPH1 and ARHGEF2 phosphorylation. However, it is very difficult to draw definite conclusions about phosphorylation efficiency without comparing substrates in the exact same conditions. It is possible that the higher molarity of EB2, and the double phosphorylation of MAP1S are the underlying reasons for the observed differences. It is therefore crucial to validate these *in vitro* substrates of CDKL5 under physiological conditions as well.

3.4   Validation of CDKL5 substrates *in vivo*

Even though *in vitro* substrates tell us a lot about the function and properties of a kinase, these assays are performed in a fabricated setting. *In vivo* experiments are therefore necessary to determine if CDKL5 also phosphorylates our newly identified substrates in physiological conditions. By using phospho-specific antibodies we can study these interactions in mammalian cell lines, mouse brain tissue and mature neurons derived from induced pluripotent stem cells of patients with CDKL5 deficiency disorder.

3.4.1   CDKL5 phosphorylates ARHGEF2 and MAP1S in cell culture

Phospho-specific antibodies against the four identified sites phosphorylated *in vitro* by CDKL5, were generated by Covalabs. CDKL5 and its substrates were overexpressed in mammalian HEK293T cells in order to achieve two goals: First, to assess if the new antibodies specifically recognise phosphorylated substrate. Second, to determine if full-length CDKL5 is capable of phosphorylating its substrates within cell culture conditions. Our inability to purify full-length analogue-sensitive CDKL5 was so-far forcing us to use the truncated kinase domain in previous experiments. This technical limitation can now be avoided.

FLAG-tagged CDKL5 KD or WT was co-expressed with HA-tagged ARHGEF2 WT or S122A in HEK293T cells, lysed and probed with the ARHGEF2 pS122-specific antibody. We concluded that the pS122 antibody is highly specific, as there is no observed band for the phosphomutant form of ARHGEF2 (Figure 10A). Excitingly, there is a significant increase in ARHGEF2 S122 phosphorylation when co-expressed with active CDKL5, confirming it as a CDKL5 substrate within cell culture conditions.

FLAG-tagged CDKL5 KD or WT was also co-expressed with HA-tagged EB2 WT or S222A in HEK293T cells, lysed and probed with the EB2 pS222-specific antibody. We can conclude that the pS222 antibody is highly specific as well, as there is no observed band for phosphomutant EB2 (Figure 10B). In contrast to ARHGEF2 however, we do not see any difference in EB2 S222 phosphorylation between co-expression with KD or WT CDKL5. This is likely to be an effect of the high endogenous phosphorylation of this site already present without active CDKL5. It is therefore possible that endogenous CDKL5 or other kinases phosphorylate this site as well.

Both identified MAP1S phosphorylation sites are located on the light chain (LC) of the protein. HA-tagged MAP1S light chain WT or S786/812A was therefore co-expressed with FLAG-tagged CDKL5 KD or WT in HEK293T cells, lysed and probed with MAP1S pS786- and pS812-specific antibody. We can conclude that both the pS786 and pS812 antibodies are highly specific, as neither of them show a band for phosphomutant MAP1S LC (Figure 10C). Interestingly, CDKL5-dependent MAP1S phosphorylation follows the observations of both
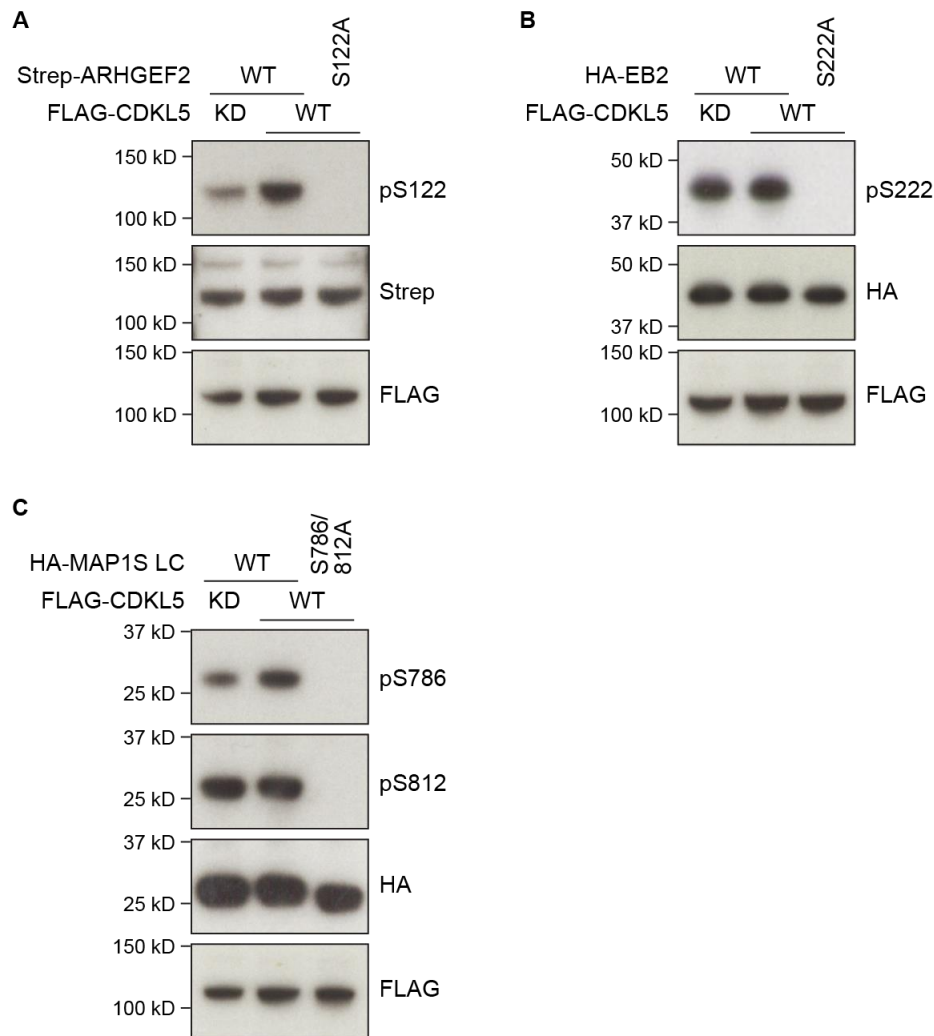
Figure 10: CDKL5-dependent phosphorylation in HEK293T cells.

FLAG-CDKL5 was co-expressed with StrepII-ARHGEF2, HA-EB2 or HA-MAP1S LC in HEK293T cells, and lysed. (A) ARHGEF2 S222 phosphorylation was visualised by Western blotting (1:2000 ARHGEF2 pS122 and FLAG, 1:1000 Strep). pS122 is phospho-specific and increased with active CDKL5. (B) EB2 S222 phosphorylation was visualised by Western blotting (1:2000 EB2 pS222, HA (Roche) and FLAG). pS222 is phospho-specific, but not increased with active CDKL5. (C) MAP1S S786 and S812 phosphorylation was visualised by Western blotting (1:2000 MAP1S pS786, MAP1S pS812, HA (Roche) and FLAG). pS786 is phospho-specific, and increased with active CDKL5. pS812 is phospho-specific, but not increased with active CDKL5.

ARHGEF2 and EB2. There is a clear increase in S786 phosphorylation when co-expressed with active CDKL5, but a difference in S812 phosphorylation between active and kinase-dead CDKL5 is lacking. High endogenous MAP1S S812 phosphorylation is believed to be the reason for this as well.

It was very surprising that the two sites that seemed most efficiently phosphorylated by CDKL5 *in vitro*, do not show any CDKL5-dependent phosphorylation in cell culture conditions. We believed that this was due to the high activity of endogenous CDKL5, or another kinase capable of phosphorylating these sites. However, CDKL5 shRNA-mediated knockdown did not result in a decrease of endogenous EB2 or MAP1S phosphorylation (data not shown). Although this was expected, as antibodies do not indicate the presence of CDKL5 in our HEK293T cells. In mitotic cells, EB2 has been shown to possibly be phosphorylated by Aurora B or CDK1 on serine 222 (Iimori et al., 2016), but inhibition of Aurora kinases and CDKs by hesperadin and roscovitine respectively, did not result in reduced phosphorylation either (data not shown). At this stage, CDKL5-dependent phosphorylation in cell culture can therefore only be ascribed to ARHGEF2 and MAP1S S786, and not EB2 and MAP1S S812.

3.4.2   EB2 and MAP1S phosphorylation is strongly reduced in Cdkl5 KO mouse brain

The most convincing evidence for kinase substrate phosphorylation comes from *in vivo* validation under physiological conditions. The previous experiments have already resulted in considerable substrates and the right tools to measure their phosphorylation. So for final confirmation, the phospho-specific antibodies can be used to detect endogenous CDKL5-dependent phosphorylation in a genetic Cdkl5 KO mouse model. Reduced phosphorylation in Cdkl5 KO mice will be considered definite proof of the identified sites being genuine CDKL5 substrates under physiological conditions.

We dissected out the cortex of five Cdkl5 +/Y and five Cdkl5 -/Y mice at postnatal day 20. We and others have seen CDKL5 protein expression levels plateauing at P20 in mouse cortex and therefore expected the strongest substrate phosphorylation at this age (Rusconi et al., 2008). By only using males, we can make use of the X-chromosomal location of the Cdkl5 gene and ensure that WT and KO mice are littermates. This minimises the biological variation between replicates. Lysed cortices were normalised for tubulin expression, and subsequently probed for all four phospho-specific antibodies.

To our excitement, we observe a very strong reduction in EB2 S222 and MAP1S S812 phosphorylation in the cortex of Cdkl5 -/Y mice (Figure 11A). The amount of phosphorylation per total protein is calculated to quantify these results, and shows that MAP1S S812 phosphorylation in Cdkl5 KO mice is reduced to ~10% of the WT level (Figure 11B, KO: 11.4 ± 1.33% of WT, n = 5, p < 0.0001). The three isoforms of EB2 run at two different sizes. In Cdkl5
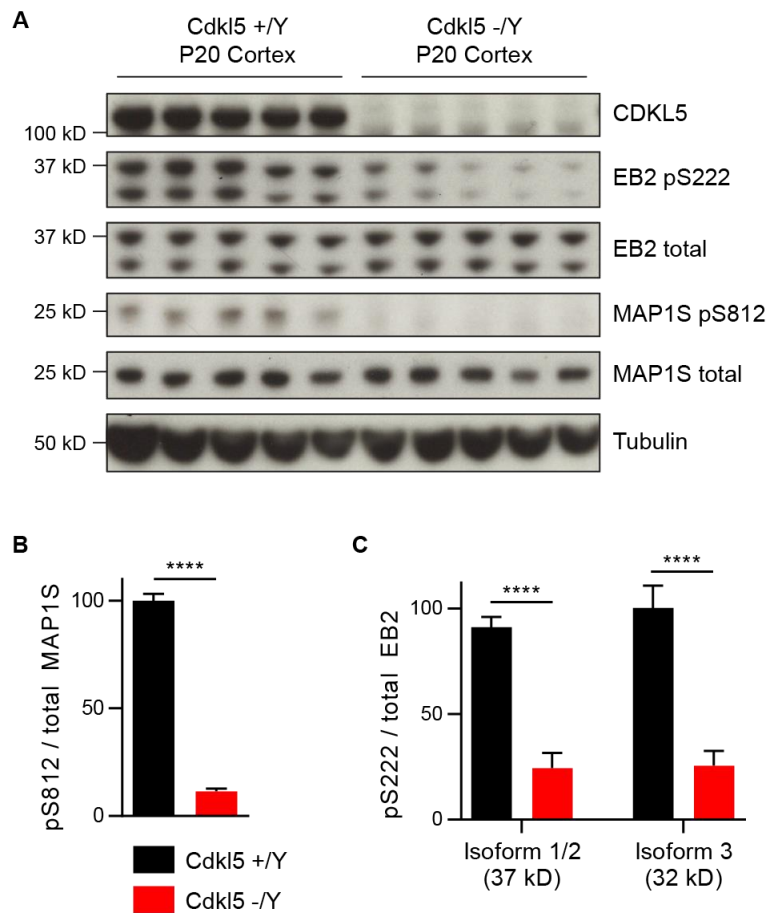
Figure 11: EB2 and MAP1S phosphorylation is strongly reduced in Cdkl5 -/Y brains.

(A) Phosphorylation of CDKL5 substrates in lysates of WT and Cdkl5 KO cortices was visualised by Western blotting (1:1000 CDKL5 (Abcam), EB2 total and MAP1S total, 1:2000 EB2 pS222, 1:500 MAP1S pS812, 1:50,000 tubulin (Sigma)). Lysate was 5x more concentrated to detect MAP1S pS812. Compared to Cdkl5 +/Y, EB2 pS222 and MAP1S pS812 is strongly reduced in Cdkl5 -/Y mouse cortical lysates. (B) Quantification of MAP1S pS812 in mouse cortex. WT normalised to 100%. Student's t-test: n = 5 animals per genotype, **** p < 0.0001, error bars are SEM. (C) Quantification of EB2 pS222 of both isoforms in mouse cortex. Sidak's multiple comparison: n = 5 animals per genotype, **** p < 0.0001, error bars are SEM.

-/Y cortex, S222 phosphorylation of both isoforms 1/2 (37 kDa) and isoform 3 (32 kDa) is reduced to ~25% of WT levels (Figure 11C, KO: isoform 1/2: 22.2 ± 6.50% of WT, p < 0.0001, isoform 3: 25.6 ± 7.00% of WT, p < 0.0001, n = 5). CDKL5 does not seem to have a preference for a specific isoform of EB2.

Unfortunately, we were unable to observe any specific signal for ARHGEF2 S122 and MAP1S S786 phosphorylation (data not shown). Based on the HEK293T experiment, we know that all antibodies are highly specific and have roughly the same efficacy. This indicates that ARHGEF2 S122 and MAP1S S786 phosphorylation abundance is too low in P20 mouse brain to be detected. This does not rule out that it is not happening though. In a similar way we can deduce that EB2 S222 phosphorylation is much more abundant then MAP1S S812 phosphorylation, as EB2 phosphorylation is shown in a 5-fold dilution of the protein lysate, and actually produces much stronger signal than MAP1S pS812. These findings confirm EB2 and MAP1S as substrates of endogenous CDKL5 under physiological conditions.

3.4.3   EB2 phosphorylation is strongly reduced in patient-derived neurons

As mentioned before, all four newly identified CDKL5 phosphorylation sites are conserved in humans (Table 8), and could therefore play important roles in the pathogenic pathways leading to CDKL5 deficiency disorder. To validate if the loss of EB2 and MAP1S phosphorylation in mice translates to human patients, we managed to obtain lysates of patient-derived mature neurons. Induced pluripotent stem cells were derived from fibroblasts of three different patients with CDKL5 deficiency disorder, and differentiated into mature neurons by the Muotri lab at UCSD. Neurons generated from the patients' parents were used as positive controls.

When we probed lysates of the human neurons with EB2 pS222, we oberved a clear reduction of phosphorylated EB2 in all three patient samples compared to their parent control (Figure 12A). Especially striking is the almost complete loss of EB2 phosphorylation in the two male patients. These patients contain a R59X mutation or a small deletion in their only copy of Cdkl5, which are assumed to result in a complete loss of CDKL5 kinase activity. This is beautifully depicted by the reduction of EB2 phosphorylation to ~15% of the parental controls in hemizygous males (Figure 12B), and strongly indicates that CDKL5 is the main kinase phosphorylating EB2 serine 222 in human neurons. This is also supported by the ~50% of EB2 phosphorylation remaining in the heterozygous female, still possessing one intact Cdkl5 allele (Figure 12B). Like in mice, both sizes of EB2 isoforms are phosphorylated by CDKL5 in a similar fashion. The low number of samples and the difference between hemizygous and heterozygous patients, makes it unqualified for statistical analyses at this stage.

Unfortunately, MAP1S phosphorylation was not detected in patient iPSC-derived mature neurons (data not shown). This is neither the case for cultured mouse primary neurons,

	Mouse			Human	
Protein	Position	Sequence		Position	Sequence
ARHGEF2	Ser122	RE**RP**T**S**A		Ser122	RE**RP**S**S**A
EB2	Ser222	PS**RP**S**S**A		Ser223	PS**RP**S**S**A
MAP1S	Ser786	PA**RP**S**S**A		Ser871	LA**RP**N**S**R
MAP1S	Ser812	RN**RP**L**S**A		Ser900	AS**RP**L**S**A

Table 8: Novel CDKL5 phosphorylation sites are conserved in humans.

All four newly identified phosphorylation sites have their RPxS consensus sequence conserved in the human proteome, signifying the possible importance of this motif. Red = phosphorylated residue, bold = CDKL5 consensus sequence.
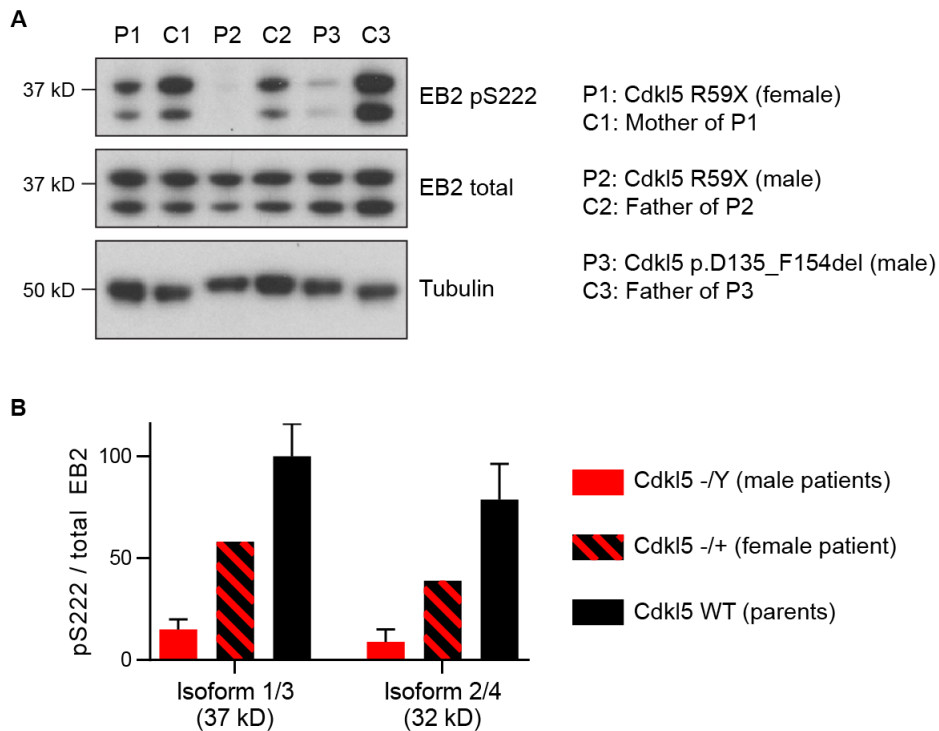
Figure 12: EB2 phosphorylation is strongly reduced in CDKL5 deficiency disorder.

(A) Phosphorylation of EB2 S222 in iPSC-derived neurons of patients with CDKL5 deficiency disorder was visualised with Western blotting (1:2000 EB2 pS222, 1:1000 EB2 total, 1:50,000 tubulin). All patient neurons show strong reductions in EB2 S222 phosphorylation compared to parent controls. (B) Quantification of A per genotype. Both EB2 isoforms show similar loss of phosphorylation dependent on the hemi- or heterozygous disruption of Cdkl5. Hemizygous: n = 2 patients, heterozygous: n = 1 patient, control: n = 3 parents, error bars are SEM. Statistical analysis is omitted due to the low sample number.

and therefore thought to be a result of using dissociated neurons instead of actual tissue. Small differences in the abundance of MAP1S phosphorylation between these two systems could be crucial and a reason that it remains under the detection limit. We therefore cannot conclude if CDKL5-dependent phosphorylation of MAP1S S812 translates to humans or not. However, EB pS222 has proven to be highly abundant and almost completely dependent on CDKL5 in both mice and humans.

3.4.4 Global phosphoproteomics confirm EB2 as CDKL5's main substrate

With the identification of RPxS as a CDKL5 consensus sequence, we have a much better grasp of possible direct CDKL5 substrates. This could potentially be used to make a better selection of targets from differences in the phosphoproteome between WT and Cdkl5 KO mice. Global phosphoproteomics will show changes in phosphorylation anywhere downstream of CDKL5 loss-of-function, but now we are able to assume that those sites containing the consensus sequence, are likely direct CDKL5 substrates.

Primary cortical cultures were made at embryonic day (E)16.5 from three Cdkl5 -/Y and three Cdkl5 +/Y mice. Each of these primary cultures was grown in K4R6 'light' or K8R10 'heavy' SILAC media in the presence of araC to limit glia division, and additional proline to prevent arginine-to-proline conversion. After 12 days-in-vitro the cultures were lysed and combined into six WT/KO pairs with opposite isotope weights. After trypsin digestion and TiO_2 phosphopeptide enrichment, ~8000 phosphorylation sites were detected by LC MS/MS (Figure 13). 72 of them contained the RPxS motif and repeated at least twice, but only three detected phosphorylation sites showed a significant difference between Cdkl5 +/Y and -/Y neurons.

In confirmation with our previous findings, EB2 S222 showed the highest reduction of phosphorylation in Cdkl5 KO mice. Interestingly, although not containing the RPxS consensus sequence, EB2 S218 and S221 phosphorylation were also found to be highly reduced. This can either mean that indirect phosphorylation of these sites is dependent on EB2 S222 phosphorylation, or that CDKL5 is also capable of directly phosphorylating these sites *in vivo*. Either way, these results independently corroborate EB2 phosphorylation being severely reduced upon loss of CDKL5 activity.

MAP1S pS786 was another RPxS-containing site which phosphorylation was consistently reduced in Cdkl5 -/Y neurons, and therefore confirmed as an endogenous *in vivo* phosphorylation site of CDKL5 as well. Only a small change and low peak intensities were observed for this site, indicating that the low abundance of this phosphorylation has probably been the reason for the phospho-specific antibody not being able to detect it before. This also argues that MAP1S pS812 is difficult to detect with mass spectrometry, as we have seen compelling evidence that it is more efficiently phosphorylated by CDKL5 than S786, but never identified in any of our mass spectrometry-based screens. An *in silico* trypsin digest of MAP1S
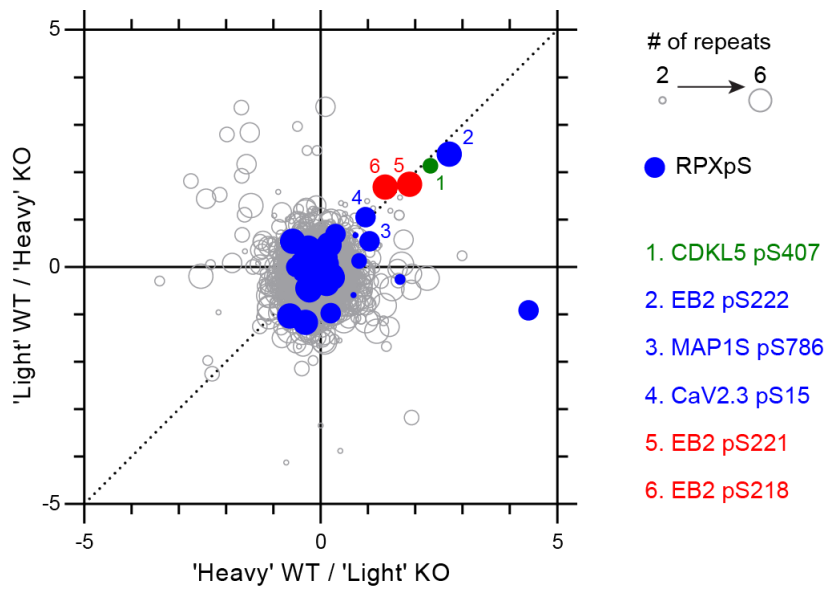
Figure 13: Global changes in the phoshoproteome of Cdkl5 KO neurons.

Mass spectrometry analysis of SILAC labelled primary cortical cultures from Cdkl5 +/Y and -/Y mice was used to determine differences in CDKL5-dependent protein phosphorylation. The origin marks no change in phosphorylation between the two genotypes. Phosphorylated sites along the dotted line are either upregulated (bottom left) or downregulated (top right) in Cdkl5 KO neurons. Significantly downregulated CDKL5 phosphorylation is labelled in green, and considered a positive marker. Sites containing the CDKL5 consensus sequence are labelled in blue and possible direct substrates. Two other strongly reduced EB2 phosphorylation sites are labelled in red. The size of a circle represents the number of samples in which the phosphorylated site was detected. The axes represent the base 2 logarithms of the ratio of each detected protein. N = 3 animals per genotype, n = 2 replicates with switched isotope labelling per animal.

indeed revealed that there are multiple cleavage sites around serine 812, probably making the resulting peptide too short to detect with LC MS/MS.

The third site following the RPxS consensus sequence, while being reduced in Cdkl5 -/Y neurons, is a novel CDKL5 substrate candidate. CaV2.3 is an R-type voltage-dependent calcium channel (VDCC). VDCCs are heavily implicated in epilepsies, sleep and pain sensation, and could therefore play an important role in the display of these symptoms in CDKL5 deficiency disorder (Weiergraber et al., 2006). Its phosphorylated serine 15 is located in the N-terminal loop of the channel which regulates its modulation by G proteins (Page et al., 1998). However, evidence for direct CaV2.3 phosphorylation by CDKL5 is still very limited, and this interaction has not been validated any further yet.

In this subchapter, we have shown that all three *in vitro* substrates of CDKL5[1-352] can be phosphorylated by full-length CDKL5 outside of a test tube. ARHGEF2 has only been validated as an *in vivo* substrate of CDKL5 when overexpressed in mammalian cell lines. This means that endogenous phosphorylation levels of ARHGEF S122 are either very low or not present at all under more physiological circumstances. Endogenous CDKL5-dependent phosphorylation of EB2 and both sites of MAP1S has been validated in Cdkl5 KO mouse neurons in multiple ways. We can therefore claim with great certainty that our newly identified targets of CDKL5 are endogenous and *in vivo* substrates. To our excitement, the loss of EB2 phosphorylation is also easily detected in neurons derived from patients with CDKL5 deficiency disorder. This gives EB2 phosphorylation the potential to be a valuable biomarker for CDKL5 activity.

3.5 CDKL5 is regulated by neuronal activity during development

Although loss of CDKL5 activity is the main pathogenic cause for CDKL5 deficiency disorder, a clear understanding of how CDKL5 activity is regulated is lacking. This is mainly because there are currently no reliable biomarkers for CDKL5 activity. It has therefore been difficult to study upstream processes and function of CDKL5 using anything other than total protein levels. However, kinase activity is generally much more likely to be regulated by conformational changes independent of protein expression or degradation (Nolen et al., 2004).

We have shown that endogenous EB2 and MAP1S phosphorylation is almost completely dependent on CDKL5 in the mouse brain. Especially EB2, which phosphorylation of serine 222 is easily detectable and absent in patient-derived neurons, has the potential of being a great biomarker for CDKL5 activity. By using these antibodies, we can measure changes in CDKL5 activity during neuronal development, and determine if neuronal activity has an effect on CDKL5 substrate phosphorylation.

3.5.1 CDKL5 activity is downregulated during neuronal development

In the mouse brain, CDKL5 mRNA and protein levels have been described by others to be upregulated during early postnatal development and maintains to be expressed during young adulthood (Hector et al., 2016; Rusconi et al., 2008). The temporal expression pattern of CDKL5 has been one of the main reasons for us to validate novel CDKL5 substrates in 20-day-old mice, but can be seen as contradicting the disease symptoms, which start immediately after birth. We therefore hypothesized that CDKL5 activity is regulated during neuronal development. CDKL5-dependent phosphorylation of EB2 and MAP1S could show a different temporal pattern than CDKL5 expression, and would be more representative of CDKL5 kinase activity.

Cortices of WT and Cdkl5 KO mice were harvested at four different ages of postnatal development, lysed and probed for CDKL5 and phosphorylated EB2 and MAP1S (Figure 14A). As expected, we observed a strong increase in total CDKL5 protein expression during postnatal development that plateaus around P20. This quite closely follows the temporal expression pattern of Cdkl5 mRNA in the whole mouse brain as described by Hector et al.

Interestingly, CDKL5-dependent EB2 and MAP1S phosphorylation show the complete opposite pattern (Figure 14A and B). EB2 is very strongly phosphorylated at serine 222 at P4, although there is also more residual phosphorylation present in Cdkl5 KO mice at this age, indicating another kinase phosphorylates the same site. During development, EB2 pS222 severely reduces, so that in P50 young adults, less than 25% of the CDKL5-dependent EB2 phosphorylation remains. Total EB2 protein levels remain constant during mouse neuronal development, and are not affected in Cdkl5 KO mice at any age.
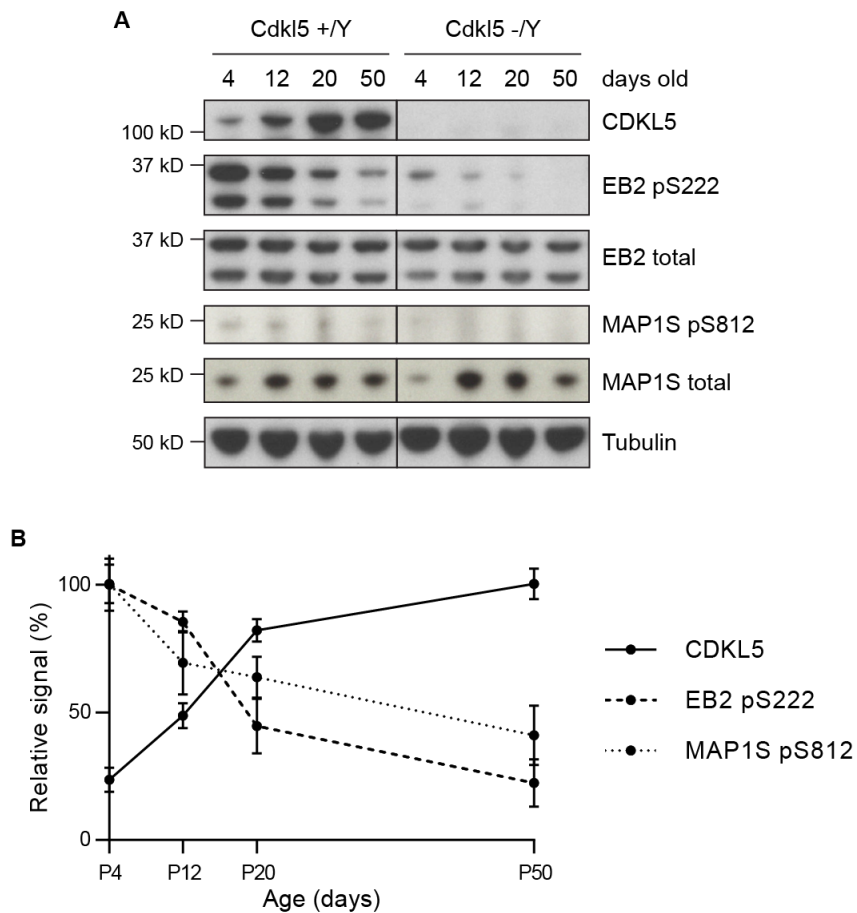
Figure 14: EB2 and MAP1S phosphorylation decreases during development.

(A) Cortices from Cdkl5 +/Y and Cdkl5 -/Y mice were harvested at different ages. Developmental changes in protein expression and phosphorylation were visualised by Western blotting (1:1000 CDKL5 (Sigma), EB2 total and MAP1S total, 1:2000 EB2 pS222, 1:500 MAP1S pS812, 1:50,000 tubulin (Sigma)). Lysate was 5x more concentrated to detect MAP1S pS812. CDKL5 protein levels clearly increase during development as is described in the literature. EB2 pS222 severely reduces during the same time, while total EB2 protein levels remain constant. MAP1S pS812 is much weaker, but also seems to decrease during development. (B) Quantification of CDKL5-dependent phosphorylation is measured by subtracting the Cdkl5 -/Y from the Cdkl5 +/Y signal. Only quantification for EB2 isoform 1/2 (37 kD) is shown. N = 3 animals per age per genotype, error bars are SEM.

MAP1S phosphorylation is much more difficult to detect than EB2 pS222, but also shows clearer bands at early ages during postnatal mouse brain development (Figure 14A). Total MAP1S protein expression has previously been reported to be constant during neurodevelopment as well (Orban-Nemeth et al., 2005). However, we observed a strong increase in expression during postnatal development. This means that per total protein, MAP1S S812 phosphorylation is much stronger at P4 than later during development (data not shown). Total MAP1S protein levels are not affected by Cdkl5 KO at any specific age, suggesting that the loss of MAP1S phosphorylation is also due to altered CDKL5 kinase activity.

CDKL5-dependent EB2 and MAP1S phosphorylation in the cortex both peak at early postnatal time points and strongly decrease during further development. This is in sharp contrast to total CDKL5 protein levels. Low levels of CDKL5 can highly phosphorylate its substrates at P4, while at P50, EB2 and MAP1S phosphorylation is strongly reduced, despite the increase in CDKL5 protein expression. We therefore suggest that CDKL5 activity is strongly regulated in the mouse brain during development. It is still possible that CDKL5 activity is unaffected and these findings are a result of substrate-specific changes in residue availability or increased phosphatase activity. The fact that both CDKL5 substrates follow the same temporal pattern makes these options less likely though. Strong CDKL5 activity immediately after birth also give a better explanation towards the early symptoms of patients with CDKL5 deficiency disorder. It would therefore also be very interesting to determine pre- and perinatal CDKL5 activity.

3.5.2 EB2 phosphorylation is regulated by neuronal activity

The interesting finding that CDKL5 activity is strongly downregulated during postnatal development independent of protein levels, made us wonder which process could be behind this. An important hallmark of neocortical development is the shift from local to large-scale network activity, accompanied by a transition from electrical to chemical synapse transmission (Luhmann et al., 2016). CDKL5 is known to be dephosphorylated upon NMDA receptor-mediated neuronal depolarisation, which could result in a fast increase of CDKL5 protein expression depending on neuronal maturation, but always eventually ends in proteosomal degradation of CDKL5 (La Montanara et al., 2015). We therefore hypothesized that neuronal depolarisation inhibits CDKL5 activity and leads to loss of EB2 and MAP1S phosphorylation.

DIV14 rat primary cortical cultures were treated with 50 mM KCl for up to an hour. The increase in extracellular KCl mimics neuronal activity by changing the chemical gradient, resulting in a strongly depolarising membrane potential of neurons. Pre-treatment for 30 minutes with 100 uM AP5, a selective NMDA receptor antagonist, was used to determine possible NDMA receptor-mediated effects. Neurons were lysed at different time points and
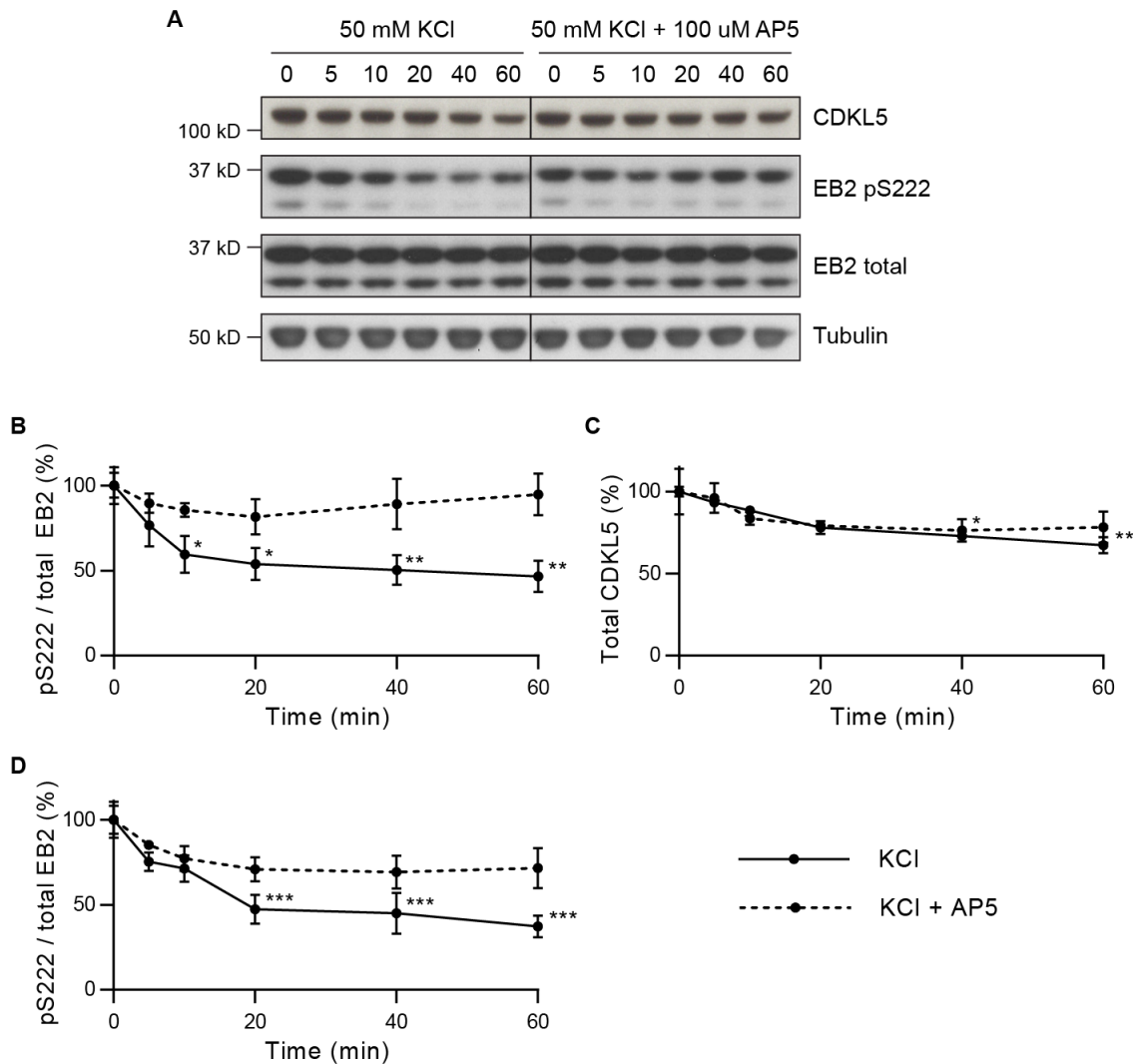
Figure 15: NMDA receptor-dependent neuronal activity reduces EB2 phosphorylation

(A) DIV14 rat primary cortical neurons are treated with 50 mM KCl with or without 30 minutes of 100 uM AP5 pre-treatment, and lysed after different amount of times. Changes in protein expression and phosphorylation are visualised by Western blotting (1:1000 CDKL5 (Sigma) and EB2 total, 1:2000 EB2 pS222, 1:50,000 tubulin (Sigma)). EB2 phosphorylation is reduced upon KCl depolarisation, but not when NMDA receptors are inhibited by AP5. (B) Quantification of EB2 phosphorylation upon neuronal activity at DIV14. EB2 pS222 is significantly decreased after 10 minutes of KCl treatment compared to the baseline control. (C) Quantification of total CDKL5 protein levels upon neuronal activity at DIV14. CDKL5 levels are slightly reduced after 40 minutes of KCl treatment compared to the baseline control. (D) Quantification of EB2 phosphorylation upon neuronal activity at DIV7. EB2 pS222 is significantly decreased after 20 minutes of KCl treatment compared to the baseline control. (B-D) Pre-treatment with AP5 does not lead to any significant differences compared to baseline controls. Dunnett's multiple comparison: n = 3 repeats, * $p < 0.05$, ** $p < 0.01$, *** $p < 0.001$, error bars are SEM.

pS812 in neuronal cultures. Most likely due to the very low abundance of this specific protein phosphorylation.

probed for CDKL5 and EB2 phosphorylation (Figure 15A). Unfortunately, we have not been able to reliably detect MAP1S

We observed a strong decrease in EB2 serine 222 phosphorylation upon KCl depolarisation (Figure 15B). Already after 10 minutes of applying KCl, EB2 phosphorylation is significantly reduced to approximately 50% of the baseline level (10 min: 59.7 ± 10.9% of 0 min, p = 0.039, 60 min: 46.7 ± 9.2% of 0 min, p = 0.0046, n = 3). When inhibiting NMDA receptors with AP5, this phenomenon is not present, suggesting important upstream mediation by glutamatergic synaptic signalling. Total EB2 protein levels remain constant and are not affected by neuronal depolarisation. Similar to Montanara et al., we see a small decrease in total CDKL5 protein levels after 40 minutes of KCl treatment, suggesting proteosomal degradation of CDKL5 (Figure 15C, 40 min: 73.0 ± 2.08% of 0 min, p = 0.027, 60 min: 67.3 ± 4.84% of 0 min, p = 0.0063, n = 3). The much later onset of CDKL5 degradation compared to reductions in EB2 phosphorylation, proposes other mechanisms that regulate CDKL5 kinase activity independent of protein turnover. The regulation of EB2 phosphorylation by NMDA receptor-mediated neuronal activity is not dependent on neuronal maturation, as we see a similar reduction in EB2 pS222 upon KCl treatment in DIV7 rat primary cortical neurons (Figure 15D, 20 min: 47.3 ± 8.51% of 0 min, p = 0.001, 60 min: 37.33 ± 6.49% of 0 min, p = 0.0001).

Although we consistently find reduced EB2 phosphorylation upon KCl treatment and are convincingly capable of preventing this with AP5, we have not been able to reproduce similar results by applying NMDA or glycine to directly stimulate NMDA receptors (data not shown). The observed findings are not caused by KCl induced changes in osmolarity either, as treatment with 50 mM NaCl has no significant effect on EB2 phosphorylation (data not shown). Although we know that EB2 phosphorylation at serine 222 is almost completely dependent on CDKL5, it is still possible that the reduction we see upon neuronal depolarisation is caused by altered phosphatase activity instead. This could be investigated by treating the cultures with phosphatase inhibitors at the same time.

In this subchapter, we have shown that we can use EB2 and MAP1S phosphorylation as biomarkers for CDKL5 activity. By doing this we have been able to proof that the phosphorylation of CDKL5 substrates has the opposite temporal pattern than CDKL5 protein expression, suggesting CDKL5 activity is strongly regulated during development. The neurodevelopmental shift from electrical to chemical synapse transmission might play a role in this, as we have given some evidence that EB2 phosphorylation is inhibited by NMDA receptor-mediated neuronal activity. We believe that these experiments are only the beginning of properly understanding the upstream regulation of CDKL5 activity, and mainly show that EB2 pS222 has the potential to be a valuable tool towards this goal.

Chapter 4. CDKL5 function

It is still an open question how loss of CDKL5 leads to the severe symptoms displayed in CDKL5 deficiency disorder. Cdkl5 KO mice have been shown to phenocopy some aspects of the human condition, but are not severely affected. On a cellular level, loss of CDKL5 has been shown to impair neuronal morphogenesis in many ways, but phenotypes have been mild and little reproducibility has been reported. The function of CDKL5 has therefore been suggested to be more important for synaptogenesis and establishing functional neuronal networks. However, electrophysiological data has been highly variable and does not seem to be reproducible between labs either. Clear consensus phenotypes for loss of CDKL5 have therefore not yet been agreed on. Together with the absence of a good understanding about CDKL5's cell-type specific or subcellular localisation, it has so far been very difficult to ascribe a function to CDKL5 in neurodevelopment.

In the previous chapter we have shown compelling evidence for the first physiological substrates of CDKL5. The three substrates we identified are all regulators of the neuronal cytoskeleton, which suggests that CDKL5 could play an overarching role in mediating microtubule stability and dynamics, and would explain the impaired neuronal morphogenesis reported by others in Cdkl5 KO mice. This second results chapter is dedicated to our identification of CDKL5's role in regulating microtubule dynamic instability. First we will show how phosphorylation by CDKL5 directly affected the microtubule-binding affinity of MAP1S, and what this meant for microtubule plus-end dynamics. We then describe how we failed to observe any impairments in neuronal morphology of Cdkl5 KO mice *in vivo* and *in vitro*. Subsequently, we give evidence for unaffected mitochondria transport and autophagy in Cdkl5 KO mice. We finish by demonstrating how we attempted to discover the function of EB2 phosphorylation.
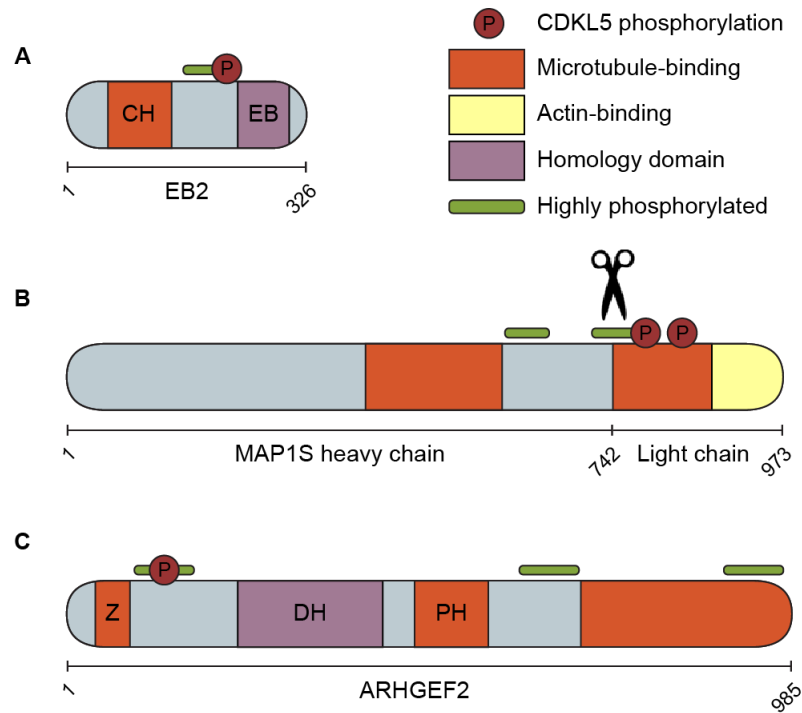
Figure 16: CDKL5 substrates are phosphorylated on or near microtubule-binding domains.
Schematics of the three CDKL5 substrates and their phosphorylation sites. (A) EB2 S222 is situated in the linker combining the microtubule-binding calponin-homology domain (CH) and the end-binding homology domain (EB). Phosphorylation of this linker is known to regulate EB2 microtubule-binding affinity. (B) MAP1S S786 and S812 are both directly located in the microtubule-binding domain of the light chain. (C) ARHGEF2 S122 is positioned near the zinc finger motif (Z) necessary for microtubule binding. Phosphorylation of other residues in this highly phosphorylated region have been shown to affect ARHGEF2 microtubule-binding affinity. DH = Dbl-homology domain, PH = pleckstrin-homology domain. All schematics drawn are based on the mouse protein. Regions containing multiple phosphorylation sites that are identified more than five times on PhosphoSitePlus are depicted in green.

4.1 Microtubule binding of CDKL5 substrates

EB2, MAP1S and ARHGEF2 are all microtubule-associated proteins which functions are directly regulated by their binding to microtubules. All three of them have well defined microtubule-binding domains important for exerting these functions. Interestingly, the residues on these proteins directly phosphorylated by CDKL5, are often located in or near their microtubule-binding domains. EB2 serine 222 is positioned in a highly phosphorylated linker connecting the microtubule-binding and end-binding homology domains (Figure 16A). Phosphorylation of the EB2 linker is known to reduce its binding affinity for microtubules (Iimori et al., 2016). Both phosphorylated MAP1S residues are directly located on the microtubule-binding domain of the light chain (Figure 16B). ARHGEF2 serine 122 is situated in a highly phosphorylated region next to the zinc finger motif known to be important for its microtubule association (Figure 16C). Phosphorylation of another serine in this region has been shown to mediate ARHGEF2's association with microtubules (Sandi et al., 2017). CDKL5 might therefore play an overarching role in microtubule regulation by mediating the microtubule-binding affinity of its substrates.

4.1.1 MAP1S phosphorylation by CDKL5 regulates its microtubular localisation

Microtubular association of proteins can be represented by their subcellular localisation to microtubules. MAP1S, EB2 and ARHGEF2 have all been shown to colocalise with microtubule fibres in various cell types, either by overexpression of fluorescent proteins or endogenous labelling with antibodies. COS7 monkey fibroblast cells are often the preferred adherent cell line for these studies as they are flat and contain a very clear microtubule array. We expect that overexpressed wild type CDKL5 substrates show clear microtubular localisation in COS7 cells and that this is altered in the phosphomutant variants. As CDKL5 protein levels are believed to be absent or very low in COS7 cells, substrates are co-expressed with active or kinase dead CDKL5 to assure they are phosphorylated.

Overexpression of the MAP1S light chain has been shown to induce microtubule stability by binding and bundling fibres (Orban-Nemeth et al., 2005). Both MAP1S phosphorylation sites are located on the microtubule-binding domain of the light chain. Microtubular localisation of MAP1S LC was therefore considered the most likely to be regulated by CDKL5 phosphorylation. COS7 cells were transfected with HA-MAP1S LC WT or S786/812A together with FLAG-CDKL5 WT or KD and fixed 24 hours later. Staining and imaging of transfected cells, clearly showed that MAP1S LC colocalises with microtubules in the absence of active CDKL5 (Figure 17A). However, when co-expressed with active CDKL5 the microtubular localisation of MAP1S LC is completely abolished. This dissociation from
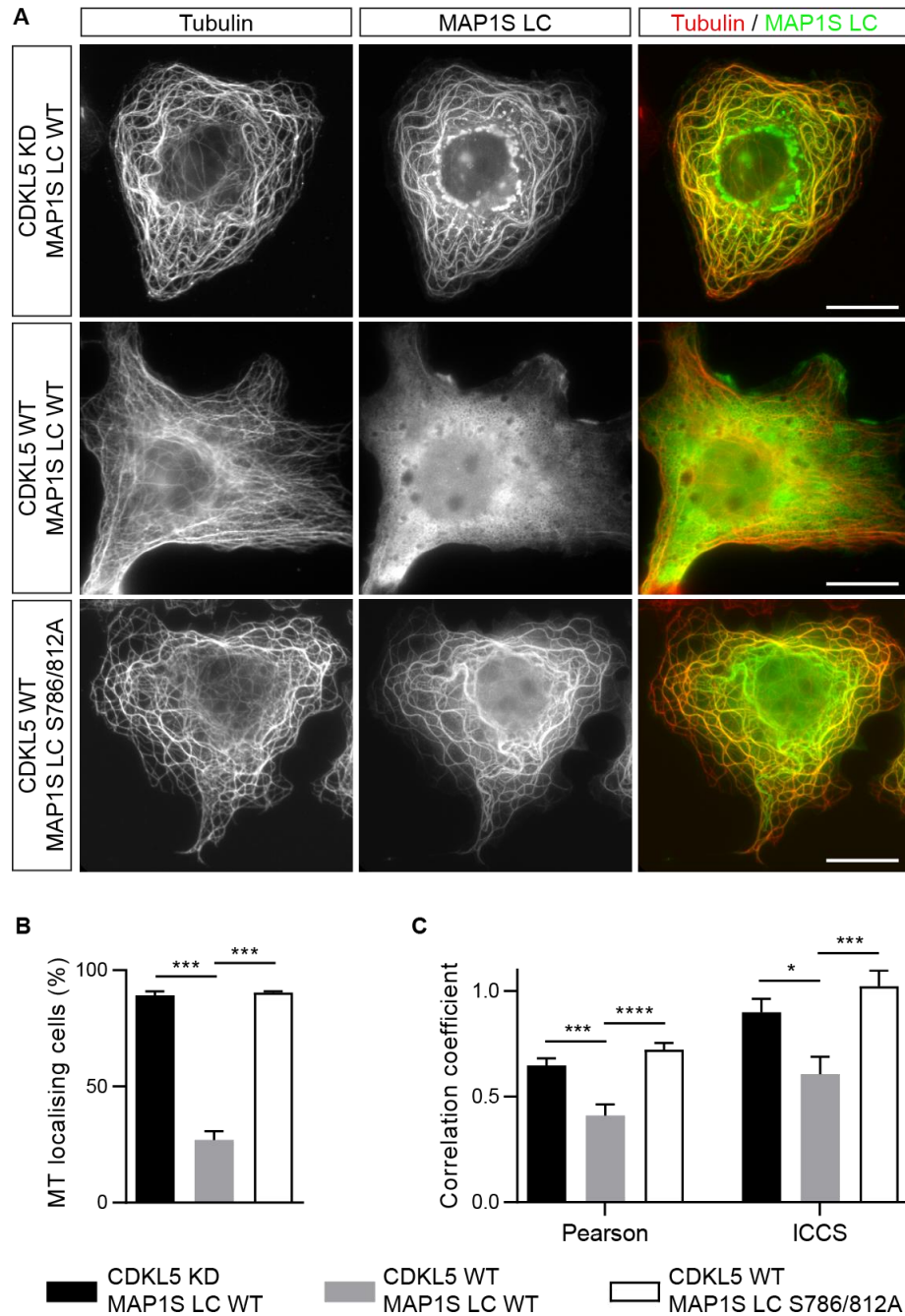
Figure 17: MAP1S microtubular localisation is regulated by CDKL5 activity.

(A) Representative images of COS7 cells overexpressed with FLAG-CDKL5 and HA-MAP1S LC and stained (1:100 FLAG, 1:1000 tubulin (Sigma), 1:500 MAP1S LC). Phosphorylated MAP1S does not localise to microtubules, but shows signs of actin localisation. Scale bar is 20 μm. (B) Quantification of the percentage of cells containing clear MAP1S LC microtubular localisation pattern. Tukey's multiple comparison: N = 2 coverslips per condition, n = 10-16 cells per coverslip, *** p < 0.001, error bars are SEM. (C) Quantification of MAP1S LC/tubulin colocalisation by Pearson correlation coefficient and spatial image cross-correlation spectroscopy (ICCS). Tukey's multiple comparison: N = 2 coverslips, n = 22-24 cells per condition, * p > 0.05, *** p > 0.001, **** p > 0.0001, error bars are SEM.

microtubules can be rescued by mutating serines 786 and 812 to alanines, confirming that CDKL5 phosphorylation on these specific sites contributes to this effect.

We quantified MAP1S light chain microtubule affinity under these different conditions by counting the number of cells containing clear microtubule localisation of MAP1S LC (Figure 17B). MAP1S LC phosphorylated at serine 786 and 812 showed a significant decrease in the percentage of cells containing clear MAP1S LC microtubule localisation (KD: 89.2 ± 1.7%, WT: 27.0 ± 3.9%, S786/812A: 90.5 ± 0.5%, n = 2, p = 0.0008). Measuring correlation coefficients of MAP1S LC and tubulin colocalisation provided a more sensitive quantification of MAP1S LC microtubule-association. Pearson and spatial image cross-correlation spectroscopy (ICCS) analysis are two separate pixel-based correlation methods that can remove the bias of visual interpretation (Comeau et al., 2006; Costes et al., 2004). Both methods confirmed a significant decrease in MAP1S LC and tubulin correlation when co-expressed with active CDKL5 (Figure 17C, Pearson: KD: 0.648 ± 0.034, n = 24, WT: 0.411 ± 0.054 , n = 23, SA: 0.723 ± 0.030, n = 22, p = 0.0003, p < 0.0001, ICCS: KD: 0.899 ± 0.065, n = 24, WT: 0.607 ± 0.082 , n = 23, SA: 1.022 ± 0.075, n = 22, p = 0.017, p = 0.0006). It has to be noted that out of focus noise is known to interfere with these measurements and could have affected the absolute values of the correlation coefficients.

MAP1S is known to bundle microtubules upon binding. We also observed this effect as microtubule fibres appear much thicker with unphosphorylated MAP1S LC that clearly localises to microtubules. Interestingly, in some cases of phosphorylated MAP1S LC, we can observe the shift from microtubule to actin localisation. The C-terminus of MAP1S LC is known to be capable of binding actin, but this property is overshadowed by its microtubule association when the complete light chain is expressed. Still, this means that by affecting the microtubule localisation of MAP1S LC through phosphorylation by CDKL5, not only microtubule stability, but also the actin cytoskeleton could be altered.

ARHGEF2 S122 and EB2 S222 are both located in a highly phosphorylated region outside of the actual microtubule-binding domain of the protein. COS7 cells were transfected with Strep-ARHGEF2 WT or S122A together with FLAG-CDKL5 WT or KD and fixed 24 hours later. Staining and imaging of transfected cells, clearly showed that ARHGEF2 colocalises with microtubules (Figure 18A). However, we did not find this to be dependent on serine 222 phosphorylation by CDKL5. We observed the characteristic circular pattern of thick microtubule fibres in all conditions of ARHGEF2 overexpression. This might be further proof that ARHGEF2 bundles microtubules and couples them to the actin cytoskeleton situated in the periphery of the cell.

Staining of co-expressed HA-EB2 WT or S222A and FLAG-CDKL5 WT or KD in COS7 cells showed that EB2 is capable of localising to microtubules, but does not seem to bundle and stabilise them (Figure 18B). We did not observe any specific changes in EB2 microtubular localisation depending on CDKL5 phosphorylation. Unfortunately, overexpression of any form of
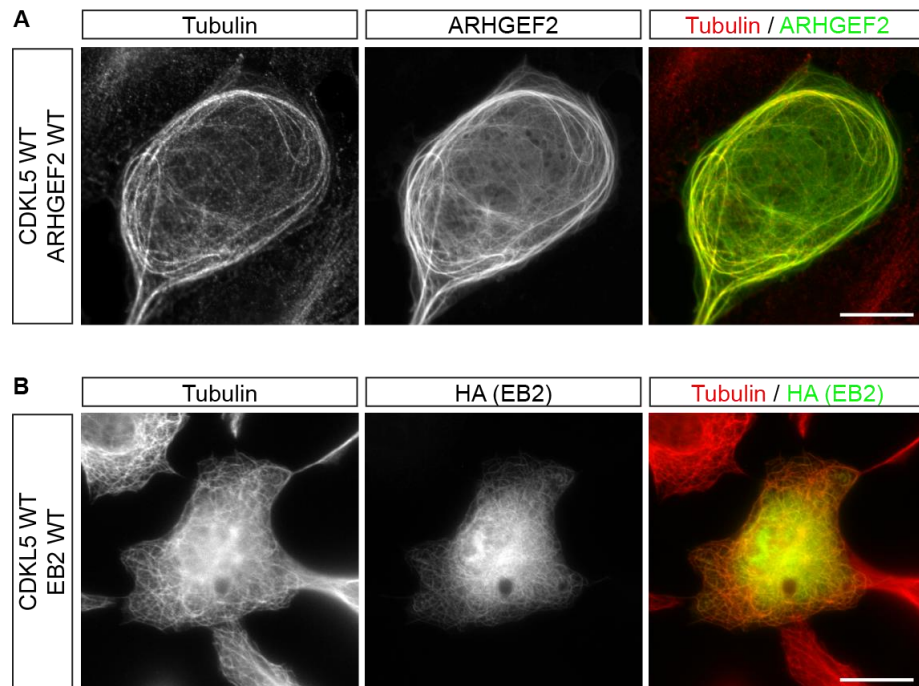
Figure 18: ARHGEF2 and EB2 localisation is unaffected by CDKL5 phosphorylation.
(A) Representative images of COS7 cells overexpressed with FLAG-CDKL5 and Strep-ARHGEF2 and stained (1:100 FLAG and tubulin (Abcam), 1:50 ARHGEF2). Independent of phosphorylation by CDKL5, ARHGEF2 strongly localise to microtubules, often causing a specific circular pattern of thick microtubule bundles. (B) Representative images of COS7 cells overexpressed with FLAG-CDKL5 and HA-EB2 and stained (1:100 FLAG, 1:1000 tubulin (Sigma) and HA (Cell Signalling)). Overexpression of EB2 did show microtubular localisation in cases, but also resulted in many unhealthy cells unfit for characterisation. This phenomenon seemed independent of phosphorylation by CDKL5. Scale bar is 20 µm.

EB2 in these cells seemed to have a negative effect on their health. Only low-expressing cells sometimes showed the microtubule localisation pattern of EB2, while high expression of the protein predominantly resulted in complete disruption of the microtubule cytoskeleton. Mutating all three serines of EB2 which phosphorylation were reduced in SILAC labelled Cdkl5 -/Y neurons, did not result in any obvious differences either (data not shown).

CDKL5 only seems to directly regulate the localisation to microtubules of MAP1S LC, and not ARHGEF2 and EB2. MAP1S is phosphorylated directly on the microtubule-binding domain, while EB2 and ARHGEF2 phosphorylation happens on different regions. The fact that these regions are known to be highly phosphorylated indicates that they could play an indirect regulatory role in microtubule localisation, but are possibly also under the control of multiple other kinases. Losing the phosphorylation of a single serine would therefore have less of an impact, and might make it very difficult to ascribe specific functions to these particular sites.

4.1.2 Phosphorylation by CDKL5 directly affects MAP1S microtubule binding affinity

CDKL5 activity regulates the localisation of MAP1S light chain to microtubules by phosphorylating two residues located on the microtubule-binding domain of the protein. This could mean that phosphorylation by CDKL5 affects the microtubule-binding affinity of MAP1S directly or indirectly by regulating MAP1S binding to another protein. In order to investigate this, we used a reductionist approach and subjected phosphorylated MAP1S to an *in vitro* microtubule co-sedimentation assay. Purified MAP1S LC has already been shown to co-sediment with microtubules in the absence of other proteins *in vitro* (Ding et al., 2006). We hypothesized that MAP1S phosphorylated by CDKL5 has reduced microtubule binding affinity and does not co-sediment with microtubules.

StrepII-tagged wild type MAP1S LC and phosphomutant S786/812A were purified from Sf9 insect cells by Vangelis Christodoulou. In order to assure phosphorylation of MAP1S serines 786 and 812, 10 µg (3 µM) MAP1S LC was incubated for 60 minutes with 0.5 µg (0.4 µM) CDKL5. CDKL5 KD and phosphomutant MAP1S LC were used as unphosphorylated negative controls. 3 µM phosphorylated or unphosphorylated MAP1S LC was incubated in the presence of 10 µM taxol-stabilized microtubules and centrifuged over a 40% glycerol cushion. This allows only heavy microtubule aggregates to sediment in the pellet, while soluble proteins remain in the supernatant. The fraction of microtubule-binding and soluble protein can then be analysed by running the lysed pellet and supernatant on Western blot.

We observed that unphosphorylated MAP1S LC strongly binds to microtubules *in vitro*, as all protein co-sedimented in the pellet when pre-incubated with inactive CDKL5 (Figure 19A). Pre-incubation with active CDKL5 resulted in a clear band observable in the soluble supernatant fraction. This band strongly reduced when mutating MAP1S serines 786 and 812 to alanines. Quantification of the microtubule bound and unbound fractions of MAP1S LC showed a
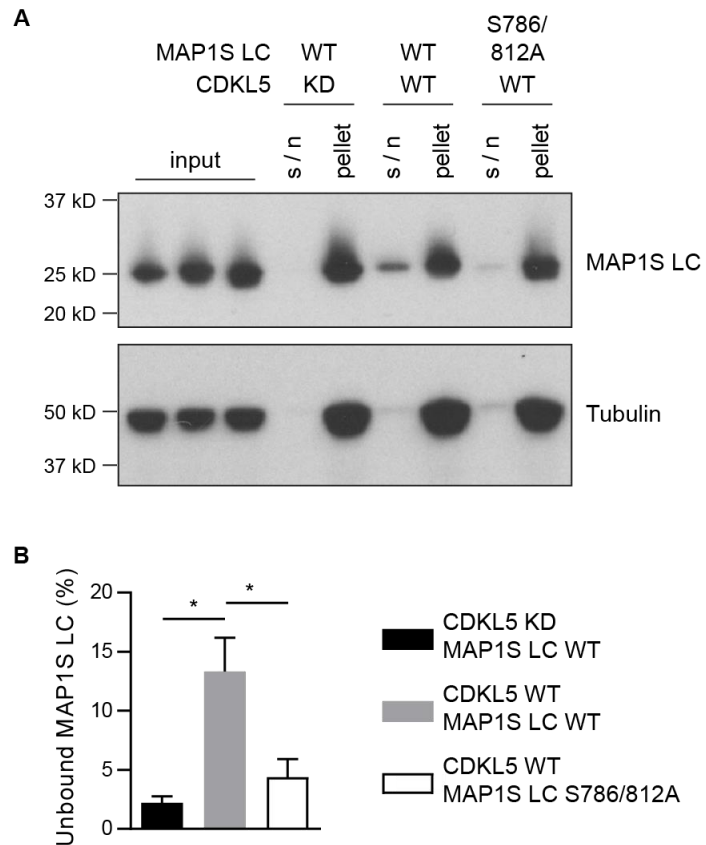
Figure 19: MAP1S microtubule binding is reduced after phosphorylation by CDKL5.

(A) A taxol-stabilised microtubule co-sedimentation assay is visualised by Western blotting (1:1000 MAP1S LC, 1:50,000 tubulin (Sigma)). Purified MAP1S light chain phosphorylated by CDKL5 binds less efficient to polymerised tubulin shown by the increase of MAP1S LC in the supernatant (s/n) fraction. 3 μM MAP1S LC was incubated in the presence of 10 uM taxol-stabilized microtubules and centrifuged over a 40% glycerol cushion. Input = 5% of total sample. (B) Quantification of unbound MAP1S LC present in the s/n fraction. Tukey's multiple comparison: n = 3 repeats, * p < 0.05, error bars are SEM.

significant 3- to 4-fold increase in soluble MAP1S when phosphorylated by CDKL5 (Figure 19B, KD: 2.23 ± 0.53% unbound, WT: 13.33 ± 2.86% unbound, SA: 4.40 ± 1.50% unbound, n = 3, p = 0.014, p = 0.036). At a 1:3 ratio of MAP1S LC to tubulin, we still see the vast majority of MAP1S being bound to microtubules. By adjusting this ratio to more equal molar concentrations, we could possibly expand the effect CDKL5 phosphorylation has on MAP1S microtubule-binding affinity. At the same time, there is no guarantee that all MAP1S is phosphorylated by CDKL5 and a complete loss of co-sedimentation is therefore not to be expected. These findings have provided evidence that CDKL5 phosphorylation of MAP1S LC directly reduces its microtubule-binding affinity.

4.1.3 Neuronal localization of CDKL5 and its substrates

CDKL5 is highly expressed during postnatal development throughout the brain, but due to the lack of a good immunofluorescent CDKL5 antibody, we still do not have a clear understanding of its subcellular localisation. We have shown that CDKL5 substrates MAP1S, EB2 and ARHGEF2 are localised to microtubules in COS7 cells and expect that this is reproducible in neurons. However, microtubules of neurons do not associate with the centrosome, thus the neuronal cytoskeleton is very distinct compared to most other cell types. It would therefore be interesting to see if CDKL5-dependent phosphorylation alters the neuronal localisation of our newly identified substrates.

As MAP1S is considered the strongest microtubule-binding substrate of CDKL5, we first tried to establish the neuronal localisation of MAP1S by overexpressing GFP- or HA-tagged MAP1S LC in rat primary neuronal cultures. However, visualising neuronal microtubules is notoriously difficult for multiple reasons. First, the thin axonal and dendritic processes make it challenging to distinguish between microtubules and cytoplasm. Second, the instability of neuronal microtubules makes them very sensitive to the method of fixation. Different labs swear by different protocols ranging from short incubation with ice-cold methanol to long exposure with PFA at 37 °C. Although we have observed cases where we were able to reproduce the microtubular localisation of MAP1S (Figure 20A), we have not yet been able to ascribe this convincingly to a specific fixation protocol. Overexpressed MAP1S LC instead often showed a diffuse, cytosolic localisation pattern.

The problems we encountered in CDKL5 substrate localisation in neurons could also be attributed to overexpression of the proteins. The resulting high expression of a protein could interfere with localisation by possible saturation of subcellular compartments, in this case microtubules. Labelling of endogenous proteins with good immunofluorescent antibodies could overcome this problem. Unfortunately, good antibodies are rare and not yet available for MAP1S and ARHGEF2. However, we recently managed to obtain an EB2 antibody that showed specific endogenous EB2 staining in rat neuronal cultures, when validated with shRNA-
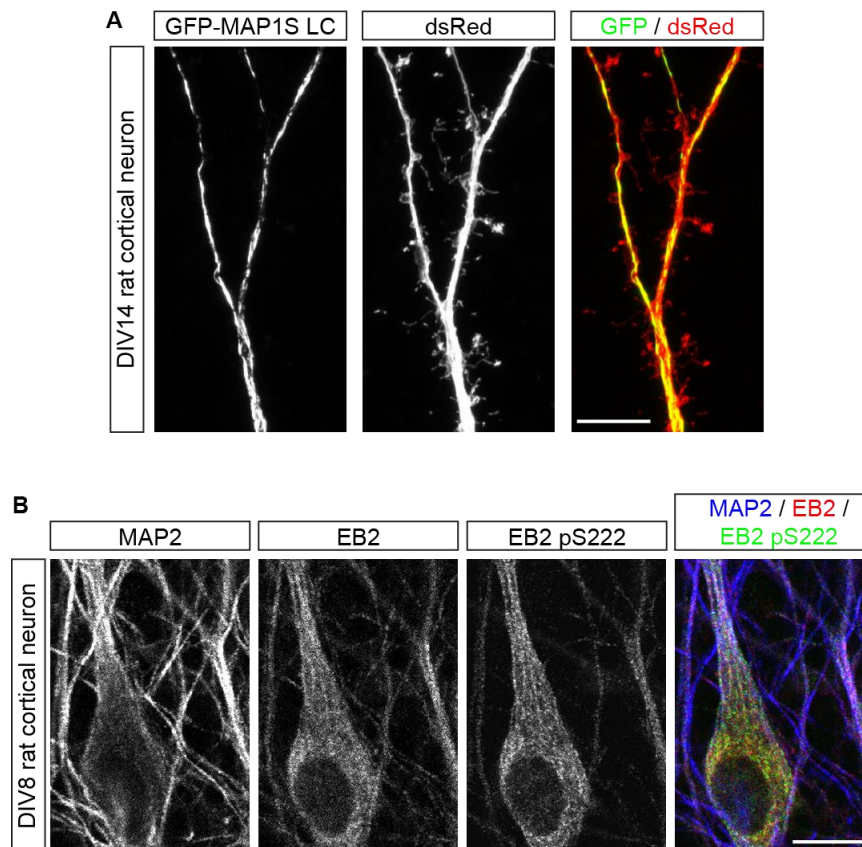
Figure 20: Neuronal localisation of CDKL5 substrates has not yet been conclusive.

(A) Example of GFP-MAP1S LC overexpressed in DIV14 rat primary cortical neurons localised to microtubules due to the absence in dendritic spines visualised by overexpressed cytosolic dsRed (OE: DIV11-14, 1:2000 GFP and dsRed). Scale bar is 10 µm. (B) Representative images of DIV8 rat primary neurons stained for endogenous EB2 (1:500 MAP2, EB2 total and EB2 pS222). EB2 co-localised with MAP2-positive microtubule fibres. Scale bar is 10 µm.

mediated knockdown (data not shown). Both endogenous total EB2 and EB2 phosphorylated at serine 222 were found to be localised at microtubules, based on the observation of colocalisation with MAP2 fibers (Figure 20B). We only managed to show this localisation pattern when fixing with methanol at -20 °C, followed by PFA fixation at RT (Jaworski et al., 2009). It would be interesting to see if we can observe CDKL5-dependent changes in EB2 localisation in Cdkl5 KO neurons in the future. EB2 pS222 also shows promising signs of being a specific biomarker of phosphorylated EB2, and thus CDKL5 activity, for immunocytochemistry. However, the antibody still needs to be validated with proper negative controls, such as Cdkl5 KO primary neurons or phosphomutant knock-in lines.

Current advances in genome editing have made it possible to map endogenous protein localisation in the mouse brain and completely avoid the use of antibodies (Mikuni et al., 2016). Single-cell labelling of endogenous proteins by CRISPR-Cas9-mediated homology-directed repair (SLENDR) uses *in utero* electroporation to sparsely insert an epitope-tag encoding sequence to a gene of interest by genome editing. We designed specific single-guide RNAs (sgRNA) targeting the start codon of CDKL5, EB2 and ARHGEF2, and the stop codon of MAP1S. We also designed corresponding ssODNs of ~200 bases to integrate an N-terminal HA-tag in the coding sequences of CDKL5, EB2 and ARHGEF2, and a C-terminal HA-tag in the coding sequence of MAP1S to target the light chain. The Cas9 and sgRNA expressing vectors, ssODNs and a EGFP transfection marker were introduced by *in utero* electroporation of E13.5 mouse embryos. Staining of 50 μm coronal sections at postnatal day 20 revealed successful electroporation, as green fluorescent neurons had sparsely integrated into the cortex. However, no HA signal was detected in any of the transfected cells.

Our failure to detect endogenous localisation by HA-staining could be due to problems specific to our proteins of interest. In order to address our ability to successfully apply this method, we obtained an sgRNA expressing vector to target CaMKIIa as a positive control. Even with this positive control, we were not able to detect any HA-specific signal, suggesting that genome editing is unsuccessful in our hands. This is most likely a technical problem due to small differences in reagents and methodology. Mikuni et al. have shown that this technique is very sensitive, depending on protein of interest and IUE age, CRISPR efficiency varied from 7.5% to less than 1% of all transfected neurons. This means that, despite multiple attempts to show it, we cannot conclude that phosphorylation by CDKL5 regulates the neuronal localisation of its substrates.

In this subchapter, we have shown that CDKL5 directly regulates the microtubule-binding affinity of MAP1S light chain. MAP1S is known to bundle and stabilise microtubules, and we see this effect when overexpressing the protein in COS7 cells. Phosphorylation of MAP1S by CDKL5 is therefore believed to destabilise microtubules. However, we have not been able to show any evidence for this mechanism in neurons. Based on our results in COS7 cells, we do not find any proof for CDKL5-dependent changes in EB2 or ARHGEF2 microtubule-binding

affinity. The position of their phosphorylation sites imply that their regulation could be more complex, and include other kinases and phosphorylation sites.

4.2 Microtubule dynamics

All novel CDKL5 substrates that we identified are microtubule binding proteins, suggesting an overarching role for CDKL5 in regulating the microtubule cytoskeleton. We presented that CDKL5 phosphorylation directly controls MAP1S microtubule-binding affinity. In HeLa cells, loss of MAP1S has been shown to alter microtubule dynamics throughout the cell cycle (Tegha-Dunghu et al., 2014). We have also identified three phosphorylation sites in a highly phosphorylated domain of EB2 that are strongly downregulated upon loss of CDKL5. End-binding proteins are key players in microtubule plus-end tracking and regulate microtubule dynamic instability. Expression of non-phosphorylatable EB2 has been shown to induce stable kinetochore microtubule dynamics in HeLa cells (Iimori et al., 2016). These studies indicate a more specific overlapping function in microtubule plus-end dynamics between CDKL5 substrates. We therefore hypothesized that microtubule dynamic instability is altered in CDKL5 KO mice.

4.2.1   Microtubule dynamic instability is altered in Cdkl5 -/Y dendrites

Microtubule dynamics can be visualised by fluorescent labelling of +TIPs as they preferentially bind to growing microtubule plus-ends. Live-cell imaging of fluorescent EB3 has been particularly used much for studying microtubule dynamic instability in neurons. The clear orientation and microtubule organisation in axons and dendrites make it relatively easy to convert live-cell imaging into kymographs. This way, properties of fluorescent EB3 comets can be used as quantifiable measurements for growing plus-ends and microtubule dynamics.

We have shown that CDKL5 expression and activity is upregulated during early postnatal development when dendritic branch patterning is happening. We therefore expect that a possible role of CDKL5 in microtubule dynamic instability would be most obvious in developing dendrites. Live-cell imaging of EB3-tdTomato comets was therefore done in dendrites of DIV14 primary cortical neurons from Cdkl5 +/Y and Cdkl5 -/Y mice. 15-16 three-minute videos at 1 frame/second of ~50 um of dendrite were taken for each genotype and converted into kymographs (Figure 21A). Fluorescent EB3 comet movement visualised by kymographs can be analysed by five characteristic measurements for microtubule dynamics: EB3 comet density, direction, distance, lifetime and velocity.

In dendrites of Cdkl5 KO neurons we observed a reduction in EB3 comet density compared to WT neurons (Figure 21B, WT: 8.58 ± 0.97, n = 16, KO: 5.11 ± 0.51, n = 15, p = 0.0042). Fewer growing plus-ends mean less dynamic and more stable microtubules in CDKL5 KO dendrites. However, it has to be noted that live imaging is not the optimal method to measure comet density, as comet density is not an intrinsic property of a single comet, but instead dependent on the quality and coverage of each video as a whole.
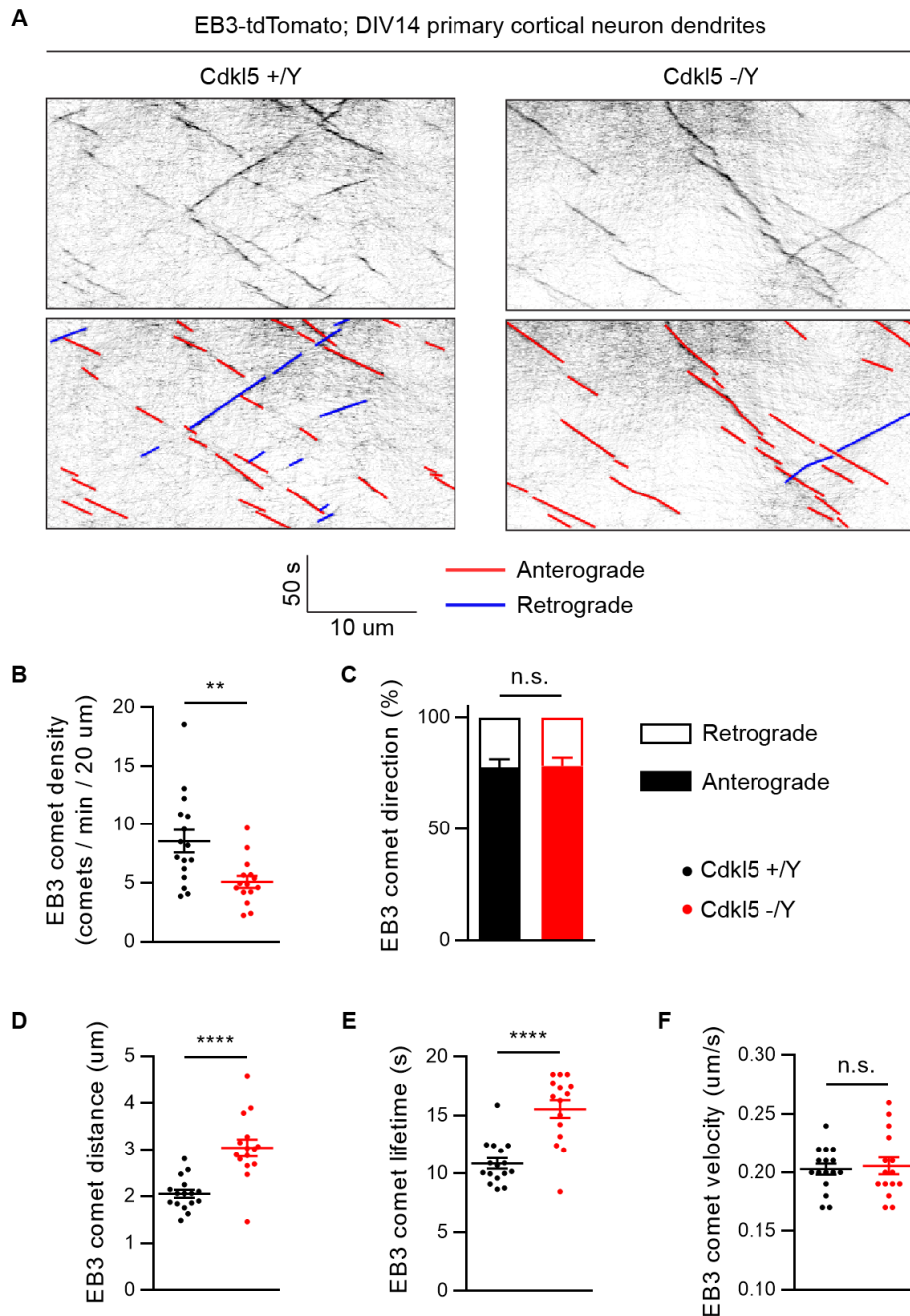
Figure 21: Microtubule dynamics are altered in DIV14 Cdkl5 -/Y dendrites.

(A) Representative kymographs of EB3-tdTomato live cell imaging in dendrites of DIV14 primary neurons. 3-minute videos of 1 frame/s. OE: DIV12.5-14. (B) EB3 comet density is significantly reduced in Cdkl5 -/Y dendrites. (C) The direction of EB3 comets is unaltered in Cdkl5 -/Y dendrites. (D) The distance covered by EB3 comets is significantly increased in Cdkl5 -/Y dendrites. (E) The lifetime of EB3 comets is significantly increased in Cdkl5 -/Y dendrites. (F) The velocity of EB3 comets is not changed in Cdkl5 -/Y dendrites. (B-F) Student t-test: WT: N = 16 neurons, n = 615 comets, KO: N = 15 neurons, n = 381 comets, n.s. = not significant, ** $p < 0.01$, **** $p < 0.0001$, error bars are SEM.

It is important to realise that both retrograde and anterograde EB3 comets are labelling growing plus-ends, and therefore measure the orientation of microtubules. Microtubules in dendrites can be oriented in both directions, but about 75% are reported to have their plus-end away from the soma. We see similar numbers in our WT neurons, which are not different in Cdkl5 KO (Figure 21C, WT: 77.65 ± 3.54 %, n = 16, KO: 78.17 ± 3.85 %, n = 15, p = 0.92). As expected, loss of CDKL5 does not result in altered microtubule orientation in dendrites.

Both the distance covered and lifetime of EB3 comets in Cdkl5 KO dendrites are significantly increased compared to WT neurons (Figure 21D and E, WT: 2.06 ± 0.09 um, 10.88 ± 0.46 s, n = 16, KO: 3.05 ± 0.18 um, 15.55 ± 0.76 s, n = 15, p < 0.0001). These changes are independent of EB3 comet velocity (Figure 21F, WT: 0.203 ± 0.0047 um/s, n = 16, KO: 0.205 ± 0.0072 um/s, n = 15, p = 0.74). The loss of short, dynamic EB3 comets and an observed increase in longer, more stable growing plus-ends, indicates less turnover between microtubule catastrophe and polymerization. Together with the overall decrease in EB3 comet density, these changes confirm drastically altered microtubule dynamic instability in dendrites of Cdkl5 KO mouse primary neurons. EB3 comet orientation, distance, lifetime and velocity are in the same order of magnitude as described previously in the literature (Ghiretti et al., 2016; Stepanova et al., 2003).

4.2.2   CDKL5 regulates microtubule dynamics via MAP1S

CDKL5-dependent changes in microtubule dynamic instability can potentially be downstream of EB2, MAP1S or both. In order to investigate via which substrate CDKL5 exerts its effect on microtubule dynamics, we performed a typical epistasis experiment. If CDKL5 functions via a specific substrate, loss of the substrate should mask the observed phenotype in Cdkl5 KO neurons. We used shRNA-mediated knockdown of EB2 and MAP1S to achieve this. Knockdown of EB2 has been successful in previous studies (Komarova et al., 2005; Yue et al., 2014), so we designed an identical short hairpin RNA. shRNA-mediated knockdown of MAP1S has not been described yet. Two new short hairpin RNAs were therefore designed to effectively target conserved sequences in the mouse and rat MAP1S gene. All three shRNAs were validated by coexpression with HA-tagged EB2 or MAP1S in HEK293T cells. Western blots showed a complete loss of the target protein when coexpressed with targeted shRNA, but not with scrambled shRNA controls (Figure 22A).

EB2 and MAP1S were knocked down by shRNAs in DIV14 Cdkl5 WT and Cdkl5 KO primary cortical neurons. Microtubule dynamics were visualised by live imaging of fluorescent EB3 as described before. Surprisingly, we did not see a significant difference in EB3 comet density between WT and Cdkl5 KO controls (Figure 22B, WT control: 6.50 ± 2.65, n = 14, KO control: 4.90 ± 2.28, n = 13, p = 0.74). Although these results are slightly trending towards
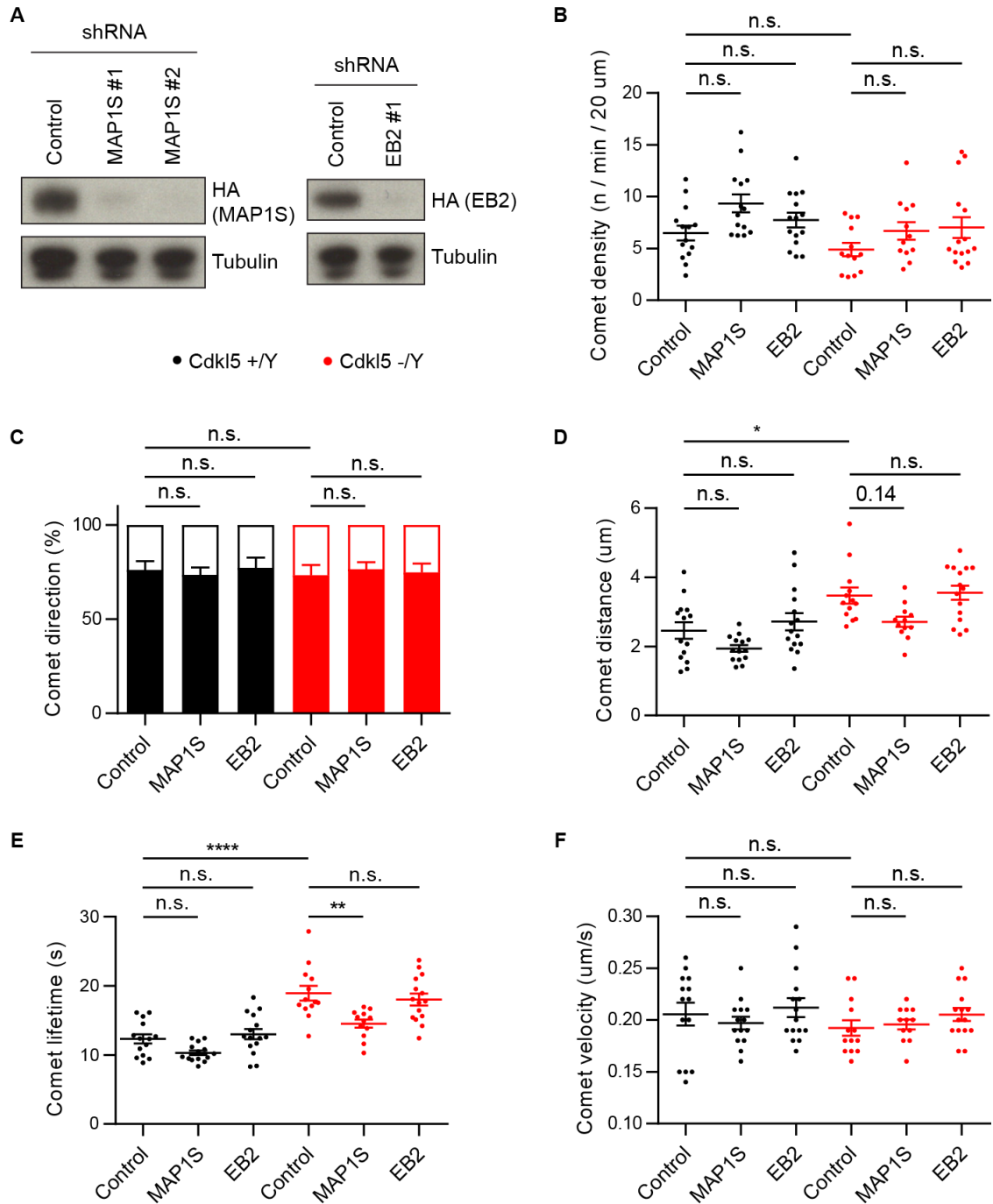
Figure 22: MAP1S knockdown rescues CDKL5-dependent microtubule dynamics.

(A) MAP1S and EB2 shRNAs are validated in Western blots of HEK293T cell lysates. HA-tagged target proteins are completely lost when co-expressed with specific shRNAs compared to scrambled controls. (B) No significant changes in EB3 comet density in dendrites of Cdkl5 +/Y or Cdkl5 -/Y neurons were detected upon CDKL5 substrate knockdown. (C) MAP1S knockdown is trending towards rescue of the increase in distance covered by EB3 comets in dendrites of Cdkl5 -/Y neurons. (D) MAP1S knockdown partially restores the increase in EB3 comet lifetime typical for dendrites of Cdkl5 -/Y neurons. (B-D) Tukey's multiple comparison: N = 12 - 15 neurons, n = 388 - 741 comets, n.s. = not significant, * $p < 0.05$, ** $p < 0.01$, **** $p < 0.0001$, error bars are SEM.

reduced microtubule dynamic instability in Cdkl5 KO neurons, it is impossible to use this measurement to determine causality of the CDKL5 substrates.

The previously observed phenotype of increased EB3 comet distance and lifetime upon loss of CDKL5 does repeat when overexpressed with scrambled shRNA controls (Figure 22C and D, WT control: 2.46 ± 0.89 um, 12.34 ± 2.50 s, n = 14, KO control: 3.47 ± 0.83 um, 18.94 ± 3.83 s, n = 13, p = 0.011, p < 0.0001). shRNA-mediated knockdown of MAP1S in Cdkl5 -/Y neurons results in a trending reduction of distance covered by EB3 comets compared to the control (KO MAP1S #1: 2.71 ± 0.50 um, n = 12, p = 0.14) and a significant decrease in EB3 comet lifetime (KO MAP1S #1: 14.53 ± 2.07 s, n = 12, p = 0.0022). Microtubule dynamics upon shRNA-mediated knockdown of MAP1S in Cdkl5 KO neurons are not significantly different from WT controls (p = 0.96, p = 0.35). MAP1S knockdown with shRNA #2 showed similar results (data not shown). No significant differences in microtubule dynamics between controls and EB2 shRNA-mediated knockdown in Cdkl5 +/Y or -/Y neurons were found (Figure 22C and D). EB3 comet direction or velocity was unaltered in any condition (Figure 22E and F).

These results suggest that CDKL5's role in regulating microtubule dynamics is partly exerted via MAP1S, but not via EB2. The loss of MAP1S phosphorylation and a resulting increase in microtubule stability, is most likely the reason behind altered microtubule dynamics in Cdkl5 KO neurons. Silencing MAP1S partly restores this imbalance in microtubule stability. Recently, CDKL5 has also been shown to affect microtubule dynamics via its interaction with IQGAP1 in COS7 cells (Barbiero et al., 2017). It is therefore possible that both pathways contribute to the altered microtubule dynamic instability in Cdkl5 KO neurons.

4.2.3 Microtubule dynamics are not affected in axons of Cdkl5 KO neurons

Barbiero et al. observed similar changes in microtubule dynamics after CDKL5 shRNA-mediated knockdown in COS7 cells. The authors were able to restore this phenotype with the neurosteroid pregnenolone, which also rescued an axon polarization defect in CDKL5 deficient neurons. We therefore hypothesized that microtubule dynamic instability could also be altered in developing axons of Cdkl5 KO neurons.

Microtubule dynamics were visualised by live imaging of EB3-tdTomato in axons of DIV4 Cdkl5 +/Y and -/Y primary cortical neurons. 13-15 three-minute videos at 1 frame/second of ~50 um of axon were taken for each genotype and converted into kymographs (Figure 23A). Microtubules in axons always direct their plus-ends away from the soma. EB3 comets therefore primarily move in the anterograde direction. We did not see any significant differences between WT and Cdkl5 axons in terms of EB3 comet density (Figure 23B, WT: 10.25 ± 0.84, n = 15, KO: 10.51 ± 0.83, n = 13, p = 0.83), distance covered by EB3 comets (Figure 23C, WT: 2.14 ± 0.11 um, n = 15, KO: 2.24 ± 0.12 um, n = 13, p = 0.52), EB3 comet lifetime (Figure 23D, WT: 11.23 ± 0.44 s, n = 15, KO: 11.92 ± 0.43 s, n = 13, p = 0.28) and EB3 comet velocity (data not shown).
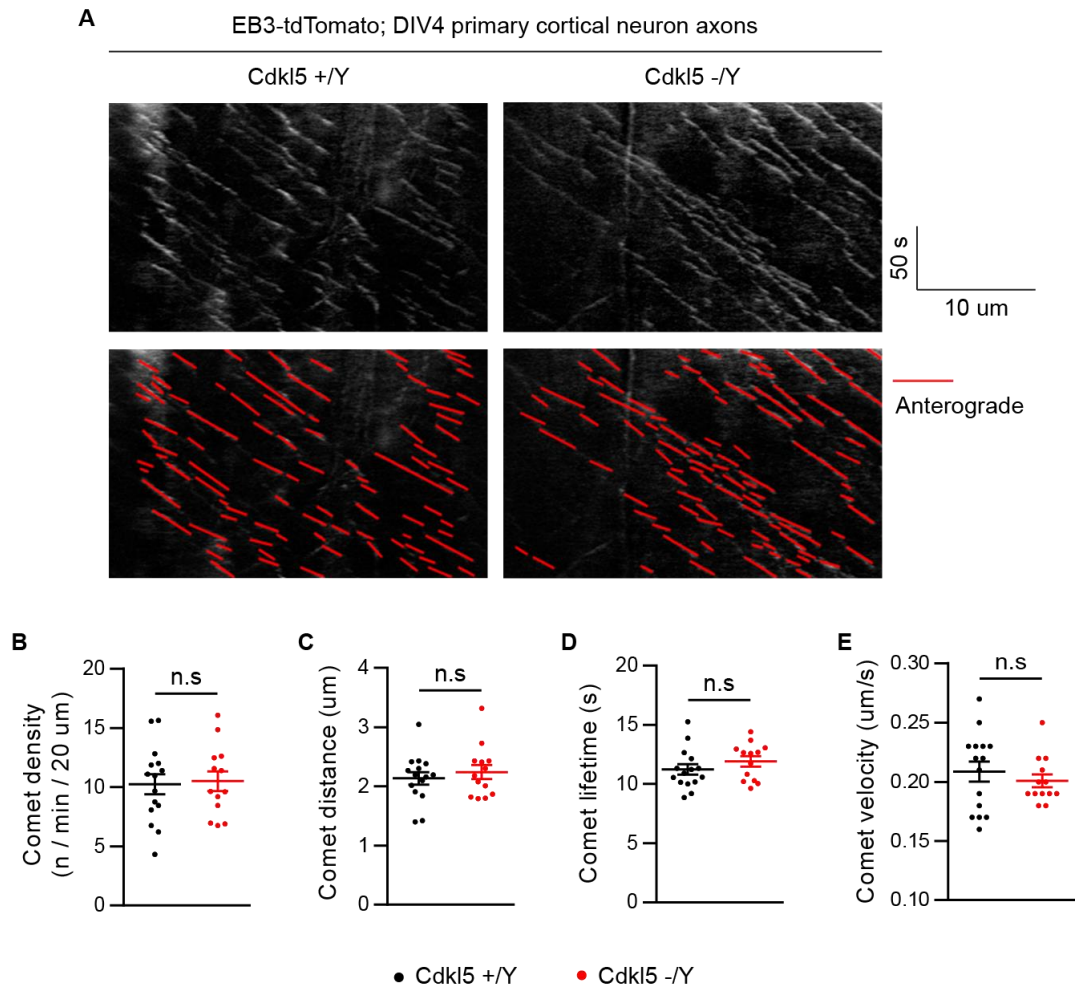
Figure 23: MT dynamics is unaltered in axons of DIV4 Cdkl5 -/Y neurons.

(A) Representative kymographs of EB3-tdTomato live cell imaging in axons of DIV4 primary cortical neurons. 3-minute videos of 1 frame/s. OE: DIV3-4. (B) EB3 comet density is not changed in axons of Cdkl5 -/Y neurons. (C) Distance covered by EB3 comets is unaltered in axons of Cdkl5 -/Y neurons. (D) EB3 comet lifetime is not changed in axons of Cdkl5 -/Y neurons. (B-D) Student t-test: WT: N = 15 neurons, n = 1249 comets, KO: N = 13 neurons, n = 949 comets, n.s. = not significant, error bars are SEM.

Unlike developing dendrites, microtubule dynamic instability in developing axons of Cdkl5 -/Y primary cortical neurons did not seem to be affected. In dendrites this phenotype is caused partially by the loss of MAP1S phosphorylation. We have shown before that expression levels of MAP1S peak around P12-20 during post-natal development of the mouse brain. A possible explanation for the absence of altered microtubule dynamics in axons at DIV4 could therefore be the natural low expression of MAP1S at this stage. This does not rule out that microtubule dynamic instability is not regulated by CDKL5 in more mature axons.

In this subchapter, we have shown that microtubule dynamic instability is altered in developing dendrites, but not axons, of Cdkl5 KO primary neurons. We observe that fewer microtubule plus-ends grow longer in time and distance, indicating an overall increase in microtubule stability. This CDKL5-dependent process has been shown to act partially via MAP1S, which corresponds with our findings that MAP1S phosphorylation by CDKL5 directly regulates its microtubule-binding affinity and thus stabilizing properties. Interestingly, EB2 does not seem to play a role in neuronal microtubule dynamics, and CDKL5 phosphorylation of this protein is therefore believed to have a different function.

4.3 *In vivo* neuronal morphology

CDKL5 has been heavily implicated in regulating neuronal morphogenesis. Multiple papers have described phenotypes in axons, dendrites and dendritic spines upon loss of CDKL5. However, these findings are often contradictory and have not yet established a clear consensus for CDKL5 function in neuronal morphology. Still, our results have shown that CDKL5 acts on the neuronal cytoskeleton by phosphorylating microtubule-binding proteins. We therefore hypothesized that the changes in microtubule dynamic instability are the foundation for previously described morphological phenotypes in CDKL5-deficient neurons. To replicate CDKL5-dependent effects on neuronal morphogenesis in the most physiological environment possible, we studied dendrite branching and dendritic spine formation in Cdkl5 KO mouse brains.

4.3.1 Dendrite morphology is not changed in Cdkl5 KO cortex

Dendrites are the input receiving branches of a neuron. The specific growth and arborisation of these microtubule-rich structures is crucial for accurate wiring and functioning of the brain. For instance, dendritic arborisation is significantly reduced in MeCP2 KO mice and patients with Rett syndrome (Armstrong et al., 1999; Stuss et al., 2012). This is especially apparent in cortical layer 5 pyramidal neurons that contain a stereotypical dendritic morphology consisting of multiple basal and one apical dendrite emanating from the soma. These neurons integrate input from all neocortical layers and project to subcortical circuits. Sparse labelling by the Thy1-GFP transgene provides a bright, Golgi-like stain that visualises the neuronal architecture of layer 5 pyramidal cells in mouse brains, which makes it possible to reconstruct them (Figure 24A).

Paraformaldehyde fixed brains were harvested from 20-day-old Cdkl5 +/Y and Cdkl5 -/Y mice expressing the Thy1-GFP transgene. The subset of fluorescent pyramidal cells in somatosensory layer 5 were imaged from 100 µm coronal sections. As a result, only the basal dendritic arbour could be reconstructed, because the vast majority of apical dendrites was cut off. To improve consistency and reduce the number of basal dendrites being cut, only neurons with somas located in the middle 50% of the section were used. With these criteria, we did not observe any significant difference in dendritic growth of L5 pyramidal cells measured by the total length of the basal dendritic arbour (Figure 24B, WT: 2293 ± 167 µm, KO: 2027 ± 154 µm, n = 19, p = 0.25).

Dendritic arborisation of these neurons can be measured by Sholl analysis. Concentric rings were drawn around the soma and the number of intersections at each radial distance quantifies the magnitude of arbour complexity. Both WT and Cdkl5 KO pyramidal neurons
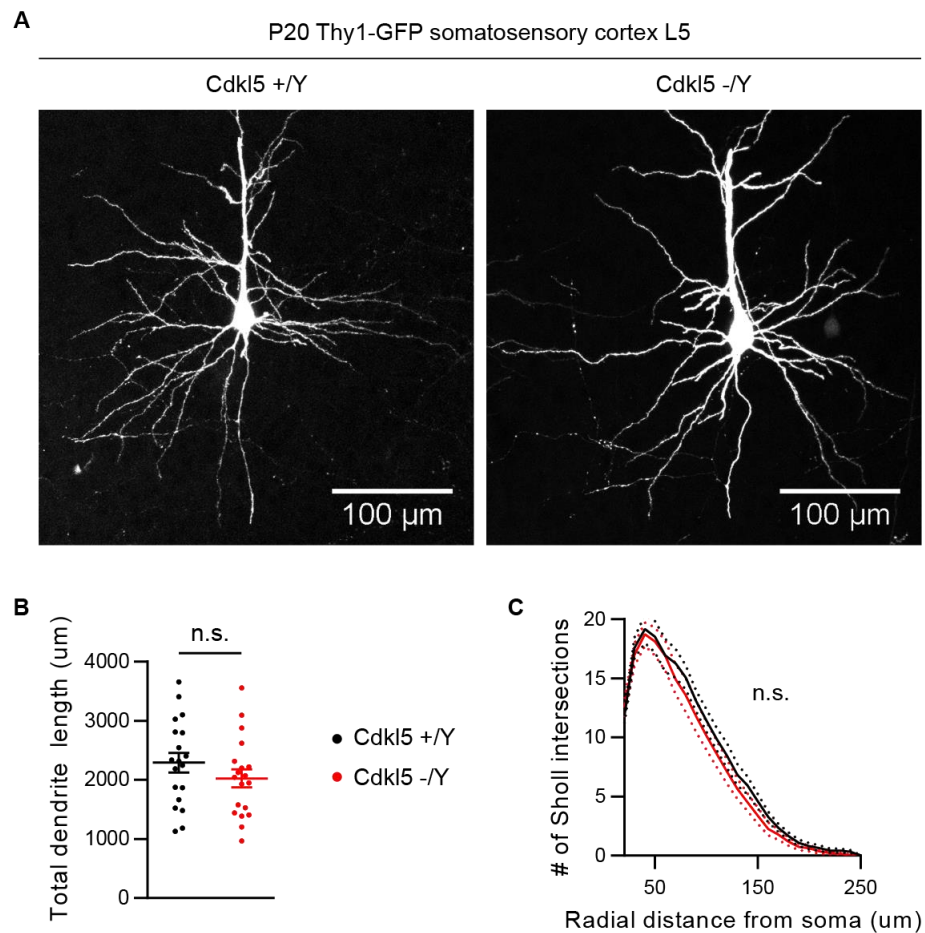
Figure 24: Dendritic growth and arborisation is unaffected in Cdkl5 KO mice.

(A) Representative images of Thy1-GFP labelled neurons in sections of somatosensory cortex layer 5 of P20 Cdkl5 +/Y and Cdkl5 -/Y mice. (B) Total length of basal dendrites is not significantly different in somatosensory cortex L5 of Cdkl5 -/Y mice. Student t-test: N = 4 animals per genotype, n = 19 neurons per genotype, n.s. = not significant, error bars are SEM. (C) Arborisation of basal dendrites is unaltered in somatosensory cortex L5 of Cdkl5 -/Y mice. Sidak's multiple comparison: N = 4 animals per genotype, n = 19 neurons per genotype, n.s. = not significant, error bars are SEM.

demonstrated curves typical for basal dendritic arborisation of these cell types without any significant difference between them (Figure 24C).

We did not observe any significant differences in the growth and arborisation of basal dendrites in layer 5 of the somatosensory cortex of Cdkl5 -/Y mice. We were unable to reconstruct the apical dendrites of these neurons and can therefore not dismiss possible alterations in those segments. Unfortunately, it was the total length and distal arborisation of the apical dendrite specifically that was shown to be reduced in Cdkl5 KO mice by others (Amendola et al., 2014). It is therefore possible that CDKL5-dependent changes in dendrite morphology *in vivo* are restricted to specific brain regions, cell types or cell compartments not studied here.

4.3.2   Dendritic spines are unaltered in Cdkl5 KO cortex

Dendritic spines are the postsynaptic structures of more than 90% of excitatory synapses in the brain. Their number and morphologies thus often represent synaptic function and neuronal circuitry. Defects in spine morphology are heavily associated with other neurodevelopmental disorders such as Fragile X and Down syndrome. The spatial and temporal regulation of these actin-rich structures is also dependent on microtubule invasion and dynamic instability (Gu et al., 2008). We therefore imaged individual dendrites of Thy1-YFP labelled pyramidal cells at higher magnification to study spine number and morphology in Cdkl5 KO mice (Figure 25A).

PFA fixed brains of P20 Cdkl5 +/Y and -/Y mice expressing Thy1-YFP were cut into 50 μm coronal sections. Secondary basal dendrites of pyramidal neurons of the somatosensory cortex layer 5 and hippocampal CA1 and CA3 were imaged. The dendritic spine density we measured in WT somatosensory cortex is very similar to the literature (Konur et al., 2003), but did not significantly change in Cdkl5 KO brains (Figure 25B, WT: 0.94 ± 0.053 spines/μm, n = 21, KO: 1.04 ± 0.069 spines/μm, n = 20, p = 0.26). Spine densities remained unaltered in hippocampal CA1 and CA3 of Cdkl5 KO mice as well (data not shown).

In vivo two-photon microscopy of the somatosensory cortex of Cdkl5 KO mice had shown a small reduction in spine density of the apical tuft at P27, which developed into a more significant decrease at P50 (Della Sala et al., 2015). In order to understand if spine density phenotypes are therefore age-dependent and perhaps not present in young Cdkl5 KO mice, we also measured spine numbers in secondary basal dendrites of P50 Cdkl5 -/Y somatosensory cortex layer 5 pyramidal cells. At this age we still did not observe significant differences in dendritic spine density between WT and Cdkl5 KO mice (Figure 25B, WT: 1.13 ± 0.057 spines/μm, n = 27, KO: 0.99 ± 0.073 spines/μm, n = 25, p = 0.14). Although a more significant trend is starting to emerge at later ages.
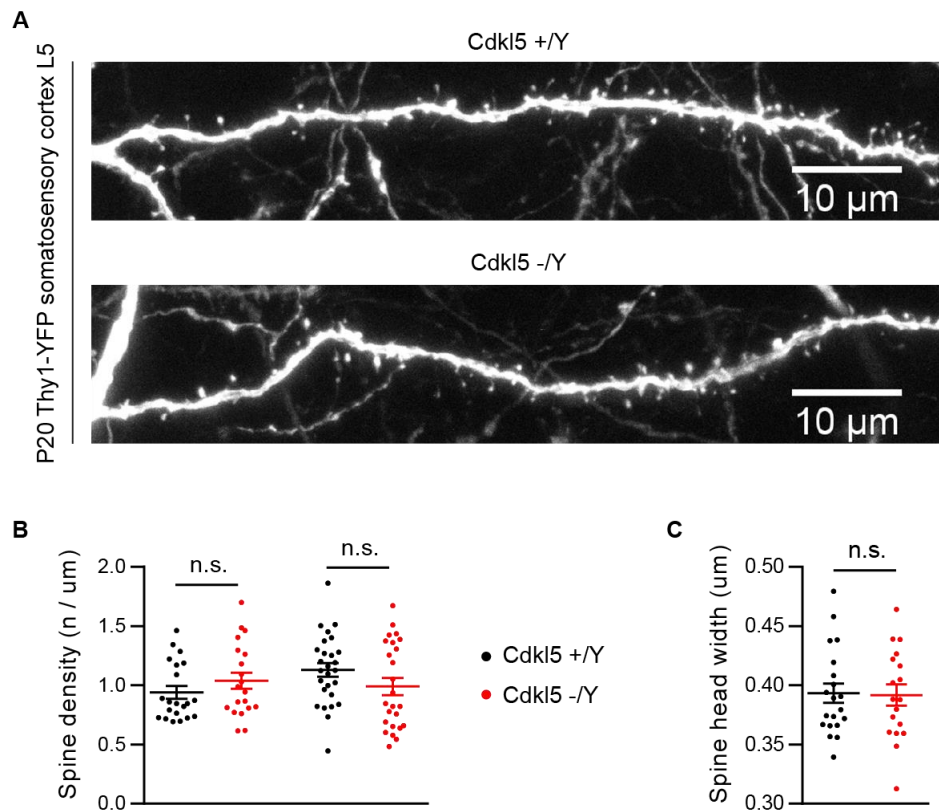
Figure 25: Dendritic spine formation is not altered in Cdkl5 KO mice.

(A) Representative images of Thy1-YFP labelled secondary basal dendrites in sections of somatosensory cortex layer 5 of P20 Cdkl5 +/Y and Cdkl5 -/Y mice. (B) Dendritic spine density is not significantly changed in basal dendrites of 20 or 50 day old Cdkl5 -/Y mice. (C) Width of dendritic spine heads in basal dendrites of P20 Cdkl5 -/Y mice is unaltered. (B and C) Student t-test: N = 20 - 27 dendrites, n = 1564 - 1916 spines, n.s. = not significant, error bars are SEM.

Dendritic spines develop from immature filopodia into mature mushroom-shaped structures. Synapses are formed onto the head of these mature spines. The head diameter of dendritic spines is therefore a measurement for spine maturation and synapse size. However, we also failed to see a difference in the average spine head width between cortical pyramidal cell dendrites of P20 WT and Cdkl5 KO mice (Figure 25C, WT: 0.393 ± 0.008 µm, n = 20, KO: 0.392 ± 0.009 µm, n = 18, p = 0.89). These results confirm that there are no obvious impairments in dendritic spine formation and maturation in basal dendrites of excitatory pyramidal neurons of Cdkl5 KO mice *in vivo*.

In this subchapter, we have shown that despite the important role of microtubule dynamic instability in neuronal dendrite and spine morphogenesis, we have not been able to identify any significant *in vivo* phenotypes regarding dendritic growth and arborisation, or spine formation and maturation in Cdkl5 KO mice. Findings of others imply that alterations in neuronal morphology in CDKL5 deficient mice might be brain region-specific and age-dependent.

Figure 26: Axon growth and polarisation is unchanged in Cdkl5 KO neurons.

(A) Representative images of GFP labelled DIV4 mouse primary cortical neurons (OE: DIV2-4, 1:2000 GFP). (B) Total axon length is not significantly different between Cdkl5 +/Y and Cdkl5 -/Y primary neurons at DIV4, but a significant increase in the total length of the dendritic branches is observed. (C) Axon polarisation is not affected in primary neurons from Cdkl5 KO mice. (B-C) Student t-test: WT: N = 4 animals, n = 52 neurons, KO: N = 2 animals, n = 26 neurons, n.s. = not significant, ** $p < 0.01$, error bars are SEM.

4.4 Morphological analysis of neuronal cultures

Altered microtubule dynamics in Cdkl5 KO neurons could still lead to impaired neuronal morphology. Remember that neuronal localisation of CDKL5 is still an open question due to the absence of a specific immunofluorescent antibody. It is therefore possible that CDKL5 activity is compensated for in specific brain regions during *in vivo* development. This could also explain the mild behavioural phenotypes of Cdkl5 mouse models. We therefore used a simpler approach to study the basics of neuronal development, without the possible compensatory mechanisms of the animal model. By characterising neuronal morphologies of dissociated primary neurons we can more extensively study the development of axons, dendrites and dendritic spines. We expected this will give us more conclusive evidence about the hypothesized function of CDKL5 and CDKL5-dependent microtubule dynamics in regulating neuronal morphogenesis.

4.4.1 Axon formation is unaffected in Cdkl5 KO primary neurons

The first developmental stage of a neuron is the formation of a single axon out of multiple neurites. This axon subsequently quickly outgrows the dendrites in a matter of days. This difficult to study process *in vivo* can be easily followed in dissociated primary cultures. RNA interference of Cdkl5 in cultured rat neurons has been shown to reduce neurite outgrowth in these early stages of development (Chen et al., 2010). EB2 has been proven to be crucial for the initial microtubule reorganisation during apico-basal epithelial differentiation (Goldspink et al., 2013) and could play a similar role in polarisation of neurons. We therefore investigated neurite formation and polarisation in early developmental stages of cultured Cdkl5 KO primary neurons.

Primary cortical neurons were cultured from Cdkl5 +/Y and Cdkl5 -/Y mouse embryos, transfected with a GFP-expressing plasmid and fixed after 4 days *in vitro* (Figure 26A). Axons and dendrites were discriminated based on morphology. At DIV4 we did not observe a significant difference in total axon length between WT and Cdkl5 KO neurons (Figure 26B, WT: 1842 ± 104 µm, n = 52, KO: 1945 ± 152 µm, n = 26, p = 0.58). Interestingly, we do see a small, but significant increase in total dendrite length of Cdkl5 KO neurons at DIV4 (Figure 26B, WT: 376.3 ± 18.0 µm, n = 52, KO: 463.6 ± 26.7 µm, n = 26, p = 0.014). This is exactly opposite of what has been reported upon shRNA-mediated knockdown of Cdkl5 in rat cultures.

Recently, polarisation defects in cultured primary neurons silenced by Cdkl5 RNA interference were published by others (Nawaz et al., 2016). However, we do not see an obvious effect of Cdkl5 KO on neuronal polarisation (Figure 26C, WT: 86.5 ± 5.7% polarised, n = 4, KO: 89.0 ± 3.0% polarised, n = 2, p = 0.79). It has to be noted though, that primary cultures contain mixed populations of cells and the presence of an axon is an important hallmark to identify

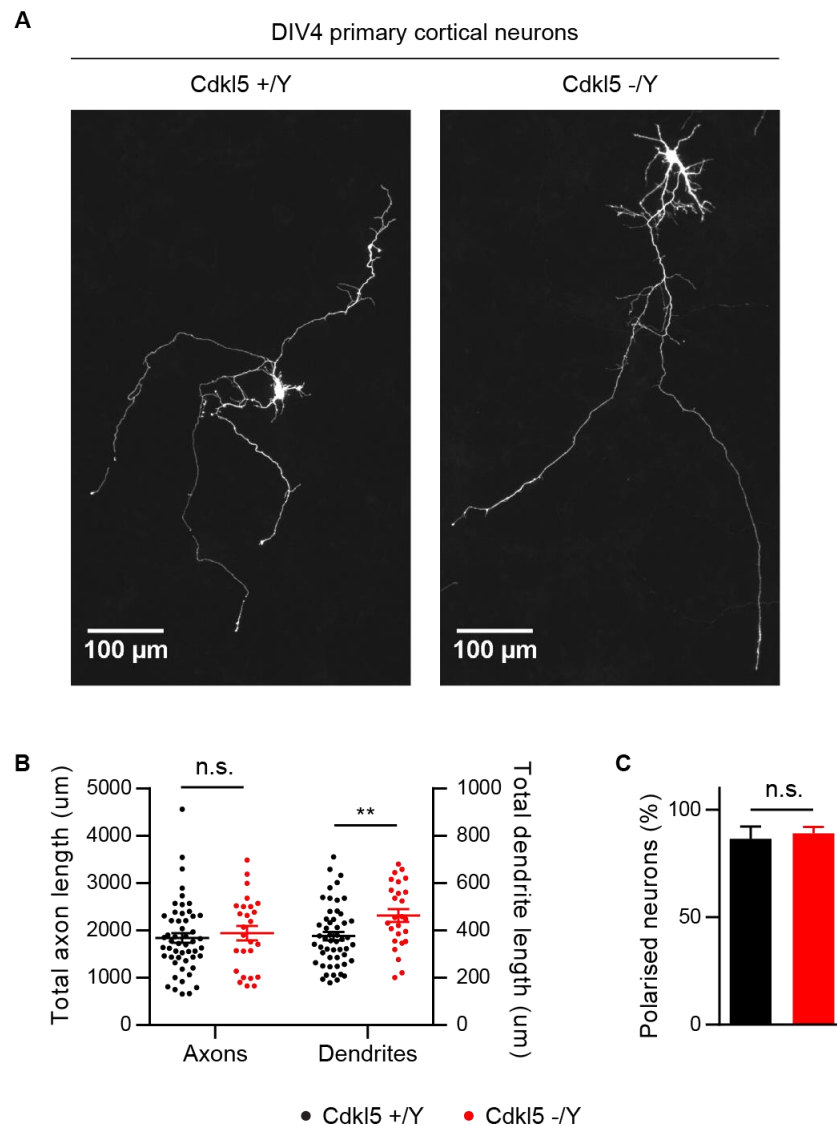**A** DIV11 primary cortical neurons

Cdkl5 +/Y   Cdkl5 -/Y
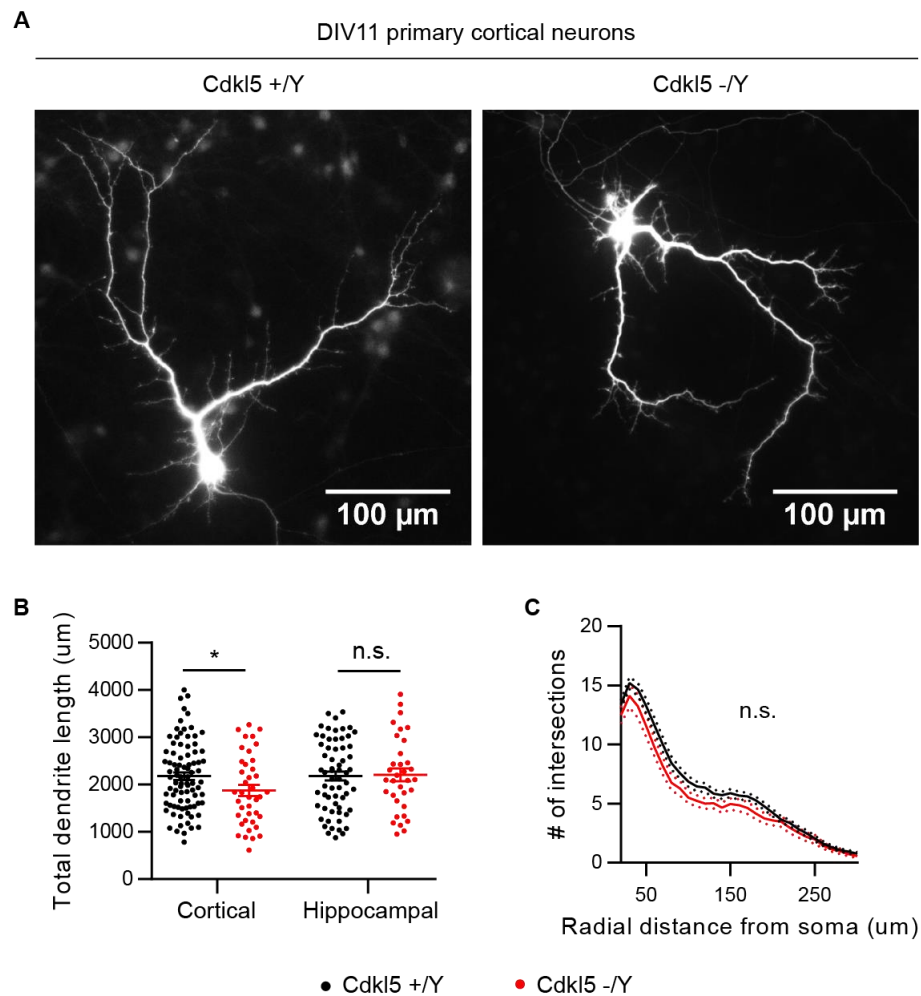
Figure 27: Dendritic growth and arborisation is not altered in Cdkl5 KO neurons.
(A) Representative images of GFP labelled DIV11 mouse primary cortical neurons (OE: DIV8-11, 1:2000 GFP). (B) At DIV11, a small, but significant reduction was observed in total dendrite length of Cdkl5 -/Y primary cortical neurons, but not in hippocampal CA3 neurons. Student's t-test: WT cortical: N = 5 animals, n = 86 neurons, hippocampal: N = 4 animals, n = 63 neurons, KO cortical: N = 3 animals, n = 40 neurons, hippocampal: N = 2 animals, n = 34 neurons, n.s. = not significant, * $p < 0.05$, error bars are SEM. (C) Dendritic arborisation is not significantly different in primary cortical neurons from Cdkl5 KO mice. Sidak's multiple comparison: WT: N = 5 animals, n = 86 neurons, KO: N = 3 animals, n = 40 neurons, n.s. = not significant, error bars are SEM.

neurons. This makes it possible that a bias towards picking healthy, polarised neurons was present in our experiment.

The disagreements with previously reported phenotypes in early developmental stages could possibly be explained by differences in cell culture conditions. Interestingly, our neurons are generally ~4 times bigger than described in Chen et al. and Nawaz et al., and therefore seem to be healthier and further developed after comparable days *in vitro*. This means we might have missed early axonal phenotypes that have already been compensated for. The small increase in early dendrite formation in Cdkl5 KO neurons for example, could actually be due to our inability to distinguish them from retracting axons without additional staining. This could have masked polarisation defects in Cdkl5 KO neurons. Still, our findings do proof that eventually there is no clear distinction in axon growth and polarisation between Cdkl5 +/Y and Cdkl5 -/Y primary neurons.

4.4.2   Dendrite morphology is not altered in Cdkl5 KO primary neurons

In the somatosensory cortex of 20-day-old Cdkl5 KO mice we did not observe an impairment in growth and arborisation of basal dendrites. In cultured primary neurons, the majority of the dendritic tree is formed in the first 14 days in vitro. In Cdkl5 KO neurons, we already noticed a small increase in total dendrite length at DIV4. If the loss of CDKL5 profoundly has an effect on dendritic growth and arborisation in cultured primary neurons, we would expect a more severe phenotype at later stages during development. Cdkl5 +/Y and Cdkl5 -/Y primary neurons were therefore transfected with a GFP-expressing plasmid and fixed after 11 days in vitro (Figure 27A).

Cdkl5 KO primary cortical neurons presented a small, but significant reduction in total dendrite length (Figure 27B, WT: 2180 ± 79 µm, n = 86, KO: 1878 ± 118 µm, n = 40, p = 0.035). Cortical cultures are known to contain a large variety of cell types, so in order to minimise the effect of biological variation, CTIP2-negative CA3 neurons were identified in primary hippocampal cultures. However, no difference in total dendrite length between DIV11 WT and Cdkl5 KO primary hippocampal CA3 neurons was detected (Figure 27B, WT: 2184 ± 95 µm, n = 63, KO: 2204 ± 136 µm, n = 24, p = 0.90). Arborisation of the dendritic tree is neither affected in Cdkl5 KO cortical or hippocampal primary neurons (Figure 27C).

These results confirm our findings in the somatosensory cortex of Cdkl5 KO mice, and show that complete loss of CDKL5 does not lead to severely altered dendritic morphology in dissociated neurons. Our methodology is considered more robust and reliable than RNA interference experiments reported by others, as shRNA-mediated knockdown could come with off-target effects. Surprisingly, another recent paper does show a significant reduction in total dendrite length of cultured Cdkl5 KO hippocampal neurons (Trazzi et al., 2016). Differences in culture conditions could therefore affect the phenotypic outcome of CDKL5 deficiency.

A DIV12-13 cortical primary neurons

Cdkl5 +/Y   Cdkl5 -/Y

Formed dendrite
Retracted dendrite

B
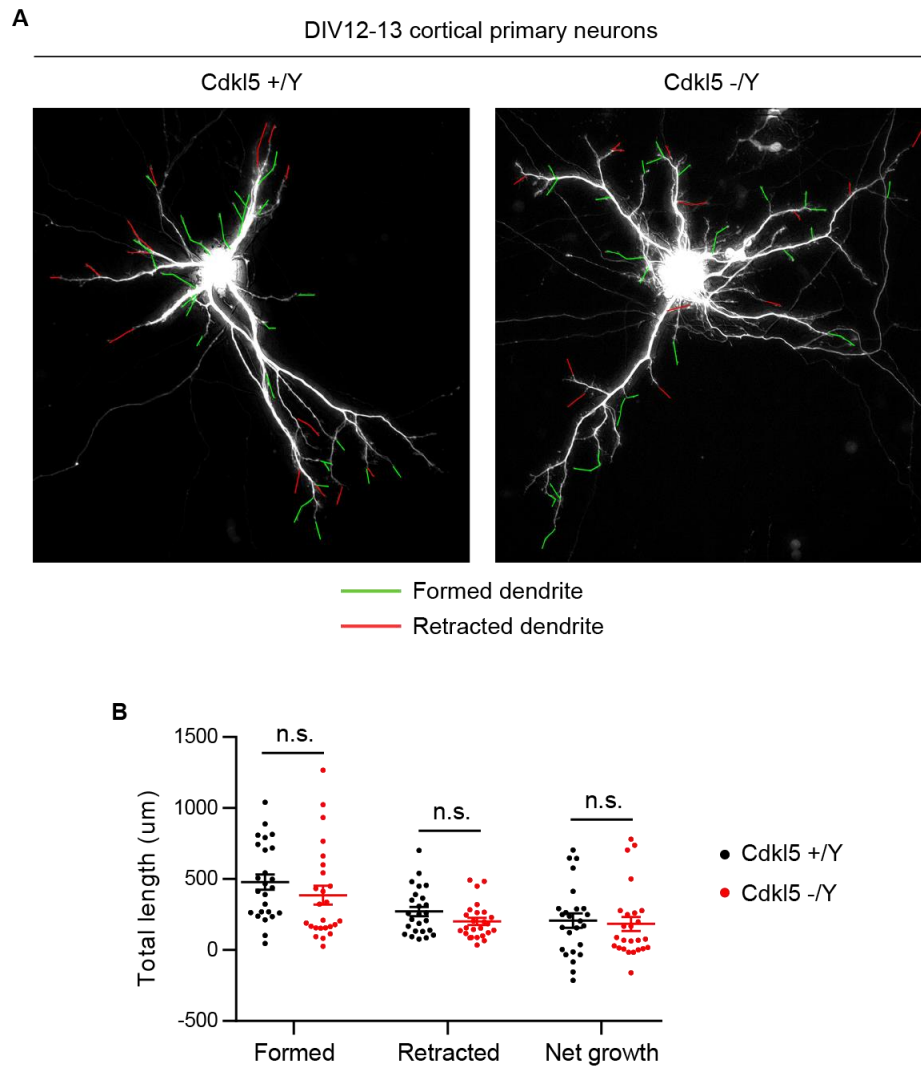
Figure 28: Dendrite dynamics are unaffected in Cdkl5 KO neurons.

(A) Representative images of GFP labelled DIV13 mouse primary cortical neurons with dendrites marked for their change compared to 24 hours prior. OE: DIV11-13. (B) Neither the total length of formed or retracted dendrites is significantly altered in Cdkl5 KO primary neurons, resulting in a similar net growth in 24 hours as WT neurons. Sidak's multiple comparison: N = 2 animals per genotype, n = 25 neurons per genotype, n.s. = not significant, error bars are SEM.

4.4.3 Dendrite dynamics are not different in Cdkl5 KO primary neurons

Patterning of the dendritic arbour is a very dynamic process. Neuronal dendrites constantly form and retract during development, which is mainly driven by the dynamicity of the microtubule cytoskeleton. Although we did not observe overall changes in dendritic growth in Cdkl5 KO neurons, it is still possible that dendrites are less dynamic as a result of impaired microtubule dynamic instability. This could have a major impact on neuronal circuit formation as correct patterning is crucial for the creation of the right synapses.

In order to address dendrite dynamics in Cdkl5 KO neurons, GFP-labelled mouse primary cortical neurons were not fixed, but imaged live after 12 days *in vitro*. 24 hours later, the same cells were visualised again. We noticed that ~5 % of the neurons died in this timespan and could not be imaged at the second time point. By overlaying the two images, dendrites that formed and retracted between DIV12 and DIV13 could be measured (Figure 28A). Between Cdkl5 +/Y and Cdkl5 -/Y neurons, there was no significant difference observed in the total length of formed dendrites (Figure 28B, WT: 479.9 ± 53.6 µm, n = 25, KO: 386.7 ± 65.4 µm, n = 25, p = 0.47), nor in the total length of retracted dendrites (Figure 28B, WT: 272.1 ± 32.7 µm, n = 25, KO: 202.9 ± 25.2 µm, n = 25, p = 0.27). The average length of dynamic dendrites was not found to be altered either (data not shown). As a result, the overall net growth between DIV12 and DIV13 of the Cdkl5 primary cortical dendritic arbour is not significantly different (Figure 28B, WT: 207.8 ± 49.7 µm, n = 25, KO: 183.8 ± 50.0 µm, n = 25, p = 0.74). This is in line with the unchanged total dendrite length found in DIV11 Cdkl5 KO primary neurons.

Impaired dynamicity of the dendritic arbour is therefore not the missing link between affected microtubule dynamics, but regular dendritic growth observed in Cdkl5 KO neurons. Together with our previous *in vivo* results, we therefore strongly believe that dynamic dendritic growth and arborisation in developing cortical neurons is not regulated by CDKL5, as these processes in Cdkl5 KO neurons behave the same as WT controls.

4.4.4 Dendritic spine formation is unchanged in Cdkl5 KO primary neurons

In the somatosensory cortex of Cdkl5 KO mice, dendritic spine density and maturation was not altered. The number of dendritic spines sharply increases in dissociated primary neurons after approximately 14 days *in vitro*. This reductionist approach might give us a better insight into a possible role of CDKL5 in dendritic spine development than *in vivo* experiments. The absence of regional layers and thus the more uncoordinated growth of cultured neurons diminishes the spatial influence on spine formation. Still, to maintain the highest degree of reproducibility, only secondary dendrites of GFP-labelled CTIP2-negative CA3 hippocampal neurons were imaged for spine density quantification (Figure 29A).

A

DIV18 hippocampal primary neurons

Cdkl5 +/Y

10 µm

Cdkl5 -/Y

10 µm

B
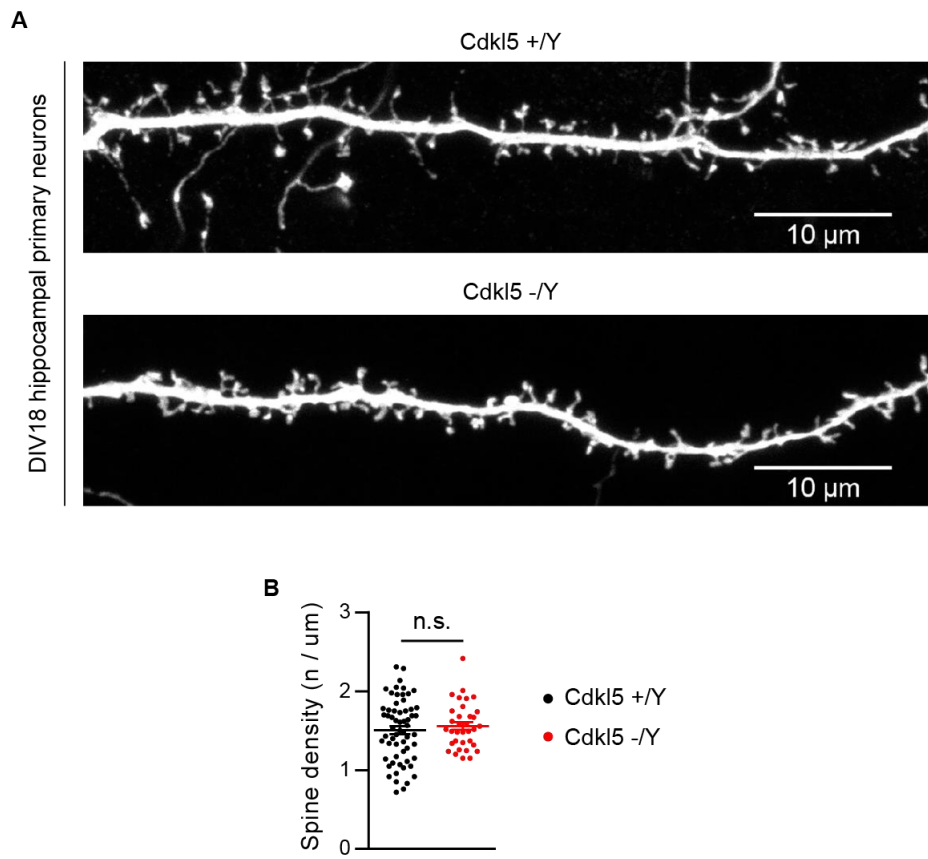
Figure 29: Dendritic spine formation is not impaired in Cdkl5 KO neurons.

(A) Representative images of GFP labelled dendrites of DIV18 mouse primary hippocampal neurons (OE: DIV11-18, 1:2000 GFP). (B) No significant change in dendritic spine density is observed in dendrites of Cdkl5 KO primary neurons. Student's t-test: WT: N = 4 animals, n = 61 dendrites, KO: N = 2 animals, n = 34 dendrites, n.s. is not significant, error bars are SEM.

We did not observe a significant difference in dendritic spine density between DIV18 Cdkl5 +/Y and Cdkl5 -/Y primary hippocampal neurons (Figure 29B, WT: 1.51 ± 0.051 spines/µm, n = 61, KO: 1.56 ± 0.050 spines/µm, n = 34, p = 0.51). As neuronal cultures often display aberrant spine structures, there is no clear morphological distinction between mature synapse-forming spines and other immature types. We therefore do not believe that *in vitro* dendritic spines are suitable for spine head measurements or functional classification.

In Cdkl5 -/Y dissociated hippocampal neurons we find the same absence of dendritic spine phenotypes as we do in the somatosensory cortex of Cdkl5 KO mice. These findings highly suggest that CDKL5 does not have a function in the formation and maturation of dendritic spines. However, others have described impaired network properties in Cdkl5 KO mice. We believe that this is caused by functional synaptic defects instead of altered formation and maintenance of synapses as suggested elsewhere.

In this subchapter, we have shown that there are no significant differences between WT and Cdkl5 KO primary neurons at multiple stages during *in vitro* development. CDKL5 therefore does not seem to play an obvious role in axon development, dendritic growth, arborisation and dynamics, or dendritic spine formation. This exactly follows the unaltered neuronal development of pyramidal cells in the somatosensory cortex of Cdkl5 KO mice *in vivo*. This means that the CDKL5-dependent changes in microtubule dynamics do not seem to have a significant effect on neuronal morphogenesis as we hypothesized.
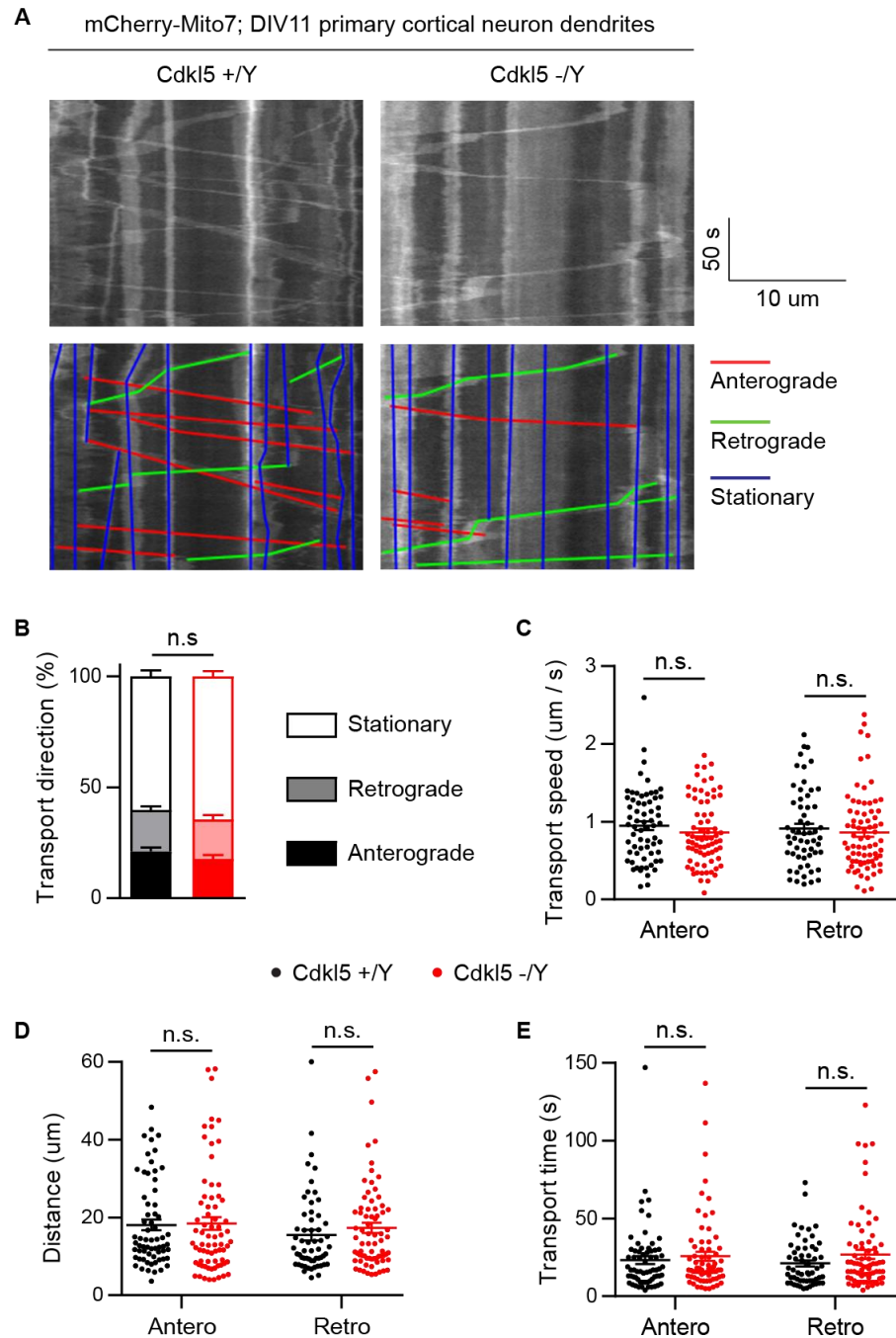
Figure 30: Mitochondrial transport is unaltered in Cdkl5 KO primary neurons.

(A) Representative kymographs of mCherry-Mito7 live cell imaging in dendrites of DIV11 primary cortical neurons. 3-minute videos of 1 frame/s. OE: DIV9-11 (B) The relative proportion of stationary, retrograde and anterograde moving mitochondria is not significantly changed in Cdkl5 KO neurons. Sidak's multiple comparison: WT: N = 5 animals, n = 15 neurons. KO: N = 5 animals, n = 18 neurons, n.s. = not significant, error bars are SEM. (C) Distance of mitochondrial transport is not significantly altered in Cdkl5 KO neurons. (D) Mitochondrial transport time is not significantly different in Cdkl5 KO neurons. (E) Transport velocity of mitochondria is not significantly affected in Cdkl5 KO neurons. (C-E) Student t-test: WT: N = 5 animals, n = 15 neurons. KO: N = 5 animals, n = 18 neurons, n.s. = not significant, error bars are SEM.

4.5 Mitochondrial transport, health and autophagy

As neuronal morphology does not seem to be affected by loss of CDKL5, we hypothesized that MAP1S and EB2 phosphorylation, and the subsequent alterations in microtubule dynamics, might result in a more functional defect. Besides regulating neuronal morphology, microtubule dynamic instability plays an important role in protein and organelle transport. It is via these microtubular tracks that cargo is delivered to the synapses by motor proteins kinesin and dynein. Defects in mitochondrial transport in neurons is crucial for synaptic homeostasis and implicated in the pathogeneses of multiple neurological disorders (Sheng and Cai, 2012). Accumulation of defective mitochondria has also been observed in MAP1S KO mice, where they have been able to link this to failed autophagosomal biogenesis and clearance (Xie et al., 2011). We therefore started to investigate potential problems in mitochondrial transport and functioning linked to autophagy, as a result of CDKL5 loss-of-function.

4.5.1 Mitochondrial transport is not affected in Cdkl5 KO primary neurons

Mitochondria provide many essential functions to the distal processes of axons and dendrites such as ATP production, calcium storage and neurotransmitter metabolism. Their transport from the soma to the dendrites is therefore necessary to maintain the demanding neuronal environment. Mitochondrial transport can be visualised by using fluorescent dye to label endogenous organelles or overexpressing fluorescent mitochondrial genes. In order to get the best spatial resolution, we overexpressed mCherry-Mito7 in mouse primary cortical neurons and live imaged them after 11 days *in vitro*. 15-18 three-minute videos at 1 frame/second of ~50 um of dendrite were taken of WT and Cdkl5 KO neurons and converted into kymographs (Figure 30A).

Kymographs were manually analysed and traced for stationary, retrograde and anterograde moving mitochondria. The population of stationary, non-moving mitochondria is similar as described in the literature (60-70%) and is not found to be altered in Cdkl5 KO primary neurons (Figure 30B, WT: 60.22 ± 2.63%, n = 15, KO: 64.49 ± 2.32%, n = 18, p = 0.50). Within the group of transported mitochondria, there is also no observed difference in directionality between Cdkl5 +/Y and Cdkl5 -/Y neurons (Figure 30B, anterograde: WT: 21.03 ± 1.87%, n = 15, KO: 17.62 ± 1.84%, n = 18, p = 0.50, retrograde: WT: 18.75 ± 1.57%, n = 15, KO: 17.90 ± 2.00%, n = 18, p = 0.75).

Mitochondria are very dynamic organelles that are subject to constant fusion and fission. Measuring properties of individual mitochondria is therefore a lot more challenging than for instance EB3 comets. The organelle does not simply appear and disappear again. We tried to quantify uninterrupted movement of mitochondrial transport and did not consider pausing. This manner of quantification did not result in a significant difference in transport distance or
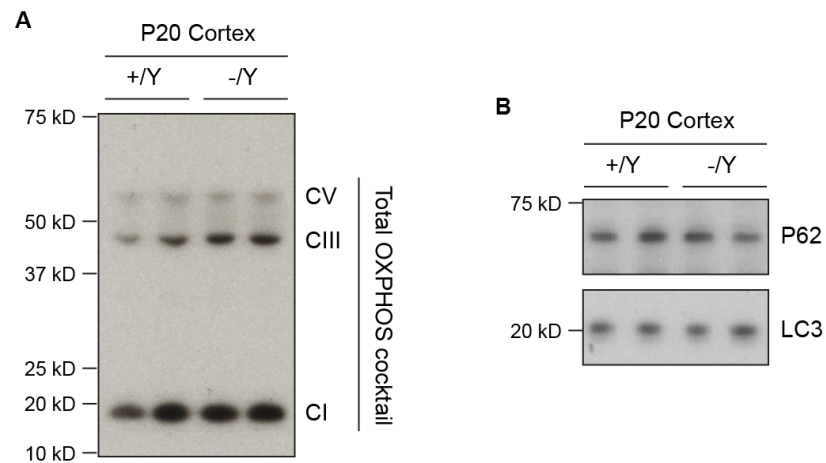
Figure 31: Mitochondrial health and autophagy are unaffected in Cdkl5 KO mice.

(A) Multiple complexes of the oxidative phosphorylation pathway in mitochondria are visualised by Western blotting of Cdkl5 +/Y and Cdkl5 -/Y cortical lysates (1:1000 total OXPHOS). No difference in assembly ratios is observed. The first lane is considered to have less total protein loaded as all three complexes are reduced compared to the other lanes, but not relatively to each other. CI = CI subunit NDUFB8, CIII = CIII core protein 2, CV = CV alpha subunit. (B) Autophagy markers P62 and LC3 are visualised by Western blotting and show no difference in expression levels in cortices of WT and Cdkl5 KO mice (1:5000 P62, 1:1500 LC3).

time of mitochondrial transport between WT and Cdkl5 KO primary neurons (Figure 30C and D, distance: WT: 16.92 ± 1.38 μm, n = 15, KO: 17.15 ± 1.45 μm, n = 18, p = 0.91, time: WT: 21.88 ± 2.07 s, n = 15, KO: 25.23 ± 2.33 s, n = 18, p = 0.30). However, there is a trend towards a small decrease in mitochondrial transport velocity in Cdkl5 KO primary neurons (Figure 30E, WT: 0.979 ± 0.058 μm/s, n = 15, KO: 0.852 ± 0.044 μm/s, n = 18, p = 0.09).

Based on these results mitochondrial transport does not seem to be impaired in dendrites of developing Cdkl5 KO primary neurons. However, we do realise that mitochondria dynamics is a lot more complex than covered in this single experiment. The small decrease in mitochondrial transport velocity makes it therefore interesting to study more extensively. This also indicates that other types of vesicular transport might be more severely affected in Cdkl5 KO neurons.

4.5.2 Mitochondrial health and autophagy is not impaired in Cdkl5 KO mice

Even though mitochondrial transport does not seem to be impaired in Cdkl5 KO mice, it is still possible that compromised mitochondrial function is the underlying reason for CDKL5 pathogenicity. MAP1S-deficient mice have been shown to accumulate autophagosomes and dysfunctional mitochondria. Microtubule binding of MAP1S also affects its direct interaction with LC3, an important protein for autophagy substrate selection (Xie et al., 2011). It is therefore not unlikely that CDKL5-dependent microtubule binding of MAP1S has a further downstream effect on mitochondrial health and autophagy. We used common markers for these two components to investigate this in Cdkl5 KO mouse brains.

Cortical lysates of 20-day-old Cdkl5 +/Y and Cdkl5 -/Y mice were probed with total OXPHOS antibody cocktail. This cocktail is suitable for analysis of all five oxidative phosphorylation complexes in mitochondria. Altered levels of assembly are known to arise as a result of physiological and/or pathological changes, and is therefore an appropriate marker for mitochondrial health and function. Although we only observed three of the five OXPHOS complexes in our preparations, there was no obvious difference in assembly between WT and Cdkl5 KO mice (Figure 31A). This suggests that mitochondrial health and function is not affected in CDKL5 KO mice.

LC3 and P62 are important components of autophagosomes and classical markers for measuring alterations in autophagy. By probing P20 mouse hippocampal lysates with antibodies against these proteins, we expected to see a difference if Cdkl5 KO results in accumulation of autophagosomes like MAP1S-deficiency does. However, we did not observe obvious differences in LC3 and P62 intensities between WT and Cdkl5 KO mice. Autophagy therefore does not seem to be impaired in Cdkl5 KO mice.
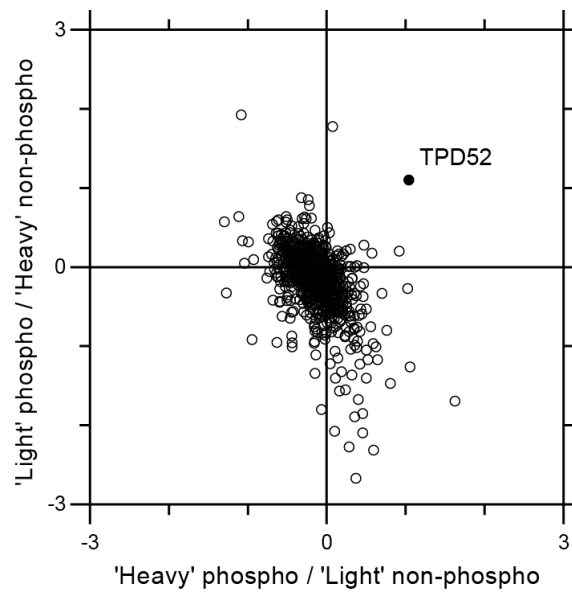
Figure 32: EB2 binds TPD52 in a phosphorylation-dependent manner.

Mass spectrometry analysis of pull-down with phosphorylated or non-phosphorylated EB2 peptides in SILAC labelled DIV12 rat primary cortical neurons. TPD52 preferentially binds phosphorylated EB2 peptide. The origin marks no change in phosphorylation between the two genotypes. The axes represent the base 2 logarithms of the ratio of each detected protein. n = 2 replicates with switched isotope labelling per pull-down.

4.6 Phosphorylation-dependent EB2 binding

We have shown that MAP1S and EB2 are physiological substrates of CDKL5 in mouse and human neurons. Besides that, we identified impaired microtubule dynamic instability in Cdkl5 KO neurons as a novel phenotype that is dependent on MAP1S binding of microtubules regulated by CDKL5-dependent phosphorylation. However, EB2 phosphorylation does not seem to play any role in regulating microtubule dynamics. This is supported by the difficulties others have had in describing EB2 neuronal functions compared to EB1 and EB3. Still, EB2 S222 phosphorylation is highly dependent on CDKL5 and seems to be its main target. We therefore tried to identify interactors of EB2 that bind in a phosphorylation-dependent manner.

4.6.1 Binding of TPD52 is dependent on EB2 phosphorylation

To test if the phosphorylation of EB2 by CDKL5 is involved in any phosphorylation-dependent interactions, we used a peptide pull-down method to identify binding proteins of EB2 in SILAC labelled neuronal lysates. We therefore generated 17 amino acid-long phosphorylated and non-phosphorylated EB2 peptides. We have previously shown that EB2 gets directly phosphorylated by CDKL5 at serine 222, and phosphorylation of this site has consistently found to be lost in CDKL5-deficient neurons. However, we also identified strong reduction of pS218 and pS221 in SILAC labelled Cdkl5 KO primary neurons, but using mass spectrometry it has been difficult to say which combination of EB2 phosphorylation is most prominent under physiological conditions. We therefore decided to use a EB2 peptide phosphorylated at both S218 and S222 for this pull-down experiment. In addition, phosphorylation of T216 has been found to be independent of CDKL5, and is included in both EB2 peptides.

Phosphorylated and non-phosphorylated EB2 peptides were conjugated to iodoacetyl agarose beads and used for pull-down of proteins in SILAC labelled DIV12 rat cortical lysates. The experiment was repeated by switching the isotope labelling. Mass spec analysis identified 1529 proteins that precipitated with EB2 peptides, of which the vast majority associated with both the phosphorylated and non-phosphorylated peptide (Figure 32). In fact, only one protein was enriched in the fraction containing phosphorylated EB2 peptide: tumor protein D52 (TPD52).

TPD52 is frequently overexpressed in cancer and is involved in the regulation of vesicle trafficking (Boutros et al., 2004). Its role in neurons has not been described yet, as it only recently has been identified as a novel synaptic protein (Biesemann et al., 2014). Therefore, the phosphorylation-dependent binding of TPD52 to EB2 might have a function in cargo transport along microtubules or synaptic targeting, but needs to be further validated first.
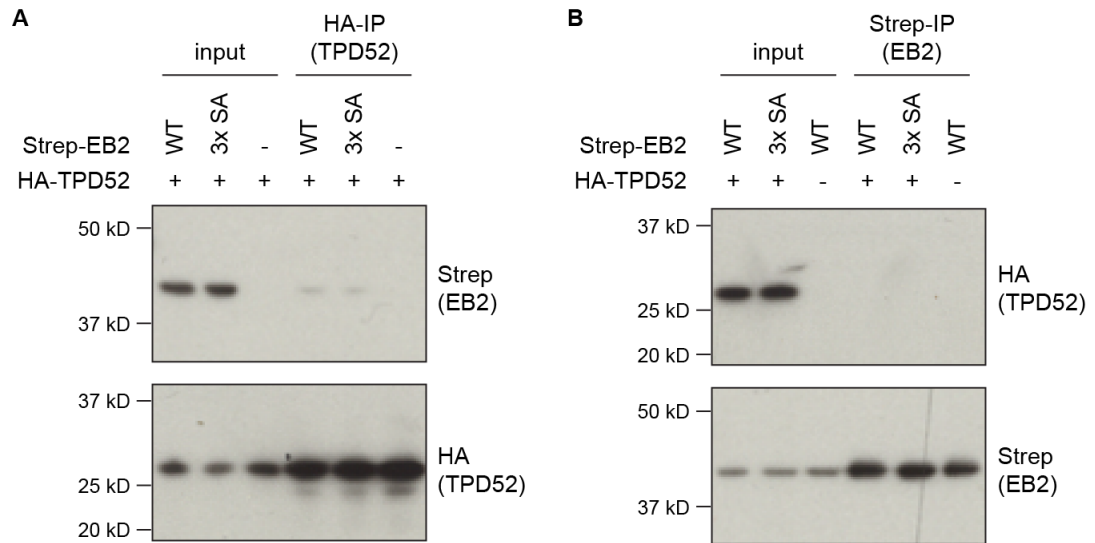
Figure 33: EB2 and TPD52 do not co-immunoprecipitate from HEK293T cells.

StrepII-tagged EB2 and HA-TPD52 were co-expressed in HEK293T cells. Immunoprecipitation by HA- or StrepII-affinity of lysates was visualised by Western blotting (1:1000 Strep, 1:2000 HA (Roche)). Input = 5% of total sample. 3x SA = S218/221/222A. (A) IP of HA-TPD52 did not show significant binding of Strep-EB2 compared to the input. (B) IP of Strep-EB2 was completely absent of any signs for HA-TPD52 interactions.

4.6.2 EB2 and TPD52 do not co-immunoprecipitate

We identified TPD52 as a potential phosphorylation-dependent binding partner of EB2. However, the screen we used to come to this finding used short EB2 peptides to pull down interactors from neuronal lysates. In order to verify if TPD52 also binds the EB2 protein in a phosphorylation-dependent manner, we overexpressed both proteins in HEK293T cells and determined protein-protein interactions by co-immunoprecipitation. We expected to see that EB2 and TPD52 co-IP, and that this interaction is abolished with phosphomutant EB2.

HA-TPD52 was co-expressed with either StrepII-tagged EB2 WT or S218/221/222A, which cannot be phosphorylated at the residues known to be dependent on CDKL5. We did not overexpress additional CDKL5 to stimulate phosphorylation of these residues, as previous experiments with the EB2 pS222 antibody showed that this site is already highly phosphorylated by endogenous kinases in HEK293T cells. TPD52 immunoprecipitation by HA-affinity of these lysates, did not result in a successful pull-down of EB2 (Figure 33A). We did observe minor bands for both wild type and phosphomutant EB2, but these are insignificant compared the input. The enrichment of TPD52 indicates efficient immunoprecipitation.

To confirm that EB2 and TPD52 do not interact in HEK293T cells, we also immunoprecipitated StrepII-tagged EB2 from HEK293T lysates overexpressing TPD52 and EB2. Again, we did not see any sign of interaction between the two proteins, while the enrichment of EB2 suggests an efficient IP (Figure 33B). We therefore had to conclude that there is no evidence for a protein-protein interaction between EB2 and TPD52. Theoretically it is still possible that EB2 was not phosphorylated at residues other than S222, and therefore did not bind TPD52. However, we would have expected to at least see some phosphorylation-independent interaction between the proteins. We therefore believe it is more likely that the result of the peptide pull-down screen was an artefact.

In this subchapter, we have shown that a phosphorylation-dependent binding partner of EB2 identified in a pull-down screen, did not hold up as valid interactor in co-IPs. By using short peptides as bait for the pull-down, we might have missed interactors that require multiple EB2 domains to bind to. EB2 phosphorylation in primary neurons is highly dependent on CDKL5, and we therefore aim to use Cdkl5 KO cultures to pull-down EB2 protein binding partners in the future instead. So far, we have to conclude that we do not know what the role of EB2 phosphorylation by CDKL5 is, or how this interaction is involved in neuronal development.

Chapter 5. Discussion

5.1 CDKL5 substrate identification

Loss of CDKL5 kinase activity is the genetic cause of a severe neurodevelopmental disorder. However, when we started this work, direct substrates of CDKL5 were largely unknown. Our main goal at the beginning of this thesis was therefore the identification of physiological CDKL5 substrates. By generating analogue-sensitive CDKL5 we were able to use chemical genetic kinase-substrate mapping to identify three putative phosphorylation targets of CDKL5: ARHGEF2, EB2 and MAP1S. We used *in vitro* kinase assays and mutagenesis to verify the direct phosphorylation of these substrates, and identified a second phosphorylation site on MAP1S. These four novel CDKL5 phosphorylation targets confirmed the preferred consensus sequence RPxS that had already been described in AMPH1 (Katayama et al., 2015). The generation of phosphospecific antibodies made it possible to validate all three candidates as physiological CDKL5 substrates. EB2 and MAP1S phosphorylation was strongly reduced in Cdkl5 KO mouse brains and cultured primary neurons, and striking loss of EB2 phosphorylation was even found in mature neurons derived from patient IPSCs. We therefore definitely succeeded in identifying novel physiological CDKL5 substrates.

5.1.1 Improving CDKL5 substrate identification

By using a chemical genetic kinase-substrate screen we successfully identified three novel CDKL5 phosphorylation targets. However, it would be foolish to assume that these are the only valid substrates of CDKL5. The failure of our screen to identify MAP1S pS812 for instance, unmistakably points out that we are dealing with a number of false negatives. To achieve full mass spectrometry coverage of the phosphoproteome, we could therefore apply other proteolytic enzymes than trypsin (Engholm-Keller and Larsen, 2013). As another way to improve sensitivity, we have also described our attempts to introduce stable isotope labelling to the samples by using SILAC or dimethyl labelling, although our NDR1 experiments showed that we were already capable of detecting phosphorylation of low abundant proteins. An important difference compared to the CDKL5 screen however, was the use of constitutively active NDR1 (Ultanir et al., 2012). The alleged difference in catalytic activity between the two kinases is likely to be the reason for the discrepancy in detection limit based on the ranking in abundance of the identified substrates in the mouse brain proteome (NDR1 substrates: #454 AAK1, #1939 Synergin γ, #2128 Rab11FIP5, #3566 RAPH1, #5315 PI4Kβ, #7052 Pannexin 2, CDKL5 substrates: #427 EB2, #969 ARHGEF2, #2073 MAP1S)(Sharma et al., 2015). It might therefore have been more fruitful if we had focused more on increasing the abundance of phosphorylation

events by improving the catalytic activity of CDKL5, or fractionation of the protein source to enrich for specific proteins. For example, subcellular compartments such as the nuclear envelope have been used as a protein source for chemical genetics in the past (Blethrow et al., 2008). In the future, we could therefore use synaptic fractions to enrich for proteins involved in neuronal transmission.

Other techniques to screen for kinase substrates in an unbiased way, such as KALIP (Xue et al., 2016), would be very interesting to apply to CDKL5 as well. Especially now that we have identified the RPxS motif as a consensus sequence for CDKL5 phosphorylation, which will make it easier to distinguish direct CDKL5 targets. With this in mind we also looked for changes in the global phosphoproteome of CDKL5 KO primary neurons, which led us to believe that CaV2.3 is a potential CDKL5 substrate as well. The low abundance of this R-type voltage-dependent calcium channel (#2330 in Sharma et al.) might have been the reason we did not detect it in the chemical genetic screen. We have therefore started a collaboration with Annette Dolphin at UCL to verify the phosphorylation by CDKL5 of this calcium channel, and investigate its potential role in CDKL5 deficiency disorder.

5.1.2 The RPxS consensus sequence

All CDKL5 substrates that we identified and validated *in vivo*, contain an RPxS phosphorylation site. This was in agreement with the residues determined to be critical for AMPH1 phosphorylation (Katayama et al., 2015). We therefore strongly believe that this is the preferred consensus sequence of CDKL5. However, this does not completely overlap with the other CDKL5 substrate candidates described in the literature (Table 9). MeCP2 and DNMT1, two highly disputed *in vitro* CDKL5 substrates of which the apparent phosphorylation sites are unknown (Kameshita et al., 2008; Mari et al., 2005), do not contain a RPxS motif. These proteins are therefore unlikely to be directly phosphorylated by CDKL5, and probably unspecific artefacts of *in vitro* kinase assays (Lin et al., 2005; Sekiguchi et al., 2013). NGL1 was identified as a CDKL5 substrate through a candidate approach, but *in vitro* kinase assays with purified proteins to determine direct phosphorylation by CDKL5, were never described (Ricciardi et al., 2012). NGL1 does not contain an RPxS motif either, and thus the reported reduction in phosphorylated NGL1 in CDKL5 deficient cells is likely to be an indirect effect. More recently, HDAC4 was identified as a substrate of CDKL5 in an unbiased screen (Trazzi et al., 2016). Although *in vitro* kinase assays and *in vivo* validation with a phosphospecific antibody were done, verification of the phosphorylation site by mutagenesis was surprisingly absent, and the reduction in endogenous phosphorylation relatively small. The reported HDAC4 phosphorylation site does not contain the RPxS motif, but interestingly, the serine at -4 does. We do not believe this is a coincidence, and hypothesize that HDAC4 is indeed a valid substrate of CDKL5, but that the wrong phosphorylation site is reported. Like we observe with EB2, loss of the directly

phosphorylated site can have an indirect effect on the phosphorylation of residues around it, and this is potentially happening with HDAC4 as well. The RPxS consensus sequence should therefore be used as a handle to quickly identify putative CDKL5 substrate candidates until conclusive evidence for direct phosphorylation of other sequences is provided.

Protein	Position	Sequence	Reference
MeCP2	n/a	n/a	(Mari et al., 2005)
DNMT1	n/a	n/a	(Kameshita et al., 2008)
NGL1	Ser631	LIRMN**S**K	(Ricciardi et al., 2012)
AMPH1	Ser293	PV**RP**R**S**P	(Sekiguchi et al., 2013)
HDAC4	Ser629	LS**R**AQ**S**S	(Trazzi et al., 2016)
ARHGEF2	Ser122	RE**RP**T**S**A	
EB2	Ser222	PS**RP**S**S**A	
MAP1S	Ser786	PA**RP**S**S**A	
MAP1S	Ser812	RN**RP**L**S**A	

Table 9: Overview of all reported CDKL5 phosphorylation target sites.

Five other putative CDKL5 substrates have been identified in the past, but MeCP2, DNMT1 and AMPH1 have only been described as *in vitro* targets, while evidence for the direct phosphorylation of NGL1 and HDAC4 is questionable. Only AMPH1 S293 contains the RPxS consensus sequence, although HDAC4 S626 interestingly does as well. Mouse sequences are presented, but are highly similar in humans.

5.1.3   Potential biomarkers for CDKL5 activity

The phosphospecific antibodies we have generated against EB2 pS222 and MAP1S pS812 showed high specificity and strong reductions of phosphorylated CDKL5 substrates *in vivo*. Especially EB2 phosphorylation was found to be highly abundant and almost completely dependent on CDKL5 in mouse and human neurons. We therefore believe that phosphorylated EB2 can potentially be used as an important biomarker for CDKL5 activity. By taking advantage of these markers for CDKL5 activity, we have been capable of showing upstream regulation of CDKL5 by NMDA receptor-dependent neuronal activity. Reduced catalytic activity precedes the previously reported CDKL5 proteosomal degradation (La Montanara et al., 2015) and could be an indirect effect of the loss of kinase activity. It would be interesting to further investigate the exact upstream mechanisms that result in inhibited CDKL5 kinase activity. For instance, a shift in subcellular CDKL5 localisation has been ascribed to extrasynaptic NDMA receptor activity specifically (Rusconi et al., 2011), but we do not know if this is also the case for altered kinase activity. The same counts for upstream kinases that might be involved in regulating CDKL5 catalytic activity.

138

Besides determining upstream regulation of CDKL5, EB2 phosphorylation can also be used as a marker for specifying temporal and spatial patterns of CDKL5 activity. We exemplified this by the surprising result that CDKL5 activity seems to completely contradict its temporal protein expression pattern. It is possible that changes in the subcellular localisation of CDKL5 are causing this effect. There have been claims that CDKL5 is mainly localised to excitatory synapses, although the evidence is still limited and often based on unspecific antibody staining (Okuda et al., 2017; Ricciardi et al., 2012). However, a developmental translocation of CDKL5 to the synapse where EB2 and MAP1S are absent, would explain why the phosphorylation of these substrates is lost at later ages. If we succeed in using the phosphospecific antibodies for immunofluorescence, we would be able to answer a lot of these questions.

Finally, EB2 and MAP1S phosphorylation could be useful tools for researchers closer to the clinical side of the spectrum. Heroic efforts are being undertaken to reinstate the lost kinase activity through gene therapy and protein replacement. Having reliable and quantifiable biomarkers for CDKL5 kinase activity are invaluable to achieve this. However, a lot more work has to be done before we can use the phosphospecific antibodies that we have generated for this purpose. Preferably CDKL5-dependent phosphorylation has to be observed in blood or CSF in order to use less invasive methods. Otherwise, different cell types such as fibroblasts might be an option. We are currently investigating if CDKL5-dependent changes in EB2 phosphorylation are being detected in different tissues than the brain. However, our results with HEK293T cells indicate that there might be other kinases present in mitotic cells that can phosphorylate EB2 at serine 222 (Iimori et al., 2016).

5.2   CDKL5 function

CDKL5 disease models have shown a variety of phenotypes involving neuronal morphogenesis. However, many of them have been very mild and not reproducible (Zhou et al., 2017). The function of CDKL5 in neuronal development is therefore still unknown. As a second goal for this thesis, we wanted to ascribe cellular functions to the phosphorylation events we identified, and link them to established phenotypes in Cdkl5 KO mice. As all three newly identified CDKL5 substrates were microtubule-associated proteins, we hypothesized an overarching role for CDKL5 in neuronal cytoskeleton regulation. We showed that MAP1S phosphorylation by CDKL5 indeed directly regulates its microtubule-binding affinity, and therefore controls microtubule bundling and stability. However, we were not able to determine any specific molecular or cellular functions for EB2 and ARHGEF2 phosphorylation. Although the microtubule cytoskeleton plays a crucial part in morphogenesis, we were not able to reproduce any aspects of impaired neuronal morphology described elsewhere. Based on the known roles of the CDKL5 substrates in microtubule dynamic instability, we did manage to discover affected microtubule plus-end dynamics in dendrites of Cdkl5 KO primary neurons. This phenotype was found to be downstream of MAP1S, and likely a result of the overstabilisation of microtubules upon the loss of MAP1S phosphorylation. Overall, we therefore believe that we have discovered important new mechanisms that establish a novel function of CDKL5 in regulating dynamics of the microtubule cytoskeleton (Figure 34). How this exactly disrupts neuronal development in the absence of CDKL5 is still unknown.
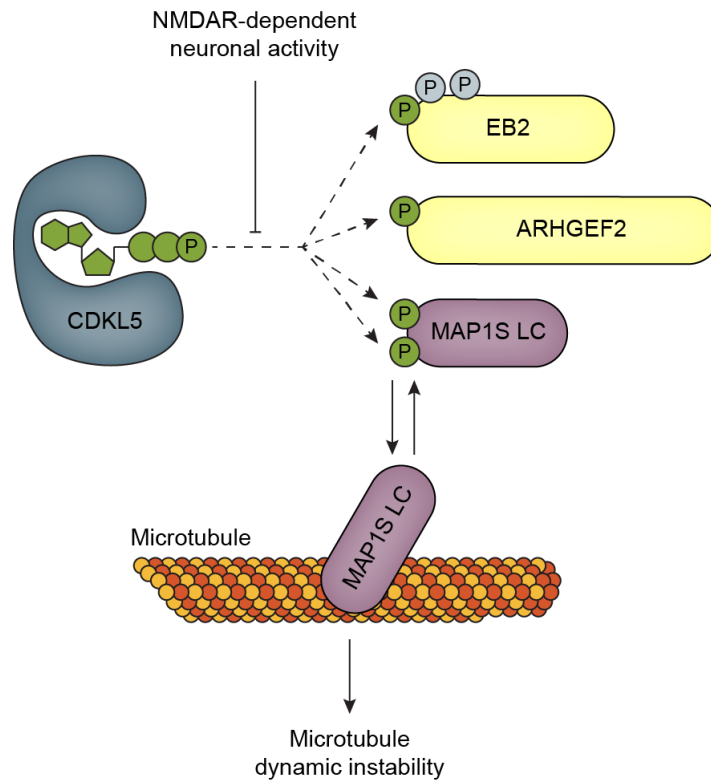
Figure 34: Summary schematic of novel CDKL5 substrates and functions.

CDKL5 has been shown to phosphorylate three novel substrates: EB2, ARHGEF2 and MAP1S. EB2 is directly phosphorylated at serine 222, but phosphorylation of serine 218 and 221 were also found to be CDKL5-dependent. ARHGEF2 is directly phosphorylated at serine 122, and CDKL5 directly phosphorylates both MAP1S serine 786 and 812. CDKL5 catalytic activity is regulated by NMDA receptor-dependent neuronal depolarisation. Phosphorylation of MAP1S mediates its microtubule-binding affinity and is responsible for altered microtubule dynamic instability observed in developing dendrites of CDKL5 KO primary neurons.

Appendix

SLENDR ssODN sequences

Guide sgRNA targets are highlighted in red. HA-tag sequence is highlighted in capitals, as well as additional mutations to lose the 5' NGG motif.

CDKL5 N-terminal HA

ccctgcttactgaataacttgtttagacgtttctttttttggtgccatgttctgtggctcacatcaaaagagCagtttgtcttcatgTACCCATACGATGTTCCAGATTACGCTaagattcctaacattggtaatgtgatgaataaatttgagatccttggggttgtcggtgaaggtaagttagaatttcacgtttgaag

MAP1S C-terminal HA

accaggcactgggcatcagggtgctgggcagtggcagcctggtgtccatgcaggacgaggccttccccgcctgcaaggtgCagttcTACCCATACGATGTTCCAGATTACGCTtagccccacgctgcagggcagcctgggaacaacagttcctcactgtgacccaggttggtgctgtggctccatgtgcaaagctagat

EB2 N-terminal HA

agggtgagcagcaagcagcggggagacacaaccctccgccccagtcagccaccgcgtgtgttccctctgtcgggagagcgccaatgTACCCATACGATGTTCCAGATTACGCTcccgggccgacccaaacgttgtccccaaatggcgagaacaacaacgacatcatccaggataacgggactatcattcctttccggaa

ARHGEF2 N-terminal HA

ggccgacgcgtgcggccggacccctcccccgccgttgctggacacccggggccgccgcgtcctcccgcggctcacgctggattatgTACCCATACGATGTTCCAGATTACGCTtctcggatcgaatccctcactcgcgcgcggatcgaccggagcaaggagcaggcaaccaaggtgggctggctctgcgaccgggcgcc

CaMKIIa C-terminal HA

gaggagacccgcgtctggcaccgcagggacggcaaatggcagatcgtccacttccacagatctggggcgccctccgtcctgccgcacTACCCTTACGACGTTCCAGACTACGCTtaaggattctttcttcctgaatctctggggtgcattaagggtattgccttgtagaggggcatgccccaggggagtggaggtggg

References

Akhmanova, A., and Hoogenraad, C.C. (2015). Microtubule minus-end-targeting proteins. Curr Biol *25*, R162-171.

Akhmanova, A., and Steinmetz, M.O. (2008). Tracking the ends: a dynamic protein network controls the fate of microtubule tips. Nature reviews Molecular cell biology *9*, 309-322.

Alvarez, V.A., Ridenour, D.A., and Sabatini, B.L. (2006). Retraction of synapses and dendritic spines induced by off-target effects of RNA interference. The Journal of neuroscience : the official journal of the Society for Neuroscience *26*, 7820-7825.

Alves-Silva, J., Sanchez-Soriano, N., Beaven, R., Klein, M., Parkin, J., Millard, T.H., Bellen, H.J., Venken, K.J., Ballestrem, C., Kammerer, R.A.*, et al.* (2012). Spectraplakins promote microtubule-mediated axonal growth by functioning as structural microtubule-associated proteins and EB1-dependent +TIPs (tip interacting proteins). The Journal of neuroscience : the official journal of the Society for Neuroscience *32*, 9143-9158.

Amano, M., Hamaguchi, T., Shohag, M.H., Kozawa, K., Kato, K., Zhang, X., Yura, Y., Matsuura, Y., Kataoka, C., Nishioka, T.*, et al.* (2015). Kinase-interacting substrate screening is a novel method to identify kinase substrates. J Cell Biol *209*, 895-912.

Amendola, E., Zhan, Y., Mattucci, C., Castroflorio, E., Calcagno, E., Fuchs, C., Lonetti, G., Silingardi, D., Vyssotski, A.L., Farley, D.*, et al.* (2014). Mapping pathological phenotypes in a mouse model of CDKL5 disorder. PloS one *9*, e91613.

Amenduni, M., De Filippis, R., Cheung, A.Y., Disciglio, V., Epistolato, M.C., Ariani, F., Mari, F., Mencarelli, M.A., Hayek, Y., Renieri, A.*, et al.* (2011). iPS cells to model CDKL5-related disorders. European journal of human genetics : EJHG *19*, 1246-1255.

Arens, J., Duong, T.T., and Dehmelt, L. (2013). A morphometric screen identifies specific roles for microtubule-regulating genes in neuronal development of P19 stem cells. PloS one *8*, e79796.

Armstrong, D.D., Dunn, J.K., Schultz, R.J., Herbert, D.A., Glaze, D.G., and Motil, K.J. (1999). Organ growth in Rett syndrome: a postmortem examination analysis. Pediatr Neurol *20*, 125-129.

Arnheim, N., and Calabrese, P. (2009). Understanding what determines the frequency and pattern of human germline mutations. Nat Rev Genet *10*, 478-488.

Baas, P.W., and Lin, S. (2011). Hooks and comets: The story of microtubule polarity orientation in the neuron. Dev Neurobiol *71*, 403-418.

Baek, S.T., Kerjan, G., Bielas, S.L., Lee, J.E., Fenstermaker, A.G., Novarino, G., and Gleeson, J.G. (2014). Off-target effect of doublecortin family shRNA on neuronal migration associated with endogenous microRNA dysregulation. Neuron *82*, 1255-1262.

Bahi-Buisson, N., Villeneuve, N., Caietta, E., Jacquette, A., Maurey, H., Matthijs, G., Van Esch, H., Delahaye, A., Moncla, A., Milh, M.*, et al.* (2012). Recurrent mutations in the CDKL5 gene: genotype-phenotype relationships. American journal of medical genetics Part A *158A*, 1612-1619.

Baj, G., Patrizio, A., Montalbano, A., Sciancalepore, M., and Tongiorgi, E. (2014). Developmental and maintenance defects in Rett syndrome neurons identified by a new mouse staging system in vitro. Front Cell Neurosci *8*, 18.

Baltussen, L., Rosianu, F., and Ultanir, S. (2017). Kinases in synaptic development and neurological diseases. Prog Neuropsychopharmacol Biol Psychiatry.

Banker, G., and Goslin, K. (1988). Developments in neuronal cell culture. Nature *336*, 185-186.

Barbiero, I., Peroni, D., Tramarin, M., Chandola, C., Rusconi, L., Landsberger, N., and Kilstrup-Nielsen, C. (2017). The neurosteroid pregnenolone reverts microtubule derangement induced by the loss of a functional CDKL5-IQGAP1 complex. Human molecular genetics *26*, 3520-3530.

Bertani, I., Rusconi, L., Bolognese, F., Forlani, G., Conca, B., De Monte, L., Badaracco, G., Landsberger, N., and Kilstrup-Nielsen, C. (2006). Functional consequences of mutations in CDKL5, an X-linked gene involved in infantile spasms and mental retardation. The Journal of biological chemistry *281*, 32048-32056.

Berwick, D.C., and Harvey, K. (2011). LRRK2 signaling pathways: the key to unlocking neurodegeneration? Trends in cell biology *21*, 257-265.

Biesemann, C., Gronborg, M., Luquet, E., Wichert, S.P., Bernard, V., Bungers, S.R., Cooper, B., Varoqueaux, F., Li, L., Byrne, J.A.*, et al.* (2014). Proteomic screening of glutamatergic mouse brain synaptosomes isolated by fluorescence activated sorting. EMBO J *33*, 157-170.

Birkenfeld, J., Nalbant, P., Yoon, S.H., and Bokoch, G.M. (2008). Cellular functions of GEF-H1, a microtubule-regulated Rho-GEF: is altered GEF-H1 activity a crucial determinant of disease pathogenesis? Trends in cell biology *18*, 210-219.

Blethrow, J., Zhang, C., Shokat, K.M., and Weiss, E.L. (2004). Design and use of analog-sensitive protein kinases. Current protocols in molecular biology / edited by Frederick M Ausubel [et al] *Chapter 18*, Unit 18 11.

Blethrow, J.D., Glavy, J.S., Morgan, D.O., and Shokat, K.M. (2008). Covalent capture of kinase-specific phosphopeptides reveals Cdk1-cyclin B substrates. Proceedings of the National Academy of Sciences of the United States of America *105*, 1442-1447.

Borg, I., Freude, K., Kubart, S., Hoffmann, K., Menzel, C., Laccone, F., Firth, H., Ferguson-Smith, M.A., Tommerup, N., Ropers, H.H.*, et al.* (2005). Disruption of Netrin G1 by a balanced chromosome translocation in a girl with Rett syndrome. European journal of human genetics : EJHG *13*, 921-927.

Boutros, R., Fanayan, S., Shehata, M., and Byrne, J.A. (2004). The tumor protein D52 family: many pieces, many puzzles. Biochemical and biophysical research communications *325*, 1115-1121.

Campbell, J.N., and Slep, K.C. (2011). alphabeta-Tubulin and microtubule-binding assays. Methods Mol Biol *777*, 87-97.

Canning, P., Krojer, T., Goubin, S., Mahajan, P., Vollmar, M., Pike, A.C.W., von Delft, F., Arrowsmith, C.H., Edwards, A.M., Bountra, C., Bullock, A (2013). Crystal Structure of the Human Cdkl5 Kinase Domain (http://www.rcsb.org/pdb/explore/explore.do?structureId=4BGQ).

Carouge, D., Host, L., Aunis, D., Zwiller, J., and Anglard, P. (2010). CDKL5 is a brain MeCP2 target gene regulated by DNA methylation. Neurobiology of disease *38*, 414-424.

Chahrour, M., and Zoghbi, H.Y. (2007). The story of Rett syndrome: from clinic to neurobiology. Neuron *56*, 422-437.

Chailangkarn, T., Trujillo, C.A., Freitas, B.C., Hrvoj-Mihic, B., Herai, R.H., Yu, D.X., Brown, T.T., Marchetto, M.C., Bardy, C., McHenry, L.*, et al.* (2016). A human neurodevelopmental model for Williams syndrome. Nature *536*, 338-343.

Chen, Q., Zhu, Y.C., Yu, J., Miao, S., Zheng, J., Xu, L., Zhou, Y., Li, D., Zhang, C., Tao, J.*, et al.* (2010). CDKL5, a protein associated with rett syndrome, regulates neuronal morphogenesis via Rac1

signaling. The Journal of neuroscience : the official journal of the Society for Neuroscience *30*, 12777-12786.

Cheng, P.L., and Poo, M.M. (2012). Early events in axon/dendrite polarization. Annu Rev Neurosci *35*, 181-201.

Cheung, Z.H., and Ip, N.Y. (2012). Cdk5: a multifaceted kinase in neurodegenerative diseases. Trends in cell biology *22*, 169-175.

Chico, L.K., Van Eldik, L.J., and Watterson, D.M. (2009). Targeting protein kinases in central nervous system disorders. Nature reviews Drug discovery *8*, 892-909.

Cline, H., and Haas, K. (2008). The regulation of dendritic arbor development and plasticity by glutamatergic synaptic input: a review of the synaptotrophic hypothesis. J Physiol *586*, 1509-1517.

Cohen, P. (2000). The regulation of protein function by multisite phosphorylation--a 25 year update. Trends Biochem Sci *25*, 596-601.

Cohen, P., and Alessi, D.R. (2013). Kinase drug discovery--what's next in the field? ACS Chem Biol *8*, 96-104.

Cohen, P., and Knebel, A. (2006). KESTREL: a powerful method for identifying the physiological substrates of protein kinases. The Biochemical journal *393*, 1-6.

Comeau, J.W., Costantino, S., and Wiseman, P.W. (2006). A guide to accurate fluorescence microscopy colocalization measurements. Biophys J *91*, 4611-4622.

Conde, C., Arias, C., Robin, M., Li, A., Saito, M., Chuang, J.Z., Nairn, A.C., Sung, C.H., and Caceres, A. (2010). Evidence for the involvement of Lfc and Tctex-1 in axon formation. The Journal of neuroscience : the official journal of the Society for Neuroscience *30*, 6793-6800.

Conde, C., and Caceres, A. (2009). Microtubule assembly, organization and dynamics in axons and dendrites. Nature reviews Neuroscience *10*, 319-332.

Costes, S.V., Daelemans, D., Cho, E.H., Dobbin, Z., Pavlakis, G., and Lockett, S. (2004). Automatic and quantitative measurement of protein-protein colocalization in live cells. Biophys J *86*, 3993-4003.

Crino, P.B. (2011). mTOR: A pathogenic signaling pathway in developmental brain malformations. Trends Mol Med *17*, 734-742.

Dallol, A., Cooper, W.N., Al-Mulla, F., Agathanggelou, A., Maher, E.R., and Latif, F. (2007). Depletion of the Ras association domain family 1, isoform A-associated novel microtubule-associated protein, C19ORF5/MAP1S, causes mitotic abnormalities. Cancer Res *67*, 492-500.

Dar, A.C., and Shokat, K.M. (2011). The evolution of protein kinase inhibitors from antagonists to agonists of cellular signaling. Annu Rev Biochem *80*, 769-795.

De Groot, C.O., Jelesarov, I., Damberger, F.F., Bjelic, S., Scharer, M.A., Bhavesh, N.S., Grigoriev, I., Buey, R.M., Wuthrich, K., Capitani, G.*, et al.* (2010). Molecular insights into mammalian end-binding protein heterodimerization. The Journal of biological chemistry *285*, 5802-5814.

Dehmelt, L., and Halpain, S. (2005). The MAP2/Tau family of microtubule-associated proteins. Genome Biol *6*, 204.

Della Sala, G., Putignano, E., Chelini, G., Melani, R., Calcagno, E., Michele Ratto, G., Amendola, E., Gross, C.T., Giustetto, M., and Pizzorusso, T. (2015). Dendritic Spine Instability in a Mouse Model of CDKL5 Disorder Is Rescued by Insulin-like Growth Factor 1. Biol Psychiatry.

Ding, J., Valle, A., Allen, E., Wang, W., Nardine, T., Zhang, Y., Peng, L., and Yang, Y. (2006). Microtubule-associated protein 8 contains two microtubule binding sites. Biochemical and biophysical research communications *339*, 172-179.

Dubos, A., Pannetier, S., and Hanauer, A. (2008). Inactivation of the CDKL3 gene at 5q31.1 by a balanced t(X;5) translocation associated with nonspecific mild mental retardation. American journal of medical genetics Part A *146A*, 1267-1279.

Ebert, D.H., and Greenberg, M.E. (2013). Activity-dependent neuronal signalling and autism spectrum disorder. Nature *493*, 327-337.

Eblen, S.T., Kumar, N.V., Shah, K., Henderson, M.J., Watts, C.K., Shokat, K.M., and Weber, M.J. (2003). Identification of novel ERK2 substrates through use of an engineered kinase and ATP analogs. The Journal of biological chemistry *278*, 14926-14935.

Engholm-Keller, K., and Larsen, M.R. (2013). Technologies and challenges in large-scale phosphoproteomics. Proteomics *13*, 910-931.

Eriksson, M., Samuelsson, H., Samuelsson, E.B., Liu, L., McKeehan, W.L., Benedikz, E., and Sundstrom, E. (2007). The NMDAR subunit NR3A interacts with microtubule-associated protein 1S in the brain. Biochemical and biophysical research communications *361*, 127-132.

Fehr, S., Wilson, M., Downs, J., Williams, S., Murgia, A., Sartori, S., Vecchi, M., Ho, G., Polli, R., Psoni, S.*, et al.* (2013). The CDKL5 disorder is an independent clinical entity associated with early-onset encephalopathy. European journal of human genetics : EJHG *21*, 266-273.

Fehr, S., Wong, K., Chin, R., Williams, S., de Klerk, N., Forbes, D., Krishnaraj, R., Christodoulou, J., Downs, J., and Leonard, H. (2016). Seizure variables and their relationship to genotype and functional abilities in the CDKL5 disorder. Neurology *87*, 2206-2213.

Feng, G., Mellor, R.H., Bernstein, M., Keller-Peck, C., Nguyen, Q.T., Wallace, M., Nerbonne, J.M., Lichtman, J.W., and Sanes, J.R. (2000). Imaging neuronal subsets in transgenic mice expressing multiple spectral variants of GFP. Neuron *28*, 41-51.

Flynn, K.C., Hellal, F., Neukirchen, D., Jacob, S., Tahirovic, S., Dupraz, S., Stern, S., Garvalov, B.K., Gurniak, C., Shaw, A.E.*, et al.* (2012). ADF/cofilin-mediated actin retrograde flow directs neurite formation in the developing brain. Neuron *76*, 1091-1107.

Fu, Z., Schroeder, M.J., Shabanowitz, J., Kaldis, P., Togawa, K., Rustgi, A.K., Hunt, D.F., and Sturgill, T.W. (2005). Activation of a nuclear Cdc2-related kinase within a mitogen-activated protein kinase-like TDY motif by autophosphorylation and cyclin-dependent protein kinase-activating kinase. Molecular and cellular biology *25*, 6047-6064.

Fuchs, C., Rimondini, R., Viggiano, R., Trazzi, S., De Franceschi, M., Bartesaghi, R., and Ciani, E. (2015). Inhibition of GSK3beta rescues hippocampal development and learning in a mouse model of CDKL5 disorder. Neurobiology of disease *82*, 298-310.

Fuchs, C., Trazzi, S., Torricella, R., Viggiano, R., De Franceschi, M., Amendola, E., Gross, C., Calza, L., Bartesaghi, R., and Ciani, E. (2014). Loss of CDKL5 impairs survival and dendritic growth of newborn neurons by altering AKT/GSK-3beta signaling. Neurobiology of disease.

Gantke, T., Boussouf, S., Janzen, J., Morrice, N.A., Howell, S., Muhlberger, E., and Ley, S.C. (2013). Ebola virus VP35 induces high-level production of recombinant TPL-2-ABIN-2-NF-kappaB1 p105 complex in co-transfected HEK-293 cells. The Biochemical journal *452*, 359-365.

Garske, A.L., Peters, U., Cortesi, A.T., Perez, J.L., and Shokat, K.M. (2011). Chemical genetic strategy for targeting protein kinases based on covalent complementarity. Proceedings of the National Academy of Sciences of the United States of America *108*, 15046-15052.

Gauthier-Fisher, A., Lin, D.C., Greeve, M., Kaplan, D.R., Rottapel, R., and Miller, F.D. (2009). Lfc and Tctex-1 regulate the genesis of neurons from cortical precursor cells. Nature neuroscience *12*, 735-744.

Geraldo, S., and Gordon-Weeks, P.R. (2009). Cytoskeletal dynamics in growth-cone steering. Journal of cell science *122*, 3595-3604.

Geraldo, S., Khanzada, U.K., Parsons, M., Chilton, J.K., and Gordon-Weeks, P.R. (2008). Targeting of the F-actin-binding protein drebrin by the microtubule plus-tip protein EB3 is required for neuritogenesis. Nature cell biology *10*, 1181-1189.

Ghiretti, A.E., Thies, E., Tokito, M.K., Lin, T., Ostap, E.M., Kneussel, M., and Holzbaur, E.L.F. (2016). Activity-Dependent Regulation of Distinct Transport and Cytoskeletal Remodeling Functions of the Dendritic Kinesin KIF21B. Neuron *92*, 857-872.

Ghosh, A., and Giese, K.P. (2015). Calcium/calmodulin-dependent kinase II and Alzheimer's disease. Molecular brain *8*, 78.

Goldspink, D.A., Gadsby, J.R., Bellett, G., Keynton, J., Tyrrell, B.J., Lund, E.K., Powell, P.P., Thomas, P., and Mogensen, M.M. (2013). The microtubule end-binding protein EB2 is a central regulator of microtubule reorganisation in apico-basal epithelial differentiation. Journal of cell science *126*, 4000-4014.

Gordon-Weeks, P.R., and Fournier, A.E. (2014). Neuronal cytoskeleton in synaptic plasticity and regeneration. J Neurochem *129*, 206-212.

Greene, N.D., and Copp, A.J. (2009). Development of the vertebrate central nervous system: formation of the neural tube. Prenat Diagn *29*, 303-311.

Gregan, J., Zhang, C., Rumpf, C., Cipak, L., Li, Z., Uluocak, P., Nasmyth, K., and Shokat, K.M. (2007). Construction of conditional analog-sensitive kinase alleles in the fission yeast Schizosaccharomyces pombe. Nat Protoc *2*, 2996-3000.

Grosso, S., Brogna, A., Bazzotti, S., Renieri, A., Morgese, G., and Balestri, P. (2007). Seizures and electroencephalographic findings in CDKL5 mutations: case report and review. Brain Dev *29*, 239-242.

Grueber, W.B., and Sagasti, A. (2010). Self-avoidance and tiling: Mechanisms of dendrite and axon spacing. Cold Spring Harb Perspect Biol *2*, a001750.

Gu, J., Firestein, B.L., and Zheng, J.Q. (2008). Microtubules in dendritic spine development. The Journal of neuroscience : the official journal of the Society for Neuroscience *28*, 12120-12124.

Gunosewoyo, H., Yu, L., Munoz, L., and Kassiou, M. (2017). Kinase targets in CNS drug discovery. Future Med Chem *9*, 303-314.

Hagebeuk, E.E., Marcelis, C.L., Alders, M., Kaspers, A., and de Weerd, A.W. (2015). Two Siblings With a CDKL5 Mutation: Genotype and Phenotype Evaluation. J Child Neurol *30*, 1515-1519.

Halpain, S., and Dehmelt, L. (2006). The MAP1 family of microtubule-associated proteins. Genome Biol *7*, 224.

Hector, R.D., Dando, O., Landsberger, N., Kilstrup-Nielsen, C., Kind, P.C., Bailey, M.E., and Cobb, S.R. (2016). Characterisation of CDKL5 Transcript Isoforms in Human and Mouse. PloS one *11*, e0157758.

Hector, R.D., Dando, O., Ritakari, T.E., Kind, P.C., Bailey, M.E., and Cobb, S.R. (2017). Characterisation of Cdkl5 transcript isoforms in rat. Gene *603*, 21-26.

Hertz, N.T., Wang, B.T., Allen, J.J., Zhang, C., Dar, A.C., Burlingame, A.L., and Shokat, K.M. (2010). Chemical genetic approach for kinase-substrate mapping by covalent capture of thiophosphopeptides and analysis by mass spectrometry. Current protocols in chemical biology *2*, 15-36.

Hirokawa, N., Niwa, S., and Tanaka, Y. (2010). Molecular motors in neurons: transport mechanisms and roles in brain function, development, and disease. Neuron *68*, 610-638.

Hoogenraad, C.C., and Bradke, F. (2009). Control of neuronal polarity and plasticity--a renaissance for microtubules? Trends in cell biology *19*, 669-676.

Hornbeck, P.V., Zhang, B., Murray, B., Kornhauser, J.M., Latham, V., and Skrzypek, E. (2015). PhosphoSitePlus, 2014: mutations, PTMs and recalibrations. Nucleic Acids Res *43*, D512-520.

Howard, J., and Hyman, A.A. (2009). Growth, fluctuation and switching at microtubule plus ends. Nature reviews Molecular cell biology *10*, 569-574.

Hu, X., Viesselmann, C., Nam, S., Merriam, E., and Dent, E.W. (2008). Activity-dependent dynamic microtubule invasion of dendritic spines. The Journal of neuroscience : the official journal of the Society for Neuroscience *28*, 13094-13105.

Huang, I.H., Hsiao, C.T., Wu, J.C., Shen, R.F., Liu, C.Y., Wang, Y.K., Chen, Y.C., Huang, C.M., del Alamo, J.C., Chang, Z.F.*, et al.* (2014). GEF-H1 controls focal adhesion signaling that regulates mesenchymal stem cell lineage commitment. Journal of cell science *127*, 4186-4200.

Huber, A.B., Kolodkin, A.L., Ginty, D.D., and Cloutier, J.F. (2003). Signaling at the growth cone: ligand-receptor complexes and the control of axon growth and guidance. Annu Rev Neurosci *26*, 509-563.

Hutti, J.E., Jarrell, E.T., Chang, J.D., Abbott, D.W., Storz, P., Toker, A., Cantley, L.C., and Turk, B.E. (2004). A rapid method for determining protein kinase phosphorylation specificity. Nature methods *1*, 27-29.

Iimori, M., Watanabe, S., Kiyonari, S., Matsuoka, K., Sakasai, R., Saeki, H., Oki, E., Kitao, H., and Maehara, Y. (2016). Phosphorylation of EB2 by Aurora B and CDK1 ensures mitotic progression and genome stability. Nat Commun *7*, 11117.

Inoue, S., and Salmon, E.D. (1995). Force generation by microtubule assembly/disassembly in mitosis and related movements. Mol Biol Cell *6*, 1619-1640.

Isrie, M., Breuss, M., Tian, G., Hansen, A.H., Cristofoli, F., Morandell, J., Kupchinsky, Z.A., Sifrim, A., Rodriguez-Rodriguez, C.M., Dapena, E.P.*, et al.* (2015). Mutations in Either TUBB or MAPRE2 Cause Circumferential Skin Creases Kunze Type. American journal of human genetics *97*, 790-800.

Jaworski, J., Kapitein, L.C., Gouveia, S.M., Dortland, B.R., Wulf, P.S., Grigoriev, I., Camera, P., Spangler, S.A., Di Stefano, P., Demmers, J.*, et al.* (2009). Dynamic microtubules regulate dendritic spine morphology and synaptic plasticity. Neuron *61*, 85-100.

Jeong, J.S., Jiang, L., Albino, E., Marrero, J., Rho, H.S., Hu, J., Hu, S., Vera, C., Bayron-Poueymiroy, D., Rivera-Pacheco, Z.A.*, et al.* (2012). Rapid identification of monospecific monoclonal antibodies using a human proteome microarray. Molecular & cellular proteomics : MCP *11*, O111 016253.

Johnson, S.A., and Hunter, T. (2005). Kinomics: methods for deciphering the kinome. Nature methods *2*, 17-25.

Joseph, R.E., and Andreotti, A.H. (2011). Controlling the activity of the Tec kinase Itk by mutation of the phenylalanine gatekeeper residue. Biochemistry *50*, 221-229.

Kalil, K., and Dent, E.W. (2014). Branch management: mechanisms of axon branching in the developing vertebrate CNS. Nature reviews Neuroscience *15*, 7-18.

Kalscheuer, V.M., Tao, J., Donnelly, A., Hollway, G., Schwinger, E., Kubart, S., Menzel, C., Hoeltzenbein, M., Tommerup, N., Eyre, H.*, et al.* (2003). Disruption of the serine/threonine kinase 9 gene causes severe X-linked infantile spasms and mental retardation. American journal of human genetics *72*, 1401-1411.

Kameshita, I., Sekiguchi, M., Hamasaki, D., Sugiyama, Y., Hatano, N., Suetake, I., Tajima, S., and Sueyoshi, N. (2008). Cyclin-dependent kinase-like 5 binds and phosphorylates DNA methyltransferase 1. Biochemical and biophysical research communications *377*, 1162-1167.

Kang, M.G., Guo, Y., and Huganir, R.L. (2009). AMPA receptor and GEF-H1/Lfc complex regulates dendritic spine development through RhoA signaling cascade. Proceedings of the National Academy of Sciences of the United States of America *106*, 3549-3554.

Kapitein, L.C., Yau, K.W., Gouveia, S.M., van der Zwan, W.A., Wulf, P.S., Keijzer, N., Demmers, J., Jaworski, J., Akhmanova, A., and Hoogenraad, C.C. (2011). NMDA receptor activation suppresses microtubule growth and spine entry. The Journal of neuroscience : the official journal of the Society for Neuroscience *31*, 8194-8209.

Katayama, S., Sueyoshi, N., and Kameshita, I. (2015). Critical Determinants of Substrate Recognition by Cyclin-Dependent Kinase-like 5 (CDKL5). Biochemistry *54*, 2975-2987.

Kaufmann, W.E., and Moser, H.W. (2000). Dendritic anomalies in disorders associated with mental retardation. Cerebral cortex *10*, 981-991.

Kilstrup-Nielsen, C., Rusconi, L., La Montanara, P., Ciceri, D., Bergo, A., Bedogni, F., and Landsberger, N. (2012). What we know and would like to know about CDKL5 and its involvement in epileptic encephalopathy. Neural plasticity *2012*, 728267.

Kleele, T., Marinkovic, P., Williams, P.R., Stern, S., Weigand, E.E., Engerer, P., Naumann, R., Hartmann, J., Karl, R.M., Bradke, F*., et al.* (2014). An assay to image neuronal microtubule dynamics in mice. Nat Commun *5*, 4827.

Komarova, Y., De Groot, C.O., Grigoriev, I., Gouveia, S.M., Munteanu, E.L., Schober, J.M., Honnappa, S., Buey, R.M., Hoogenraad, C.C., Dogterom, M*., et al.* (2009). Mammalian end binding proteins control persistent microtubule growth. J Cell Biol *184*, 691-706.

Komarova, Y., Lansbergen, G., Galjart, N., Grosveld, F., Borisy, G.G., and Akhmanova, A. (2005). EB1 and EB3 control CLIP dissociation from the ends of growing microtubules. Mol Biol Cell *16*, 5334-5345.

Konur, S., Rabinowitz, D., Fenstermaker, V.L., and Yuste, R. (2003). Systematic regulation of spine sizes and densities in pyramidal neurons. Journal of neurobiology *56*, 95-112.

Kriegstein, A., and Alvarez-Buylla, A. (2009). The glial nature of embryonic and adult neural stem cells. Annu Rev Neurosci *32*, 149-184.

Krishnaraj, R., Ho, G., and Christodoulou, J. (2017). RettBASE: Rett Syndrome Database Update. Hum Mutat.

Krylyshkina, O., Anderson, K.I., Kaverina, I., Upmann, I., Manstein, D.J., Small, J.V., and Toomre, D.K. (2003). Nanometer targeting of microtubules to focal adhesions. J Cell Biol *161*, 853-859.

La Montanara, P., Rusconi, L., Locarno, A., Forti, L., Barbiero, I., Tramarin, M., Chandola, C., Kilstrup-Nielsen, C., and Landsberger, N. (2015). Synaptic synthesis, dephosphorylation and degradation: a novel paradigm for an activity-dependent neuronal control of CDKL5. The Journal of biological chemistry.

Lai, Y.C., Kondapalli, C., Lehneck, R., Procter, J.B., Dill, B.D., Woodroof, H.I., Gourlay, R., Peggie, M., Macartney, T.J., Corti, O*., et al.* (2015). Phosphoproteomic screening identifies Rab GTPases as novel downstream targets of PINK1. EMBO J *34*, 2840-2861.

Le Dreau, G., and Marti, E. (2012). Dorsal-ventral patterning of the neural tube: a tale of three signals. Dev Neurobiol *72*, 1471-1481.

Lefebvre, J.L., Sanes, J.R., and Kay, J.N. (2015). Development of dendritic form and function. Annu Rev Cell Dev Biol *31*, 741-777.

Lein, E.S., Hawrylycz, M.J., Ao, N., Ayres, M., Bensinger, A., Bernard, A., Boe, A.F., Boguski, M.S., Brockway, K.S., Byrnes, E.J*., et al.* (2007). Genome-wide atlas of gene expression in the adult mouse brain. Nature *445*, 168-176.

Lewis, S.A., and Cowan, N. (1990). Microtubule bundling. Nature *345*, 674.

Lin, C., Franco, B., and Rosner, M.R. (2005). CDKL5/Stk9 kinase inactivation is associated with neuronal developmental disorders. Human molecular genetics *14*, 3775-3786.

Liu, H., Yue, J., Huang, H., Gou, X., Chen, S.Y., Zhao, Y., and Wu, X. (2015). Regulation of Focal Adhesion Dynamics and Cell Motility by the EB2 and Hax1 Protein Complex. The Journal of biological chemistry *290*, 30771-30782.

Liu, L., Xie, R., Yang, C., and McKeehan, W.L. (2009). Dual function microtubule- and mitochondria-associated proteins mediate mitotic cell death. Cell Oncol *31*, 393-405.

Liu, Z., Xu, D., Zhao, Y., and Zheng, J. (2010). Non-syndromic mild mental retardation candidate gene CDKL3 regulates neuronal morphogenesis. Neurobiology of disease *39*, 242-251.

Livide, G., Patriarchi, T., Amenduni, M., Amabile, S., Yasui, D., Calcagno, E., Lo Rizzo, C., De Falco, G., Ulivieri, C., Ariani, F.*, et al.* (2015). GluD1 is a common altered player in neuronal differentiation from both MECP2-mutated and CDKL5-mutated iPS cells. European journal of human genetics : EJHG *23*, 195-201.

Lo Martire, V., Alvente, S., Bastianini, S., Berteotti, C., Silvani, A., Valli, A., Viggiano, R., Ciani, E., and Zoccoli, G. (2017). CDKL5 deficiency entails sleep apneas in mice. J Sleep Res.

London, M., and Hausser, M. (2005). Dendritic computation. Annu Rev Neurosci *28*, 503-532.

Luhmann, H.J., Sinning, A., Yang, J.W., Reyes-Puerta, V., Stuttgen, M.C., Kirischuk, S., and Kilb, W. (2016). Spontaneous Neuronal Activity in Developing Neocortical Networks: From Single Cells to Large-Scale Interactions. Front Neural Circuits *10*, 40.

Mann, M. (2006). Functional and quantitative proteomics using SILAC. Nature reviews Molecular cell biology *7*, 952-958.

Manning, G., Whyte, D.B., Martinez, R., Hunter, T., and Sudarsanam, S. (2002). The protein kinase complement of the human genome. Science *298*, 1912-1934.

Mari, F., Azimonti, S., Bertani, I., Bolognese, F., Colombo, E., Caselli, R., Scala, E., Longo, I., Grosso, S., Pescucci, C.*, et al.* (2005). CDKL5 belongs to the same molecular pathway of MeCP2 and it is responsible for the early-onset seizure variant of Rett syndrome. Human molecular genetics *14*, 1935-1946.

Marin, O., and Rubenstein, J.L. (2003). Cell migration in the forebrain. Annu Rev Neurosci *26*, 441-483.

Maurer, S.P., Fourniol, F.J., Bohner, G., Moores, C.A., and Surrey, T. (2012). EBs recognize a nucleotide-dependent structural cap at growing microtubule ends. Cell *149*, 371-382.

Mazziotti, R., Lupori, L., Sagona, G., Gennaro, M., Della Sala, G., Putignano, E., and Pizzorusso, T. (2017). Searching for biomarkers of CDKL5 disorder: early-onset visual impairment in CDKL5 mutant mice. Human molecular genetics.

Meiri, D., Marshall, C.B., Greeve, M.A., Kim, B., Balan, M., Suarez, F., Bakal, C., Wu, C., Larose, J., Fine, N.*, et al.* (2012). Mechanistic insight into the microtubule and actin cytoskeleton coupling through dynein-dependent RhoGEF inhibition. Mol Cell *45*, 642-655.

Merriam, E.B., Millette, M., Lumbard, D.C., Saengsawang, W., Fothergill, T., Hu, X., Ferhat, L., and Dent, E.W. (2013). Synaptic regulation of microtubule dynamics in dendritic spines by calcium, F-actin, and drebrin. The Journal of neuroscience : the official journal of the Society for Neuroscience *33*, 16471-16482.

Mikuni, T., Nishiyama, J., Sun, Y., Kamasawa, N., and Yasuda, R. (2016). High-Throughput, High-Resolution Mapping of Protein Localization in Mammalian Brain by In Vivo Genome Editing. Cell *165*, 1803-1817.

Miller, C.J., and Turk, B.E. (2016). Rapid Identification of Protein Kinase Phosphorylation Site Motifs Using Combinatorial Peptide Libraries. Methods Mol Biol *1360*, 203-216.

Mirzaa, G.M., Paciorkowski, A.R., Marsh, E.D., Berry-Kravis, E.M., Medne, L., Alkhateeb, A., Grix, A., Wirrell, E.C., Powell, B.R., Nickels, K.C.*, et al.* (2013). CDKL5 and ARX mutations in males with early-onset epilepsy. Pediatr Neurol *48*, 367-377.

Mohan, R., and John, A. (2015). Microtubule-associated proteins as direct crosslinkers of actin filaments and microtubules. IUBMB Life *67*, 395-403.

Mok, J., Im, H., and Snyder, M. (2009). Global identification of protein kinase substrates by protein microarray analysis. Nat Protoc *4*, 1820-1827.

Montini, E., Andolfi, G., Caruso, A., Buchner, G., Walpole, S.M., Mariani, M., Consalez, G., Trump, D., Ballabio, A., and Franco, B. (1998). Identification and characterization of a novel serine-threonine kinase gene from the Xp22 region. Genomics *51*, 427-433.

Muly, E.C., Nairn, A.C., Greengard, P., and Rainnie, D.G. (2008). Subcellular distribution of the Rho-GEF Lfc in primate prefrontal cortex: effect of neuronal activation. The Journal of comparative neurology *508*, 927-939.

Nawaz, M.S., Giarda, E., Bedogni, F., La Montanara, P., Ricciardi, S., Ciceri, D., Alberio, T., Landsberger, N., Rusconi, L., and Kilstrup-Nielsen, C. (2016). CDKL5 and Shootin1 Interact and Concur in Regulating Neuronal Polarization. PloS one *11*, e0148634.

Nectoux, J., Fichou, Y., Cagnard, N., Bahi-Buisson, N., Nusbaum, P., Letourneur, F., Chelly, J., and Bienvenu, T. (2011). Cell cloning-based transcriptome analysis in cyclin-dependent kinase-like 5 mutation patients with severe epileptic encephalopathy. J Mol Med (Berl) *89*, 193-202.

Niwa, S. (2015). Kinesin superfamily proteins and the regulation of microtubule dynamics in morphogenesis. Anat Sci Int *90*, 1-6.

Nolen, B., Taylor, S., and Ghosh, G. (2004). Regulation of protein kinases; controlling activity through activation segment conformation. Mol Cell *15*, 661-675.

O'Donnell, M., Chance, R.K., and Bashaw, G.J. (2009). Axon growth and guidance: receptor regulation and signal transduction. Annu Rev Neurosci *32*, 383-412.

Oi, A., Katayama, S., Hatano, N., Sugiyama, Y., Kameshita, I., and Sueyoshi, N. (2017). Subcellular distribution of cyclin-dependent kinase-like 5 (CDKL5) is regulated through phosphorylation by dual specificity tyrosine-phosphorylation-regulated kinase 1A (DYRK1A). Biochemical and biophysical research communications *482*, 239-245.

Okuda, K., Kobayashi, S., Fukaya, M., Watanabe, A., Murakami, T., Hagiwara, M., Sato, T., Ueno, H., Ogonuki, N., Komano-Inoue, S.*, et al.* (2017). CDKL5 controls postsynaptic localization of GluN2B-containing NMDA receptors in the hippocampus and regulates seizure susceptibility. Neurobiology of disease *106*, 158-170.

Orban-Nemeth, Z., Simader, H., Badurek, S., Trancikova, A., and Propst, F. (2005). Microtubule-associated protein 1S, a short and ubiquitously expressed member of the microtubule-associated protein 1 family. The Journal of biological chemistry *280*, 2257-2265.

Page, K.M., Canti, C., Stephens, G.J., Berrow, N.S., and Dolphin, A.C. (1998). Identification of the amino terminus of neuronal Ca2+ channel alpha1 subunits alpha1B and alpha1E as an essential

determinant of G-protein modulation. The Journal of neuroscience : the official journal of the Society for Neuroscience *18*, 4815-4824.

Pearson, G., Robinson, F., Beers Gibson, T., Xu, B.E., Karandikar, M., Berman, K., and Cobb, M.H. (2001). Mitogen-activated protein (MAP) kinase pathways: regulation and physiological functions. Endocr Rev *22*, 153-183.

Pizzo, R., Gurgone, A., Castroflorio, E., Amendola, E., Gross, C., Sassoe-Pognetto, M., and Giustetto, M. (2016). Lack of Cdkl5 Disrupts the Organization of Excitatory and Inhibitory Synapses and Parvalbumin Interneurons in the Primary Visual Cortex. Front Cell Neurosci *10*, 261.

Ptacek, J., Devgan, G., Michaud, G., Zhu, H., Zhu, X., Fasolo, J., Guo, H., Jona, G., Breitkreutz, A., Sopko, R.*, et al.* (2005). Global analysis of protein phosphorylation in yeast. Nature *438*, 679-684.

Ramaswamy, S., and Markram, H. (2015). Anatomy and physiology of the thick-tufted layer 5 pyramidal neuron. Front Cell Neurosci *9*, 233.

Ricciardi, S., Ungaro, F., Hambrock, M., Rademacher, N., Stefanelli, G., Brambilla, D., Sessa, A., Magagnotti, C., Bachi, A., Giarda, E.*, et al.* (2012). CDKL5 ensures excitatory synapse stability by reinforcing NGL-1-PSD95 interaction in the postsynaptic compartment and is impaired in patient iPSC-derived neurons. Nature cell biology *14*, 911-923.

Rusconi, L., Kilstrup-Nielsen, C., and Landsberger, N. (2011). Extrasynaptic N-methyl-D-aspartate (NMDA) receptor stimulation induces cytoplasmic translocation of the CDKL5 kinase and its proteasomal degradation. The Journal of biological chemistry *286*, 36550-36558.

Rusconi, L., Salvatoni, L., Giudici, L., Bertani, I., Kilstrup-Nielsen, C., Broccoli, V., and Landsberger, N. (2008). CDKL5 expression is modulated during neuronal development and its subcellular distribution is tightly regulated by the C-terminal tail. The Journal of biological chemistry *283*, 30101-30111.

Ryan, X.P., Alldritt, J., Svenningsson, P., Allen, P.B., Wu, G.Y., Nairn, A.C., and Greengard, P. (2005). The Rho-specific GEF Lfc interacts with neurabin and spinophilin to regulate dendritic spine morphology. Neuron *47*, 85-100.

Sandi, M.J., Marshall, C.B., Balan, M., Coyaud, E., Zhou, M., Monson, D.M., Ishiyama, N., Chandrakumar, A.A., La Rose, J., Couzens, A.L.*, et al.* (2017). MARK3-mediated phosphorylation of ARHGEF2 couples microtubules to the actin cytoskeleton to establish cell polarity. Sci Signal *10*.

Sassa, T., Gomi, H., and Itohara, S. (2004). Postnatal expression of Cdkl2 in mouse brain revealed by LacZ inserted into the Cdkl2 locus. Cell Tissue Res *315*, 147-156.

Sayas, C.L., and Avila, J. (2014). Regulation of EB1/3 proteins by classical MAPs in neurons. Bioarchitecture *4*, 1-5.

Scala, E., Ariani, F., Mari, F., Caselli, R., Pescucci, C., Longo, I., Meloni, I., Giachino, D., Bruttini, M., Hayek, G.*, et al.* (2005). CDKL5/STK9 is mutated in Rett syndrome variant with infantile spasms. Journal of medical genetics *42*, 103-107.

Sekiguchi, M., Katayama, S., Hatano, N., Shigeri, Y., Sueyoshi, N., and Kameshita, I. (2013). Identification of amphiphysin 1 as an endogenous substrate for CDKL5, a protein kinase associated with X-linked neurodevelopmental disorder. Archives of biochemistry and biophysics *535*, 257-267.

Shah, K., Liu, Y., Deirmengian, C., and Shokat, K.M. (1997). Engineering unnatural nucleotide specificity for Rous sarcoma virus tyrosine kinase to uniquely label its direct substrates. Proceedings of the National Academy of Sciences of the United States of America *94*, 3565-3570.

Sharma, K., Schmitt, S., Bergner, C.G., Tyanova, S., Kannaiyan, N., Manrique-Hoyos, N., Kongi, K., Cantuti, L., Hanisch, U.K., Philips, M.A*., et al.* (2015). Cell type- and brain region-resolved mouse brain proteome. Nature neuroscience *18*, 1819-1831.

Sheng, M., and Kim, E. (2011). The postsynaptic organization of synapses. Cold Spring Harb Perspect Biol *3*.

Sheng, Z.H., and Cai, Q. (2012). Mitochondrial transport in neurons: impact on synaptic homeostasis and neurodegeneration. Nature reviews Neuroscience *13*, 77-93.

Sit, S.T., and Manser, E. (2011). Rho GTPases and their role in organizing the actin cytoskeleton. Journal of cell science *124*, 679-683.

Sivilia, S., Mangano, C., Beggiato, S., Giuliani, A., Torricella, R., Baldassarro, V.A., Fernandez, M., Lorenzini, L., Giardino, L., Borelli, A.C*., et al.* (2016). CDKL5 knockout leads to altered inhibitory transmission in the cerebellum of adult mice. Genes Brain Behav *15*, 491-502.

Song, K., Hu, W., Yue, F., Zou, J., Li, W., Chen, Q., Yao, Q., Sun, W., and Liu, L. (2015). Transforming Growth Factor TGFbeta Increases Levels of Microtubule-Associated Protein MAP1S and Autophagy Flux in Pancreatic Ductal Adenocarcinomas. PloS one *10*, e0143150.

Spruston, N. (2008). Pyramidal neurons: dendritic structure and synaptic integration. Nature reviews Neuroscience *9*, 206-221.

Steger, M., Tonelli, F., Ito, G., Davies, P., Trost, M., Vetter, M., Wachter, S., Lorentzen, E., Duddy, G., Wilson, S*., et al.* (2016). Phosphoproteomics reveals that Parkinson's disease kinase LRRK2 regulates a subset of Rab GTPases. Elife *5*.

Stenner, F., Liewen, H., Gottig, S., Henschler, R., Markuly, N., Kleber, S., Faust, M., Mischo, A., Bauer, S., Zweifel, M*., et al.* (2013). RP1 is a phosphorylation target of CK2 and is involved in cell adhesion. PloS one *8*, e67595.

Stepanova, T., Slemmer, J., Hoogenraad, C.C., Lansbergen, G., Dortland, B., De Zeeuw, C.I., Grosveld, F., van Cappellen, G., Akhmanova, A., and Galjart, N. (2003). Visualization of microtubule growth in cultured neurons via the use of EB3-GFP (end-binding protein 3-green fluorescent protein). The Journal of neuroscience : the official journal of the Society for Neuroscience *23*, 2655-2664.

Stiess, M., Maghelli, N., Kapitein, L.C., Gomis-Ruth, S., Wilsch-Brauninger, M., Hoogenraad, C.C., Tolic-Norrelykke, I.M., and Bradke, F. (2010). Axon extension occurs independently of centrosomal microtubule nucleation. Science *327*, 704-707.

Stuss, D.P., Boyd, J.D., Levin, D.B., and Delaney, K.R. (2012). MeCP2 mutation results in compartment-specific reductions in dendritic branching and spine density in layer 5 motor cortical neurons of YFP-H mice. PloS one *7*, e31896.

Suter, D.M., and Miller, K.E. (2011). The emerging role of forces in axonal elongation. Prog Neurobiol *94*, 91-101.

Takano, T., Wu, M., Nakamuta, S., Naoki, H., Ishizawa, N., Namba, T., Watanabe, T., Xu, C., Hamaguchi, T., Yura, Y*., et al.* (2017). Discovery of long-range inhibitory signaling to ensure single axon formation. Nat Commun *8*, 33.

Takano, T., Xu, C., Funahashi, Y., Namba, T., and Kaibuchi, K. (2015). Neuronal polarization. Development *142*, 2088-2093.

Tang, S., Wang, I.J., Yue, C., Takano, H., Terzic, B., Pance, K., Lee, J.Y., Cui, Y., Coulter, D.A., and Zhou, Z. (2017). Loss of CDKL5 in Glutamatergic Neurons Disrupts Hippocampal Microcircuitry and Leads

to Memory Impairment in Mice. The Journal of neuroscience : the official journal of the Society for Neuroscience *37*, 7420-7437.

Tao, J., Van Esch, H., Hagedorn-Greiwe, M., Hoffmann, K., Moser, B., Raynaud, M., Sperner, J., Fryns, J.P., Schwinger, E., Gecz, J.*, et al.* (2004). Mutations in the X-linked cyclin-dependent kinase-like 5 (CDKL5/STK9) gene are associated with severe neurodevelopmental retardation. American journal of human genetics *75*, 1149-1154.

Tegha-Dunghu, J., Bausch, E., Neumann, B., Wuensche, A., Walter, T., Ellenberg, J., and Gruss, O.J. (2014). MAP1S controls microtubule stability throughout the cell cycle in human cells. Journal of cell science *127*, 5007-5013.

Toriyama, M., Kozawa, S., Sakumura, Y., and Inagaki, N. (2013). Conversion of a signal into forces for axon outgrowth through Pak1-mediated shootin1 phosphorylation. Curr Biol *23*, 529-534.

Trazzi, S., Fuchs, C., Viggiano, R., De Franceschi, M., Valli, E., Jedynak, P., Hansen, F.K., Perini, G., Rimondini, R., Kurz, T.*, et al.* (2016). HDAC4: a key factor underlying brain developmental alterations in CDKL5 disorder. Human molecular genetics *25*, 3887-3907.

Ultanir, S.K., Hertz, N.T., Li, G., Ge, W.P., Burlingame, A.L., Pleasure, S.J., Shokat, K.M., Jan, L.Y., and Jan, Y.N. (2012). Chemical genetic identification of NDR1/2 kinase substrates AAK1 and Rabin8 Uncovers their roles in dendrite arborization and spine development. Neuron *73*, 1127-1142.

Ultanir, S.K., Yadav, S., Hertz, N.T., Oses-Prieto, J.A., Claxton, S., Burlingame, A.L., Shokat, K.M., Jan, L.Y., and Jan, Y.N. (2014). MST3 Kinase Phosphorylates TAO1/2 to Enable Myosin Va Function in Promoting Spine Synapse Development. Neuron *84*, 968-982.

Vale, R.D. (2003). The molecular motor toolbox for intracellular transport. Cell *112*, 467-480.

van Beuningen, S.F., Will, L., Harterink, M., Chazeau, A., van Battum, E.Y., Frias, C.P., Franker, M.A., Katrukha, E.A., Stucchi, R., Vocking, K.*, et al.* (2015). TRIM46 Controls Neuronal Polarity and Axon Specification by Driving the Formation of Parallel Microtubule Arrays. Neuron *88*, 1208-1226.

Vilor-Tejedor, N., Alemany, S., Forns, J., Caceres, A., Murcia, M., Macia, D., Pujol, J., Sunyer, J., and Gonzalez, J.R. (2016). Assessment of Susceptibility Risk Factors for ADHD in Imaging Genetic Studies. J Atten Disord.

Volk, M., Maver, A., Hodzic, A., Lovrecic, L., and Peterlin, B. (2017). Transcriptome Profiling Uncovers Potential Common Mechanisms in Fetal Trisomies 18 and 21. OMICS *21*, 565-570.

Wang, I.T., Allen, M., Goffin, D., Zhu, X., Fairless, A.H., Brodkin, E.S., Siegel, S.J., Marsh, E.D., Blendy, J.A., and Zhou, Z. (2012). Loss of CDKL5 disrupts kinome profile and event-related potentials leading to autistic-like phenotypes in mice. Proceedings of the National Academy of Sciences of the United States of America *109*, 21516-21521.

Weaving, L.S., Christodoulou, J., Williamson, S.L., Friend, K.L., McKenzie, O.L., Archer, H., Evans, J., Clarke, A., Pelka, G.J., Tam, P.P.*, et al.* (2004). Mutations of CDKL5 cause a severe neurodevelopmental disorder with infantile spasms and mental retardation. American journal of human genetics *75*, 1079-1093.

Weiergraber, M., Kamp, M.A., Radhakrishnan, K., Hescheler, J., and Schneider, T. (2006). The Ca(v)2.3 voltage-gated calcium channel in epileptogenesis--shedding new light on an enigmatic channel. Neurosci Biobehav Rev *30*, 1122-1144.

Williams, M.E., de Wit, J., and Ghosh, A. (2010). Molecular mechanisms of synaptic specificity in developing neural circuits. Neuron *68*, 9-18.

Williamson, S.L., Giudici, L., Kilstrup-Nielsen, C., Gold, W., Pelka, G.J., Tam, P.P., Grimm, A., Prodi, D., Landsberger, N., and Christodoulou, J. (2012). A novel transcript of cyclin-dependent kinase-like 5

(CDKL5) has an alternative C-terminus and is the predominant transcript in brain. Human genetics *131*, 187-200.

Witte, H., Neukirchen, D., and Bradke, F. (2008). Microtubule stabilization specifies initial neuronal polarization. J Cell Biol *180*, 619-632.

Wong, E.Y., Tse, J.Y., Yao, K.M., Lui, V.C., Tam, P.C., and Yeung, W.S. (2004). Identification and characterization of human VCY2-interacting protein: VCY2IP-1, a microtubule-associated protein-like protein. Biol Reprod *70*, 775-784.

Wong, R.O., and Ghosh, A. (2002). Activity-dependent regulation of dendritic growth and patterning. Nature reviews Neuroscience *3*, 803-812.

Xie, R., Nguyen, S., McKeehan, K., Wang, F., McKeehan, W.L., and Liu, L. (2011). Microtubule-associated protein 1S (MAP1S) bridges autophagic components with microtubules and mitochondria to affect autophagosomal biogenesis and degradation. The Journal of biological chemistry *286*, 10367-10377.

Xu, G., Yue, F., Huang, H., He, Y., Li, X., Zhao, H., Su, Z., Jiang, X., Li, W., Zou, J.*, et al.* (2016). Defects in MAP1S-mediated autophagy turnover of fibronectin cause renal fibrosis. Aging (Albany NY) *8*, 977-985.

Xue, L., Arrington, J.V., and Tao, W.A. (2016). Identification of Direct Kinase Substrates via Kinase Assay-Linked Phosphoproteomics. Methods Mol Biol *1355*, 263-273.

Xue, L., and Tao, W.A. (2013). Current technologies to identify protein kinase substrates in high throughput. Front Biol (Beijing) *8*, 216-227.

Yau, K.W., van Beuningen, S.F., Cunha-Ferreira, I., Cloin, B.M., van Battum, E.Y., Will, L., Schatzle, P., Tas, R.P., van Krugten, J., Katrukha, E.A.*, et al.* (2014). Microtubule minus-end binding protein CAMSAP2 controls axon specification and dendrite development. Neuron *82*, 1058-1073.

Yoshimura, Y., and Miki, H. (2011). Dynamic regulation of GEF-H1 localization at microtubules by Par1b/MARK2. Biochemical and biophysical research communications *408*, 322-328.

Yue, F., Li, W., Zou, J., Chen, Q., Xu, G., Huang, H., Xu, Z., Zhang, S., Gallinari, P., Wang, F.*, et al.* (2015). Blocking the association of HDAC4 with MAP1S accelerates autophagy clearance of mutant Huntingtin. Aging (Albany NY) *7*, 839-853.

Yue, F., Li, W., Zou, J., Jiang, X., Xu, G., Huang, H., and Liu, L. (2017). Spermidine Prolongs Lifespan and Prevents Liver Fibrosis and Hepatocellular Carcinoma by Activating MAP1S-Mediated Autophagy. Cancer Res *77*, 2938-2951.

Yue, J., Xie, M., Gou, X., Lee, P., Schneider, M.D., and Wu, X. (2014). Microtubules regulate focal adhesion dynamics through MAP4K4. Developmental cell *31*, 572-585.

Yuste, R., and Bonhoeffer, T. (2004). Genesis of dendritic spines: insights from ultrastructural and imaging studies. Nature reviews Neuroscience *5*, 24-34.

Zhang, C., Kenski, D.M., Paulson, J.L., Bonshtien, A., Sessa, G., Cross, J.V., Templeton, D.J., and Shokat, K.M. (2005). A second-site suppressor strategy for chemical genetic analysis of diverse protein kinases. Nature methods *2*, 435-441.

Zhou, A., Han, S., and Zhou, Z.J. (2017). Molecular and genetic insights into an infantile epileptic encephalopathy - CDKL5 disorder. Front Biol (Beijing) *12*, 1-6.

Zhu, Y.C., Li, D., Wang, L., Lu, B., Zheng, J., Zhao, S.L., Zeng, R., and Xiong, Z.Q. (2013). Palmitoylation-dependent CDKL5-PSD-95 interaction regulates synaptic targeting of CDKL5 and dendritic spine development. Proceedings of the National Academy of Sciences of the United States of America *110*, 9118-9123.